Technische Universität München
Physik Department T70

Aspects of False Vacuum Decay

Wenyuan Ai

Vollständiger Abdruck der von der Fakultät für **Physik** der Technischen Universität München zur Erlangung des akademischen Grades eines

Doktors der Naturwissenschaften (Dr. rer. nat.)

genehmigten Dissertation.

Vorsitzender: Prof. Dr. Wilhelm Auwärter

Prüfer der Dissertation:

1. Prof. Dr. Björn Garbrecht
2. Prof. Dr. Andreas Weiler

Die Dissertation wurde am 22.03.2019 bei der Technischen Universität München eingereicht und durch die Fakultät für **Physik** am 02.04.2019 angenommen.

Abstract

False vacuum decay is the first-order phase transition of fundamental fields. Vacuum instability plays a very important role in particle physics and cosmology. Theoretically, any consistent theory beyond the Standard Model must have a lifetime of the electroweak vacuum longer than the age of the Universe. Phenomenologically, first-order cosmological phase transitions can be relevant for baryogenesis and gravitational wave production. In this thesis, we give a detailed study on several aspects of false vacuum decay, including correspondence between thermal and quantum transitions of vacuum in flat or curved spacetime, radiative corrections to false vacuum decay and, the real-time formalism of vacuum transitions.

Zusammenfassung

Falscher Vakuumzerfall ist ein Phasenübergang erster Ordnung fundamentaler Felder. Vakuuminstabilität spielt in der Teilchenphysik und Kosmologie eine sehr wichtige Rolle. Theoretisch muss für jede konsistente Theorie, die über das Standardmodell hinausgeht, die Lebensdauer des elektroschwachen Vakuums länger sein als das Alter des Universums. Phänomenologisch können kosmologische Phasenübergänge erster Ordnung für die Baryogenese und die Produktion von Gravitationswellen relevant sein. In dieser Arbeit geben wir eine detaillierte Studie zu verschiedenen Aspekten des falschen Vakuumzerfalls, einschließlich der Korrespondenz zwischen thermischen und Quantenübergängen des Vakuums in flachen oder gekrümmten Raumzeiten, Strahlungskorrekturen zu falschem Vakuumzerfall und den Formalismus realer Zeiten für Vakuumübergänge.

The bulk of this manuscript is based on the articles which were written during this Ph.D. thesis, a list of which is shown below:

- ⋆ W. Y. Ai, B. Garbrecht and C. Tamarit, "Functional methods for false vacuum decay in real time," arXiv:1905.04236 [hep-th].

- ⋆ W. Y. Ai, "Correspondence between Thermal and Quantum Vacuum Transitions around Horizons," JHEP **1903** 164 (2019) [arXiv:1812.06962 [hep-th]].

- ⋆ W. Y. Ai, B. Garbrecht and P. Millington, "Radiative effects on false vacuum decay in Higgs-Yukawa theory," Phys. Rev. D **98**, 076014 (2018) [arXiv:1807.03338 [hep-th]].

Notations

- $Z_E[0]$ — Euclidean partition function without source
- $Z[\beta]$ — thermal partition function at temperature $1/\beta$
- $\mu, \nu, ...$ — taking values $0, ..., 3$ or $1, ..., 4$ in the Minkowski case or the Euclidean case, respectively.
- $i, j, ...$ — taking values $1, 2, 3$ denoting the spatial indices
- $\Delta^{(4)}$, ∂^2 — four-dimensional Laplacian, both are interchangeably used in this thesis
- ∇ — three-dimensional derivative operator
- B — mostly used as the bounce action, also as subscript for "bounce"
- Γ — decay rate
- Γ — effective action
- ϵ, 0^+ — infinitesimal positive number as used in the Feynman $i\epsilon$-prescription
- Except for appendices A and D, we take $\hbar = c = k_B = 1$ throughout this thesis

Contents

Chapter 1

Introduction

It is remarkable that the abundant world that we live in can be described and explained at the very fundamental level by dozens of fundamental particles and four fundamental interactions between them: gravity, electromagnetic, weak and strong interactions. All the known particles that constitute the matter and interactions except for gravity can be very well described by the standard model (SM) of particle physics [1]. Gravity is described by general relativity (GR) [2]. It turns out that all the particles are excitations of some more fundamental objects that we call quantum fields. False vacuum decay is the first-order phase transition of such fundamental quantum fields. One surprising feature in the SM is that the electromagnetic interaction and the weak interaction are unified and they appear to be different aspects of this unified theory only after the electroweak symmetry breaking. Such an electroweak sector in the SM provides a crucial phenomenological motivation for the study of false vacuum decay.

In the SM, the Higgs doublet is responsible for all the masses of other particles via the mechanism of spontaneous symmetry breaking (SSB) where the Higgs field obtains a non-vanishing vacuum expectation value (VEV). The non-vanishing VEV of the Higgs field generates masses for other particles through the Yukawa interactions. To illustrate SSB, let us write down the Lagrangian for the Higgs doublet

$$\mathcal{L}_{\text{Higgs}} = \eta^{\mu\nu}(\partial_\mu\phi)\partial_\nu\phi - V(\phi), \tag{1.1}$$

where the Minkowski metric is $\eta^{\mu\nu} = \text{diag}(1, -1, -1, -1)$ and

$$V(\phi) = -\mu^2\phi^\dagger\phi + \lambda(\phi^\dagger\phi)^2. \tag{1.2}$$

Here ϕ is the Higgs doublet, in components

$$\phi = \begin{pmatrix}\phi_1\\ \phi_2\end{pmatrix}. \tag{1.3}$$

For $\lambda > 0$, $\mu^2 > 0$, the potential has an infinite set of degenerate minima satisfying

$$\phi^\dagger\phi = \frac{\mu^2}{2\lambda} \equiv \frac{v^2}{2}.$$

The degeneracy of the minima reflects the global $SU(2)_L \times U(1)_Y$ symmetry[1] of the theory. The vacuum picks a particular point in the degenerate minima which we take as

$$\langle 0|\phi|0\rangle = \frac{1}{\sqrt{2}}\begin{pmatrix}0\\ v\end{pmatrix}. \tag{1.4}$$

[1] It must be gauged in order to introduce the electroweak gauge fields.

In this way, the Higgs doublet obtains a non-zero VEV and the $SU(2)_L \times U(1)_Y$ symmetry of the electroweak theory is spontaneously broken by the vacuum state. It turns out that $v = 246$ GeV and the corresponding minimum is called the electroweak vacuum which is stable at the tree-level.

However, the Higgs potential suffers from quantum corrections. In particular, the coupling constants must be running when the energy scale, or correspondingly the field value, changes. The running of the coupling constants satisfies the renormalization group equation (taking the coupling λ as an example)

$$\mu \frac{\partial \lambda}{\partial \mu} = \beta(\mu), \tag{1.5}$$

where μ is the running energy scale. The beta function $\beta(\mu)$ receives contributions from all fields that couple with the Higgs. The dominant contributions come from the Higgs itself and the top quark. With the matter content in the SM, especially with the 125 GeV Higgs boson [3, 4] and the 173 GeV top quark [5], the Higgs quartic coupling λ turns to be negative at around 10^{11} GeV, developing a new minimum deeper than the electroweak vacuum.[2] Thus the electroweak vacuum in the SM is unstable. State-of-the-art calculations suggest that the lifetime of the electroweak vacuum in the SM is much longer than the age of our Universe, leading to the metastable scenario [6, 7, 8, 9, 10, 11]. The metastable scenario implies that the SM can be extrapolated up to the Planck scale with no problem of consistency in principle.

The calculation of the electroweak vacuum lifetime is very important because it could provide significant implications on new physics beyond the SM. For example, had the calculations suggested a lifetime of the electroweak vacuum shorter than the age of the Universe, there would have to be new heavy degrees of freedom that make an important contribution to the beta function of the Higgs quartic coupling. The decay rate is calculated from the running couplings with precision up to next-to-next-to-leading order (NNLO) [7, 8]. However, in comparison to the running couplings, the radiative corrections to the actual tunneling problem are known less accurately. In particular, in order to describe the tunneling process, one must resort to an inhomogeneous background field configuration which is called the bounce (see Chap. 2 for details). And the beta functions for the running couplings do not account for the effects from the inhomogeneity of the background. Actually, the previous calculations are based on the Coleman-Weinberg potential [12] which only applies to homogeneous backgrounds. Thus a new method that accounts for gradient effects from the inhomogeneous background as well as determines systematically the radiative corrections to the bounce and the decay rate is needed. This will be one of the topics in this thesis.

On the other hand, the metastable scenario could be challenged when gravity effects are taken into account. In particular, black holes, as nucleation seeds, may affect the process of vacuum decay. It was shown that the false vacuum decay catalyzed by microscopic black holes could have a much larger decay rate [13, 14, 15, 16]. The bubble nucleation around a Schwarzschild black hole is typically described by an $O(3) \times O(2)$-bounce solution, the so-called static bounce. The $O(2)$-symmetry is due to the periodic Euclidean Schwarzschild time. It is debated in the literature that whether such static bounce solution describes

[2] Note that the running of the $U(1)$-coupling leads to $\lambda > 0$ again at super-Planckian energies.

false vacuum decay at zero temperature or at finite temperature. Before the physical meaning of the static bounce is clear, the enhancement of the decay rate is under suspicion. For example, if the static bounce describes a false vacuum decay at finite temperature while realistic black holes are in the vacuum, then in order to implement the catalyzation one needs to surround a black hole with a thermal plasma. Hence, another topic in this thesis is to investigate the interpretations for the static bounce in the Euclidean Schwarzschild spacetime. As we will see, there is a correspondence that the static bounce solution describes either a thermal transition of vacuum in the static region outside of a Schwarzschild spacetime or a quantum transition in a maximally extended Kruskal-Szekeres spacetime, corresponding to the viewpoints of the external static observers and of the freely falling observers, respectively.

Besides the electroweak metastability that we have mentioned, false vacuum decay has many other applications in phenomenological studies. One particularly important application is the electroweak phase transition that happened during the cooling of the Universe. Today, there exists overwhelming evidence suggesting the big bang picture of the Universe [17, 18]. In this picture, the observable Universe originates from the expansion of a much smaller and hotter universe at earlier times. During the expansion of the Universe, the temperature decreases. Since at finite temperature, the Higgs potential can receive a thermal mass along with other effects, the broken electroweak symmetry can be restored at high temperature in the early Universe. During the cooling, the Universe thus experienced a phase transition from the symmetric phase to the broken phase which we call electroweak phase transition.[3] While in the SM, the electroweak phase transition is cross-over [19, 20], it can be of first order in a variety of beyond SM models [21, 22, 23, 24, 25, 26, 27, 28], leading to the nucleation of bubbles. The subsequent collisions and mergers of the nucleated bubbles can produce gravitational waves [29, 30, 31, 32]. Moreover, these bubbles may turn out to be pivotal for generating the cosmic matter-antimatter asymmetry [33, 34, 35, 36].

Underlying all the phenomenological studies, there is a standard description for the vacuum transition, the Callan-Coleman formalism [37] which makes use of the Euclidean path integral. In this formalism, one aims to calculate the energy for the unstable vacuum, in particular, to extract an imaginary part therein and then relate the imaginary part of the energy to the decay rate. This is very similar to solving a static Schördinger equation via a variation method. However, the picture for the dynamical tunneling process is not clear in the Euclidean formalism. In particular, in Callan-Coleman formalism, the obtained decay rate is interpreted as for the transition from the false vacuum to a classical critical bubble while this interpretation has never been rigorously justified. In addition, there are some other conceptual ambiguities in the existing descriptions for false vacuum decay. For instance, why quantum tunneling, as a *dynamical* process, can be understood by solving a *static* Schördinger equation? How can the energy of an unstable state possesses an imaginary part which seemingly is in contradiction with the Hermiticity of the Hamiltonian? Can the tunneling process be understood in the real-time Minkowski path integral instead of the Euclidean path integral? Are there any correspondences or interpretations of the instantons that only appear in the Euclidean field theory? In the

[3] There are of course other possible phase transitions such as the QCD phase transition from the phase of quark-gluon plasma to the hadron phase.

last part of this thesis, we aim to answer these conceptual questions. We will provide a real-time picture of quantum tunneling (and hence false vacuum decay) in the Minkowski path integral. By applying the optical theorem to the unstable vacuum, we obtain the decay rate from the imaginary part of the matrix M in $S = \mathbf{1} + iM$ where S is the transition amplitude form the false vacuum to itself. We will discuss new insights from this optical-theorem derivation of the vacuum decay rate.

Chapter 2

False Vacuum Decay in Flat Spacetime at Zero and Finite Temperature

A theoretical description of phase transitions wes originally given in the context of statistical physics [38, 39], which was generalized to quantum phase transitions in Refs. [40, 41, 37] (see also Ref. [42]). The seminal works [41, 37] were later extended to the case of false vacuum decay at finite temperature by Affleck [43] and Linde [44, 45]. In this chapter, we will first review the standard Callan-Coleman formalism in a simple particle tunneling example which will be generalized to false vacuum decay subsequently. We will in particular build the picture of bubble nucleation and the subsequent bubble growth in the thin-wall approximation. At last, we will extend the discussion of false vacuum decay at zero temperature to that at finite temperature.

2.1 Quantum tunneling in quantum mechanics

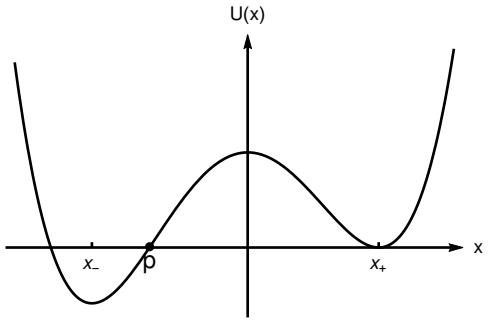

Figure 2.1: A potential $U(\Phi)$ which has an unstable minimum. The dot marked by "**p**" is the turning point.

Let us consider a particle tunneling problem in a potential with two non-degenerate minima, as shown in Fig. 2.1. In the classical theory, the particle located at the local minimum (with sufficiently small momentum) is stable. However, in quantum theory, it can transit to the global minimum through quantum tunneling. The archetypal model studied by Coleman and Callan [41, 37] is given by the following action

$$S_M = \int \mathrm{d}t\ \mathcal{L}_M = \int \mathrm{d}t\ \left[\frac{1}{2}\left(\frac{\mathrm{d}x}{\mathrm{d}t}\right)^2 - U(x)\right], \tag{2.1}$$

where

$$U(x) = -\frac{1}{2}\mu^2 x^2 + \frac{1}{3!}gx^3 + \frac{1}{4!}\lambda x^4 + U_0. \tag{2.2}$$

Here μ^2, g and λ are all positive parameters. The potential $U(x)$ has two non-degenerate minima at $x_\pm$. The constant U_0 is introduced for convenience to ensure that the potential vanishes at the higher minimum.

In order to obtain the tunneling rate, Callan and Coleman consider the following *Euclidean* transition amplitude

$$Z_E[0] = \langle x_+|e^{-H\mathcal{T}}|x_+\rangle = \int \mathcal{D}\Phi\, e^{-S_E}, \tag{2.3}$$

where S_E is the classical Euclidean action. The Euclidean path integral follows completely from the Euclidean transition amplitude by a standard derivation of the Feynman path integral. Nevertheless, a quick way to arrive at the Euclidean path integral is the Wick rotation, i.e., we can simply take $t(\equiv x_0) \to -i\tau(\equiv -ix_4)$, $T \to -i\mathcal{T}$ and $S_M \to iS_E$ in the Minkowski path integral. Written explicitly,

$$S_E = \int \mathrm{d}\tau \, \left[\frac{1}{2}\left(\frac{\mathrm{d}x}{\mathrm{d}t}\right)^2 + U(x)\right]. \tag{2.4}$$

Note in the Euclidean action, the sign in front of the potential is flipped and therefore we have a potential $-U(x)$. An immediate consequence is that, for the boundary conditions indicated by the above Euclidean transition amplitude, the Euclidean action permits non-trivial classical solutions. One of which turns out to be pivotal in describing the tunneling process as we will show shortly.

If we insert in the partition function a complete set of energy eigenstates, i.e.

$$\langle x_+|e^{-H\mathcal{T}}|x_+\rangle = \sum_n e^{-E_n\mathcal{T}} \langle x_+|n\rangle\langle n|x_+\rangle \,, \tag{2.5}$$

then for large $\mathcal{T}$, only the lowest-lying energy eigenstate will survive. Therefore

$$\lim_{\mathcal{T}\to\infty} \langle x_+|e^{-H\mathcal{T}}|x_+\rangle = e^{-E_0\mathcal{T}} \, |\langle x_+|0\rangle|^2, \tag{2.6}$$

giving us the information of the lowest energy E_0 and the corresponding wave function $|\langle x_+|0\rangle|^2$. The spirit of the Callan-Coleman method is to calculate the energy E_0 of the approximate ground state $|0\rangle$ near x_+ via Eqs. (2.6) and (2.3) . Since this state is unstable, we expect that its energy E_0 possesses an imaginary part which can be further related to the decay rate according to the evolution behavior: $\exp(-iE_0t)|0\rangle = \exp(-i(\mathrm{Re}E_0)t) \cdot \exp((\mathrm{Im}E_0)t)|0\rangle$. That is[4]

$$\Gamma = -2\,\mathrm{Im}E_0 = \frac{2}{\mathcal{T}}\,\mathrm{Im}\left(\ln Z_E[0] - \ln|\langle x_+|0\rangle|^2\right) = \frac{2}{\mathcal{T}}\,\mathrm{Im}\left(\ln Z_E[0]\right), \tag{2.7}$$

where in the last equality we have used the fact that $\ln|\langle x_+|0\rangle|^2$ does not contribute to the imaginary part.

[4]There is a sign ambiguity in extracting the imaginary part; the extraction should proceed in a way such that $\Gamma > 0$.

One can perform the calculation for the Euclidean path integral using the method of steepest descent. The stationary points are obtained from the equation of motion (EoM)

$$-\frac{\mathrm{d}^2x(\tau)}{\mathrm{d}\tau^2}+U'(x(\tau))=0, \tag{2.8}$$

where $'$ denotes the derivative with respect to x. The boundary conditions are $x|_{\tau\to\pm\infty}=x_+$. Eq. (2.8) is the EoM for a particle of unit mass moving in a potential minus U. Therefore,

$$E=\frac{1}{2}\left(\frac{\mathrm{d}x}{\mathrm{d}\tau}\right)^2-U(x) \tag{2.9}$$

is a constant of motion.

In the limit $\mathcal{T}\to\infty$, we have three solutions: the trivial false vacuum solution $x_F(\tau)\equiv x_+$, the *bounce* $x_B(\tau)$ and a third one called the *shot* in Refs. [46, 47], $x_S(\tau)$. The bounce solution is responsible for the tunneling process as we will explain later. Pictorially, the bounce solution corresponds to a particle initially at x_+ rolling through the valley in $-U(x)$, reaching the turning point "$\mathbf{p}$" and then rolling back to x_+—hence the name bounce, see Fig. 2.2. To understand the shot, recall that the particle can have a non-vanishing velocity at x_+ such that it is kicked off from x_+ and moves to another potential top at x_- with asymptotically vanishing velocity and rolls back. The requirement of that the particle stops exactly at x_- instead of some point before it comes from the condition $\mathcal{T}\to\infty$; otherwise, the motion will be finished too quickly.

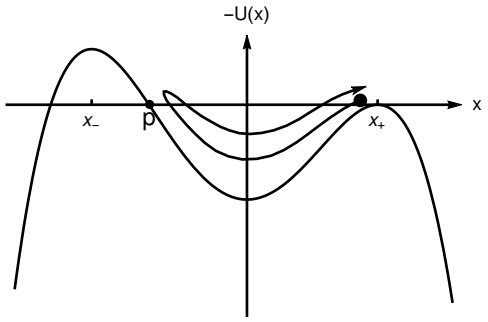

Figure 2.2: The bounce as a solution of the Euclidean EoM. Note that the potential in the Euclidean spacetime is upside down compared with that in Minkowski spacetime.

We can expand the path integral in Eq. (2.3) around these stationary points. Expanding $x(\tau)=x_a(\tau)+\Delta x_a(\tau)$ where $a=F,B,S$, we have

$$\begin{aligned}
&\langle x_+|e^{-H\mathcal{T}}|x_+\rangle\\
&\approx\sum_a\left(e^{-S_E[x_a]}\int\mathcal{D}\Delta x_a\; e^{-\int_{-\mathcal{T}/2}^{\mathcal{T}/2}\mathrm{d}\tau\left[\frac{1}{2}\Delta x_a(\tau)\left(-\partial_\tau^2+U''(x_a(\tau))\right)\Delta x_a(\tau)+\frac{1}{3!}(g+\lambda x_a(\tau))\Delta x_a^3(\tau)+\frac{\lambda}{4!}\Delta x_a^4(\tau)\right]}\right)\\
&\equiv Z_E^F[0]+Z_E^B[0]+Z_E^S[0].
\end{aligned} \tag{2.10}$$

In Ref. [37], only the expansions around x_F and x_B are considered in evaluating the above Euclidean transition amplitude. The reasons, though subtle, are the following:

(1). The expansion around the shot, $Z_E^S[0]$, is dominant in Eq. (2.10) but gives the energy for the global ground state rather than the one for the false ground state $|0\rangle$ near x_+. But we want to calculate the energy for $|0\rangle$.

(2). Since we want to study the tunneling process for the false ground state around x_+, we shall only consider the stationary points in which the particle has low initial energy. Thus only x_F and x_B need to be considered.

$Z_E^F[0]$ can be calculated in a standard way as a perturbative theory in a trivial background and we obtain up to one-loop order

$$Z_E^F[0] = \mathcal{N}\left[\det\left(-\partial_\tau^2 + U''(x_+)\right)\right]^{-1/2}, \tag{2.11}$$

where the factor $\mathcal{N}$ on the RHS is a normalization factor to make the path integral properly well-defined which shall be always fixed by a physical condition. Computing $Z_E^B[0]$ is less nontrivial. Because of the inhomogeneous background x_B, we must look into the eigenspectrum of the fluctuation operator evaluated at x_B,

$$\left(-\partial_\tau^2 + U''(x_B(\tau))\right) f_n^B(\tau) = \lambda_n^B f_n^B(\tau). \tag{2.12}$$

In terms of the eigenfunctions, $\Delta x_B(\tau)$ can be written as

$$\Delta x_B(\tau) = \sum_n c_n^B f_n^B(\tau). \tag{2.13}$$

Then the measure $\mathcal{D}\Delta x_B$ can be defined as[5]

$$\mathcal{D}\Delta x_B = \prod_n \frac{1}{\sqrt{2\pi}} \mathrm{d}c_n^B. \tag{2.14}$$

It turns out that the fluctuation operator $-\partial_\tau^2 + U''(x_B)$ contains a negative eigenvalue which we denote as λ_0^B.[6] Therefore, a naive Gaussian functional integral around the bounce gives a divergent result. This divergence is not a problem of our theory but only comes from that we did not use the method of steepest descent correctly. The direction associated with the negative eigenvalue is not the steepest descent direction but instead a steepest *ascent* direction. To correctly make use of the method of steepest descent, one needs to complexify the paths $x(\tau)$ and then perform the path integral on a deformed middle-dimensional contour. Such a procedure can be very generically carried out with the help of Picard-Lefschetz theory [48, 49] as we will describe in detail in Chap. 6.

For now, it is sufficient to take only care of the particular negative mode whose eigenvalue is λ_0^B. This means that we can focus on a one-dimensional subspace in the whole function space that passes through the bounce x_B along the direction associated with the negative mode. Denote the functions in this one-dimensional subspace as $x(\tau;\zeta)$. It was observed by Callan and Coleman that the stationary point x_F is also in this subspace [37].

[5]The factor $1/\sqrt{2\pi}$ in the measure was chosen for convenience and is not important since the path integral must be properly normalized anyway; the final physical quantities do not depend on the choice of this factor.

[6]The notation that the subscript "0" denotes the negative mode instead of the zero modes was originally used by Callan and Coleman [37] and we follow them in this thesis.

It was further pointed out in Ref. [47] that the shot is in this subspace too. The relations between all these stationary points in this one-dimensional subspace are explained in Fig. 2.3. The dependence of the Euclidean action on these paths is shown in Fig. 2.4.

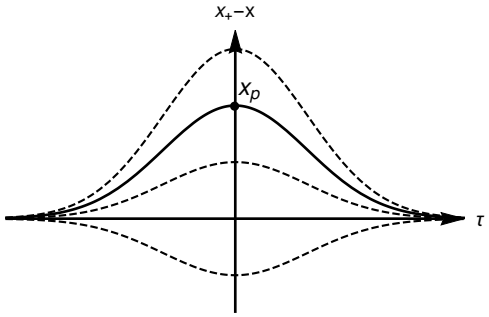

Figure 2.3: A family of symmetric paths from x_+ to itself: $x(\tau;\zeta)$, parameterized by ζ. Take the τ-axis—the trivial false vacuum solution—as the base point $x(\tau;0)$. The path with its maximum x_p, indicating the turning point, is the bounce $x(\tau;b) \equiv x_B(\tau)$, for some number b. The paths above the bounce $x(\tau;\zeta > 0)$ are the quantum paths with escape point outer than the turning point $\mathbf{p}$, containing the shot at some point $\rho = s > b$ which we did not plot explicitly.

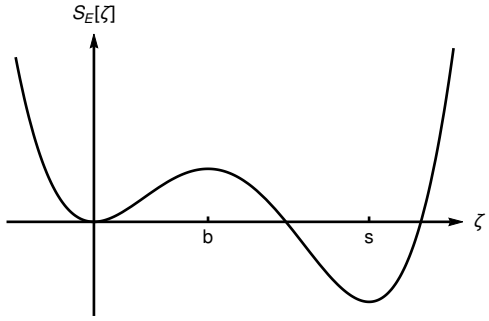

Figure 2.4: The dependence of the Euclidean action $S_E[x(\tau;\zeta)]$ on the parameter ζ. The stationary points in the plot are at $\zeta = 0, b, s$ corresponding to x_F, x_B and x_S, respectively.

Since the bounce appears as a maximum of the Euclidean action in this subspace, it was argued by Callan and Coleman that when integrating over ζ, one must analytically continue ζ to the upper complex plane from the point $\zeta = b$ along the direction given by $\mathrm{Re}\,\zeta = b$. Thus performing the Gaussian functional integral around the saddle point[7] x_B gives us an expected imaginary result as well as an unexpected factor $1/2$ since we integrate over only $\mathrm{Im}\zeta \in [0, \infty)$.

The bounce has $E = 0$. Thus, the bounce action has relation

$$B \equiv S[x_B] = \int_{-\infty}^{\infty} \mathrm{d}\tau \left(\frac{\mathrm{d}x_B}{\mathrm{d}\tau}\right)^2 = \int_0^{x_p} \mathrm{d}x \sqrt{U(x)}. \tag{2.15}$$

[7]In this thesis, "stationary point" and "saddle point" are used exchangeably.

Note that B is to be distinguished from the superscript or subscript for the bounce saddle point.

Aside from the negative mode f_0^B, the operator $-\partial_\tau^2 + U''(x_B)$ also has a zero mode. To see this, we can act on the EoM (2.8) with the operator ∂_τ. Then we have

$$\left(-\partial_\tau^2 + U''(x_B)\right) \partial_\tau x_B(\tau) = 0. \tag{2.16}$$

Thus we obtain a zero mode $f_1^B = B^{-1/2}\partial_\tau x_B$ where the normalization factor comes from Eq. (2.15). This zero mode is the Goldstone mode from the SSB of the time-translation symmetry. Actually, for a given bounce solution $x_B(\tau)$, one can obtain another one by shifting the bounce center to $-\tau_c$, i.e.,

$$x_B(\tau) \to x_B(\tau + \tau_c). \tag{2.17}$$

Here τ_c appears as a free parameter. The integral over the zero mode can be traded for an integral over the collective coordinate τ_c of the bounce [50]. To see this, consider a small change Δc_1. Then we have

$$\Delta x = f_1^B \Delta c_1. \tag{2.18}$$

On the other hand, the change Δx under a shift $\Delta\tau_c$ of the bounce center is

$$\Delta x = \frac{\partial x_B}{\partial \tau}\Delta\tau_c = \sqrt{B} f_1^B \Delta\tau_c, \tag{2.19}$$

where in the last equality we used the expression for the zero mode. Comparing Eqs. (2.18) and (2.19), one obtains

$$\mathrm{d}c_1 = \sqrt{B}\mathrm{d}\tau_c. \tag{2.20}$$

Thus the integral over c_1 has been traded for that over the collective coordinate τ_c which gives us a factor

$$\mathcal{T}\left(\frac{B}{2\pi}\right)^{1/2}. \tag{2.21}$$

Combing the analyses on the negative mode and the zero mode, one finally obtains

$$Z_E^B[0] = \frac{1}{2}\mathcal{N}\mathcal{T}\left(\frac{B}{2\pi}\right)^{1/2}\left[\det{}'\left(-\partial_\tau^2 + U''(x_B)\right)\right]^{-1/2} e^{-B}, \tag{2.22}$$

where $\det'$ implies that the zero eigenvalue of the operator $-\partial_\tau^2 + U''(x_B)$ is to be omitted when computing the determinant.

Now we almost have arrived at the Callan-Coleman's formula for the tunneling rate but still miss one last point. In Eq. (2.10), we can consider all possible multi-bounce configurations—which go back and forth from x_+ N times, for arbitrary N—as approximate saddle points. And the expansions around all these approximate saddle points should contribute to the full transition amplitude. Once we sum over all these expansions, the multi-bounce configurations exponentiate and lead to the following decay rate formula

$$\Gamma \;=\; \frac{2}{\mathcal{T}}\,\mathrm{Im}\, Z_E[0], \tag{2.23}$$

where one shall consider only the one-bounce configuration in evaluating the partition function and require a normalization condition $Z_E^F[0] = 1$.[8] For details, see Ref. [37, 51]. We therefore obtain the decay rate at one-loop order

$$\Gamma = \left(\frac{B}{2\pi}\right)^{1/2} \left|\frac{\det'\left[-\partial_\tau^2 + U''(x_B)\right]}{\det\left[-\partial_\tau^2 + U''(x_+)\right]}\right|^{-1/2} e^{-B}. \tag{2.24}$$

In Appendix. A, we show how to evaluate the functional ratio in the above formula from two different methods.

2.2 False vacuum decay at zero temperature

The discussion given in the last section can be immediately generalized to quantum field theory without obstacles.

We consider the same model but simply replace the degree of freedom x by a field Φ:

$$S_M[\Phi] = \int \mathrm{d}^4x\, \mathcal{L}_M = \int \mathrm{d}^4x \left[\frac{1}{2}\eta^{\mu\nu}(\partial_\mu\Phi)\partial_\nu\Phi - U(\Phi)\right], \tag{2.25}$$

where $\mu, \nu = 0, ..., 3$ and

$$U(\Phi) = -\frac{1}{2}\mu^2\Phi^2 + \frac{1}{3!}g\Phi^3 + \frac{1}{4!}\lambda\Phi^4 + U_0. \tag{2.26}$$

Again, the constant U_0 is introduced to ensure that the potential vanishes at the metastable minimum. The local and global minima are denoted as φ_+ and φ_-, respectively. φ_+ and φ_- are usually called the false vacuum and the true vacuum, respectively. This terminology, though we sometimes follow, is however not quite correct since the false and true vacua are not the field configuration eigenstates, but instead are (false or true) ground states. Of course, false vacuum can not be a real ground state but should be understood as a resonant state, thus can decay. Therefore, we will instead denote the false and true vacuum by $|\mathrm{FV}\rangle$ and $|\mathrm{TV}\rangle$, respectively. It is easy to obtain $\varphi_\pm \approx \pm\, v + \mathcal{O}(g/\sqrt{\lambda})$, where $v = \sqrt{6\mu^2/\lambda}$.

The decay of the false vacuum can be described as follows. A system initially in the false vacuum can penetrate the potential barrier and materialize at an escape field configuration $\varphi_{\mathrm{bubble}}$ at a time, say $t = 0$, after which it evolves classically. The Minkowski transition amplitude describing this process is given as

$$\langle\varphi_{\mathrm{bubble}}|e^{-iHT}|\mathrm{FV}\rangle \sim \langle\varphi_{\mathrm{bubble}}|e^{-iHT}|\varphi_+\rangle = \int \mathcal{D}\Phi\, e^{iS_M}, \tag{2.27}$$

where H is the Hamiltonian and T is the amount of time in this transition. Since there is no classical solutions with the boundary conditions indicated in the above transition amplitude and with low initial energy, we do not have stationary points in the Minkowski path

[8] This normalization condition amounts to choose the effective potential such that it is zero when evaluated at x_+. Except for the argument of the exponentiation of the multi-instantons by Callan and Coleman, there will be another motivation for this requirement that will be clear when we discuss the real-time formalism of quantum tunneling.

integral upon which we can do perturbative calculations. Therefore a direct calculation of the Minkowski transition amplitude (2.27) is difficult. We will show in Chap. 6 that one can complexify the paths in the path integral and deform the integral contour such that it passes complex saddle points which enable us to perform a perturbative calculation.

For now, let us follow Callan and Coleman, considering instead the following *Euclidean* transition amplitude

$$Z_E[0] = \langle \varphi_+ | e^{-H\mathcal{T}} | \varphi_+ \rangle = \int \mathcal{D}\Phi \, e^{-S_E}, \tag{2.28}$$

where the classical Euclidean action $S_E[\Phi]$ reads

$$S_E = \int \mathrm{d}^4 x \, \left[\frac{1}{2} \delta^{\mu\nu} (\partial_\mu \Phi) \partial_\nu \Phi + U(\Phi) \right]. \tag{2.29}$$

Here, $\delta^{\mu\nu}$ is the Kronecker symbol and we now use μ, ν to denote $1, ..., 4$. The formula for the decay rate is given by Eq. (2.23).

Along the lines of the last section, we have the following differences:

(1). The EoM for the bounce now is

$$-\partial^2 \varphi \, + \, U'(\varphi) = 0, \tag{2.30}$$

where $'$ denotes the derivative with respect to the field φ. The boundary conditions are $\varphi|_{\tau \to \pm\infty} = \varphi_+$ and $\dot{\varphi}|_{\tau=0} = 0$ where the dot denotes the derivative with respect to τ. The latter condition is due to the turning of the "particle" at $\tau = 0$ described in Fig. 2.2. For the action to be finite, we also require $\varphi|_{r \to \infty} = \varphi_+$ where $r = |\mathbf{x}|$.

(2). The functional operator becomes $-\Delta^{(4)} + U''(\varphi_a)$ where $\Delta^{(4)}$ is the four-dimensional Laplacian.

(3). Besides the time-translation symmetry, we have space-translation symmetries in the field theory. Therefore, we will have four zero modes associated with the SSB of these symmetries. The integral over these zero modes gives

$$V\mathcal{T} \left(\frac{B}{2\pi} \right)^2, \tag{2.31}$$

where we still use B to denote the classical bounce action in the field theory.

With the above differences properly handled, we obtain the false vacuum decay rate per unit volume at one-loop order

$$\Gamma/V = \left(\frac{B}{2\pi} \right)^2 \left| \frac{\det' \left[-\Delta^{(4)} + U''(\varphi_B) \right]}{\det \left[-\Delta^{(4)} + U''(\varphi_+) \right]} \right|^{-1/2} e^{-B}. \tag{2.32}$$

2.3 The bubble growth after the nucleation

We have derived the rate for false vacuum decay but have gained little on the picture of the nucleated field configuration φ_{bubble} and its motion after the nucleation. For that, we need to take a closer look at the bounce solution.

Coleman proved that the $O(4)$-symmetric bounce solution gives the least Euclidean action and hence dominants the tunneling process [41]. Considering such $O(4)$-symmetry, one can work in four-dimensional hyperspherical coordinates, in which the equation for the bounce takes the form

$$-\frac{\mathrm{d}^2\varphi}{\mathrm{d}\rho^2} - \frac{3}{\rho}\frac{\mathrm{d}\varphi}{\mathrm{d}\rho} + U'(\varphi) = 0\,, \tag{2.33}$$

with $\rho^2 = \tau^2 + r^2$. The boundary conditions become $\varphi|_{\rho\to\infty} = \varphi_+$. The solution must be regular at the origin, and we therefore require that $\mathrm{d}\varphi/\mathrm{d}\rho|_{\rho=0} = 0$. The solution is a *four-dimensional* soliton that interpolates between the local minimum φ_+ and the turning point closer to φ_-. With a careful comparison with the Wentzel-Kramers-Brillouin (WKB) analysis, Coleman showed that the bounce is actually the most probable escape path for the tunneling process [41]. From the Minkowski point of view, the classical field makes a quantum jump (at $t = 0$) to the state of

$$\varphi_{\mathrm{bubble}}(t = 0,\ \mathbf{x}) = \varphi_B(\tau = 0,\ \mathbf{x}), \tag{2.34}$$

$$\frac{\partial}{\partial t}\varphi_{\mathrm{bubble}}(t = 0,\ \mathbf{x}) = 0. \tag{2.35}$$

Afterwards, it evolves according to the classical field EoM

$$-\partial_t^2\varphi_{\mathrm{bubble}}(t, \mathbf{x}) + \nabla^2\varphi_{\mathrm{bubble}}(t, \mathbf{x}) = U'(\varphi_{\mathrm{bubble}}(t, \mathbf{x})). \tag{2.36}$$

According to Eq. (2.34), $\varphi_{\mathrm{bubble}}(t = 0, \mathbf{x})$ describes a *three-dimensional* spherically symmetric soliton that interpolates between the local minimum φ_+ and the turning point closer to φ_-.

In the thin-wall approximation [41] (see also Ref. [52]), applicable when the minima are quasi-degenerate, i.e., when the cubic coupling g is very small, we may safely neglect the damping term in Eq. (2.33), as well as the contribution from the cubic self-interaction $g\varphi^3$. In this approximation, Eq. (2.33) has the well-known kink solution [53]

$$\varphi_B(\rho) \equiv v\,\tanh[\gamma\,(\rho - R)] \equiv v\,u, \tag{2.37}$$

where $\gamma = \mu/\sqrt{2}$. Apparently, in this case, $\varphi_{\mathrm{bubble}}(t = 0, \mathbf{x})$ is a bubble with its wall located at R and separating the false and true vacua. The slice $\varphi_{\mathrm{bubble}}(t = 0, \mathbf{x})$ is called the critical bubble. The radius of the critical bubble R is obtained by extremizing the bounce action

$$B = \int d^4x\,\left[\frac{1}{2}\left(\frac{\mathrm{d}\varphi_B}{\mathrm{d}\rho}\right)^2 + U(\varphi_B)\right]. \tag{2.38}$$

This gives

$$R = \frac{12\gamma}{gv} \tag{2.39}$$

and

$$B = 8\pi^2 R^3\gamma^3/\lambda. \tag{2.40}$$

The solution to Eq. (2.36) can be directly obtained by analytically continuing the bounce solution:

$$\varphi_{\text{bubble}}(t, \mathbf{x}) = \varphi_B(\rho = \sqrt{-t^2 + r^2}). \tag{2.41}$$

The motion of the thin wall then follows the hyperboloid

$$-t^2 + r^2 = R^2. \tag{2.42}$$

We describe the thin-wall bounce and the motion of the bubble in Fig. 2.5.

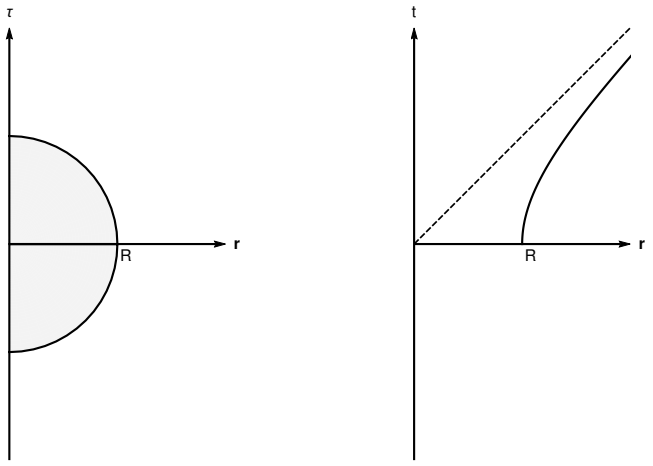

(a) (b)

Figure 2.5: On the left panel is the bounce in the thin-wall approximation. The solid circle represents the "bubble wall" in the Euclidean spacetime, separating the true vacuum (inside) from the false vacuum (outside). On the right panel is the motion of the bubble wall (solid half-hyperboloid) in the Minkowski spacetime after the nucleation ($t \geq 0$); the dashed line is the light cone.

2.4 False vacuum decay at finite temperature

Once we obtain the description of vacuum transition at zero temperature, it is natural to generalize it to the case of finite temperature. Vacuum transitions at finite temperature are perhaps more relevant for cosmological phase transitions, that may occur at finite temperature.

At finite temperature, one instead considers the following partition function (assuming we are considering a canonical ensemble)

$$Z[\beta] = \mathrm{Tr}\left[e^{-\beta H}\right], \tag{2.43}$$

where $1/\beta$ is the temperature. The partition function can be rewritten as

$$\begin{aligned} Z[\beta] = \mathrm{Tr}\left[e^{-\beta H}\right] &= \int \mathcal{D}\phi \, \langle\phi|e^{-\beta H}|\phi\rangle \\ &= \int \mathcal{D}\phi \int_{\Phi(0,\mathbf{x})=\phi}^{\Phi(\beta,\mathbf{x})=\phi} \mathcal{D}\Phi \; e^{-\int_0^\beta \mathrm{d}\tau \int \mathrm{d}^3\mathbf{x} \, \mathcal{L}_E}, \end{aligned} \tag{2.44}$$

where $\mathcal{L}_E$ is the Lagrangian in Euclidean space ($S_E \equiv \int \mathrm{d}^4x\ \mathcal{L}_E$). The integral over ϕ can be simply eliminated by imposing a periodic condition for the quantum field Φ. That is

$$Z[\beta] = \int_{\Phi(0,\mathbf{x})=\Phi(\beta,\mathbf{x})} \mathcal{D}\Phi\ e^{-\int_0^\beta \mathrm{d}\tau \int \mathrm{d}^3\mathbf{x}\ \mathcal{L}_E}. \tag{2.45}$$

Thus the thermal field theory is equivalent to a Euclidean quantum field theory periodic (or anti-periodic if we consider fermionic fields) in the Euclidean time. For more on thermal field theory, see Ref. [54].

To understand false vacuum decay at finite temperature, one has two different strategies: top-down or bottom-up.

2.4.1 Top-down

By "top-down", we mean that we will study vacuum transition at finite temperature mostly by observations and directly construct the decay rate therefrom.

It was observed by Linde that one can understand the vacuum transition at finite temperature by studying the bounce solution periodic in the Euclidean time. For clarification, we will only look at the $\tau - x_1$ plane. The bounce solution at zero temperature is depicted in Fig. 2.6(a). As the temperature increases, the periodicity of the Euclidean time becomes narrower. At temperature $1/\beta \lesssim R^{-1}$, the repeated bounces become to be closer with each other and finally overlap when $1/\beta \gtrsim R^{-1}$, see Fig. 2.6(b). When the temperature $1/\beta$ is much larger than R^{-1}, then the bounce solution becomes essentially a cylinder. At this high-temperature limit, the bounce is independent of the Euclidean time and becomes an $O(3)$-symmetric field configuration.

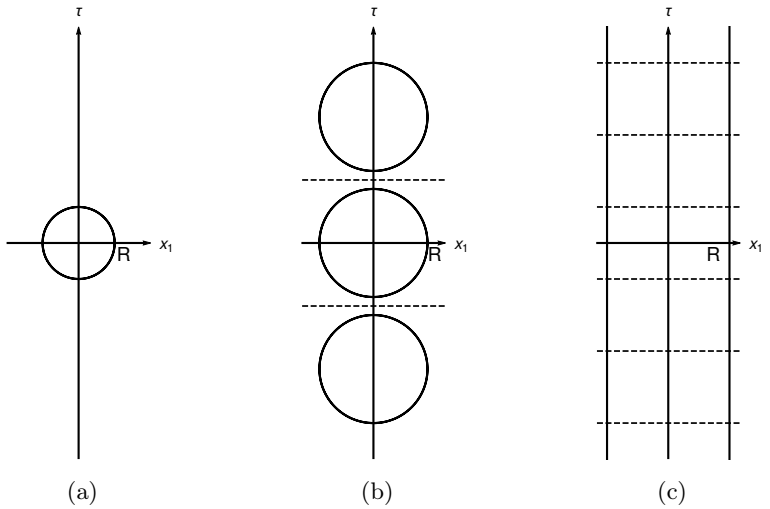

Figure 2.6: Bounce solution at different values of temperature. (a) $1/\beta = 0$; (b) $1/\beta \lesssim R^{-1}$; (c) $1/\beta \gg R^{-1}$. For simplicity, we have shown bubbles in the thin-wall regime. The vertical interval between two dashed lines represents a full periodicity in the Euclidean time.

The case of Fig. 2.6(b) might be termed as thermally assisted quantum tunneling [55]

since it still corresponds to a tunneling process from the false vacuum to the bubble state but with assistance of the thermal effects.

Fig. 2.6(c) describes a three-dimensional field configuration reduced from a four-dimensional τ-independent bounce solution. We will use φ_b to denote the bounce solutions satisfying the static condition, in comparison with the $O(4)$ bounces denoted by φ_B. When φ_b appears in a three-dimensional integral, it should be understood as a slice configuration at an arbitrary time τ. One may think that φ_b is the stationary point of the following energy functional

$$E[\varphi] \equiv S_3[\varphi] = \int \mathrm{d}^3\mathbf{x} \left[\frac{1}{2}(\nabla\varphi)^2 + U(\varphi)\right]. \tag{2.46}$$

We will discuss below how this energy functional should be modified. For now, let us continue with Eq. (2.46). One can see that the "particle" is thermally excited all the way to the top of the barrier (the stationary point of Eq. (2.46)) and no transition under the barrier. We will call the transition described by Fig. 2.6(c) as *thermal* transition. Thermal transitions are of most interest for us since cosmological phase transitions often belong to them. In Chap. 3, we will show that there is a correspondence between quantum and thermal transitions around horizons.

The integral over τ in $S_E[\varphi_b]$ is simply reduced to multiplication by β, i.e., $S_E[\varphi_b] = \beta S_3[\varphi_b]$. Since φ_b has no dependence on τ, it does not break the τ-translation symmetry and therefore we only have three zero modes. By comparing with Eq. (2.32), one may write the decay rate at high temperature as

$$\Gamma_{\mathrm{therm}}/V = \frac{1}{\beta}\left(\frac{S_3[\varphi_b]}{2\pi}\right)^2 \left|\frac{\det'\left[-\nabla^2 + U''(\varphi_b)\right]}{\det\left[-\nabla^2 + U''(\varphi_+)\right]}\right| e^{-\beta S_3[\varphi_b]}. \tag{2.47}$$

Equation (2.47) is, however, oversimplified since it has not taken the thermal effects on the potential into account.

In order to introduce the finite temperature effective potential, we consider the partition function with source

$$Z[\beta; J] \equiv e^{-W[J]} = \int_{\Phi(0,\mathbf{x})=\Phi(\beta,\mathbf{x})} \mathcal{D}\Phi\; e^{-\int_0^\beta \mathrm{d}\tau \int \mathrm{d}^3\mathbf{x}\,(\mathcal{L}_E - J(x)\Phi(x))}. \tag{2.48}$$

One can obtain the one-point function with source J via

$$\varphi = \langle\Omega|\Phi|\Omega\rangle_J = \frac{\delta \ln Z[J]}{\delta J}. \tag{2.49}$$

We define the effective action via a Legendre transform of $W[J]$

$$\Gamma[\varphi] = W[J] + \int_0^\beta \mathrm{d}\tau \int \mathrm{d}^3\mathbf{x}\; J(x)\varphi(x). \tag{2.50}$$

It can be easily shown that

$$\frac{\delta\Gamma[\varphi]}{\delta\varphi} = J, \tag{2.51}$$

which is called the quantum EoM or Schwinger-Dyson equation, here for the case of one-point function. The stationary points of $Z[\beta]$ should really satisfy the Schwinger-Dyson equation without source

$$\frac{\delta\Gamma[\varphi]}{\delta\varphi} = 0. \tag{2.52}$$

The effective action provides a quantum version of the principle of least action. Compared with the classical action, it automatically includes all the quantum and thermal corrections. For constant background field configurations, $\varphi =$ constant, we can further define the effective potential

$$U_{\text{eff}}(\varphi, \beta) = \frac{1}{V\beta}\Gamma[\varphi], \tag{2.53}$$

where we have written out the temperature dependence in the effective potential explicitly. Similarly, the effective potential contains quantum and thermal corrections compared with the classical potential.

Though the effective potential is obtained for constant fields, one may still apply it to Eq. (2.46) and define the energy functional at finite temperature as

$$E[\varphi, \beta] \equiv S_3[\varphi, \beta] = \int \mathrm{d}^3\mathbf{x} \left[\frac{1}{2}(\nabla\varphi)^2 + U_{\text{eff}}(\varphi, \beta)\right]. \tag{2.54}$$

With this definition, Linde proposed the decay rate at one-loop [44, 45]

$$\Gamma_{\text{therm}}/V = \frac{1}{\beta}\left(\frac{S_3[\varphi_b, \beta]}{2\pi}\right)^2 \left|\frac{\det'\left[-\nabla^2 + U''_{\text{eff}}(\varphi_b, \beta)\right]}{\det\left[-\nabla^2 + U''_{\text{eff}}(\varphi_+, \beta)\right]}\right| e^{-\beta S_3[\varphi_b, \beta]}, \tag{2.55}$$

where φ_b is a solution to

$$-\frac{\mathrm{d}^2\varphi}{\mathrm{d}r^2} - \frac{2}{r}\frac{\mathrm{d}\varphi}{\mathrm{d}r} + U'_{\text{eff}}(\varphi, \beta) = 0, \tag{2.56}$$

subjected to the boundary conditions $\varphi|_{r\to\infty} = \varphi_+$ and $\mathrm{d}\varphi/\mathrm{d}r|_{r=0} = 0$. It should be emphasized that this formula is obtained by analogy with the decay rate at zero temperature and thus still need to be justified. We will see below that Eq. (2.55) suffers from modifications.

2.4.2 Bottom-up

By "bottom-up", we mean that we will first provide a proper definition of the decay rate at finite temperature and then derive the one-loop result from first principles.

Comparing with Eq. (2.7), it is natural to define the decay rate at finite temperature as

$$\Gamma_{\text{therm}} = \frac{2}{\beta}\,\text{Im}\,\ln Z[\beta] = -2\,\text{Im}F \tag{2.57}$$

where $F = -(\ln Z[\beta])\beta$ is the free energy. Affleck showed that formula (2.57) may be modified slightly to [43]

$$\Gamma_{\text{therm}} = -\frac{\beta\sqrt{|\lambda_0^b|}}{\pi}\,\text{Im}F \tag{2.58}$$

because of the classical thermodynamic fluctuations. Here λ_0^b is the negative mode when we expand the path integral around the stationary point φ_b. Multiplying $\sqrt{|\lambda_0^b|}$ will then cancel the same factor from ImF in the decay rate. However, we will insist on using Eq. (2.57) as the definition of the vacuum decay rate at finite temperature for several reasons. First, the main reason that leads Affleck to propose the modified formula is the classical decay rate at high temperature. This classical decay rate is derived from the classical partition function while we are studying the transition of a quantum field, although at finite temperature. Second, the general derivation in Ref. [43] seems to rely on the leading WKB formulas for the transmission. Therefore the resulted formula may differ from Eq. (2.57) by a factor related to the negative mode which may only appear beyond the semiclassical WKB approximations. Third, as we will show in the next chapter, formula (2.57) will correctly lead to the correspondence [56] between thermal and quantum transitions of vacuum which is consistent with Unruh effect [57] and black hole complementary principle [58].

Once we have the definition (2.57), we can simply evaluate the path function $Z[\beta]$. By a similar argument, the logarithm in Eq. (2.57) can be removed because the multi-bounce configurations exponentiate. Thus we are led to

$$\Gamma_{\rm therm} = \frac{2}{\beta}\,{\rm Im}\; Z[\beta], \tag{2.59}$$

where one shall only consider the one-bounce stationary point. We may expand the partition function around the trivial false vacuum and the $O(3)$ bounce φ_b,[9]

$$Z[\beta] = Z^F[\beta] + Z^b[\beta]. \tag{2.60}$$

Since φ_a (with $a = F, b$) are the stationary points without source, one can set $J = 0$ in Eq. (2.50). Thus one has

$$Z^a[\beta] = e^{-\Gamma[\varphi_a]}. \tag{2.61}$$

If one normalizes the partition function properly to set $Z^F[\beta] = 1$, then we finally arrive at

$$\Gamma_{\rm therm} = \frac{2}{\beta}\,{\rm Im}\; e^{-\Gamma[\varphi_b]}. \tag{2.62}$$

Now we can discuss why Linde's formula (2.55) suffers from modifications. First the bounce φ_b should be a solution to (2.52) subjecting to the static condition $\partial\varphi_b/\partial\tau = 0$ and the boundary conditions $\varphi_b|_{r\to\infty} = \varphi_+$, ${\rm d}\varphi/{\rm d}r|_{r=0} = 0$.[10] Apparently, the EoM (2.52) is different from Eq. (2.56). In particular, the latter does not capture the effects from the inhomogeneity of the background field. Although such effects are not important in the thin-wall limit and at zero temperature [59, 60], it is not clear whether they are important or not at finite temperature. This will be investigated in the future. Second, there is a double-counting problem in Linde's formula. While the finite temperature effective

[9] Again, there could be a shot stationary point but it is irrelevant for the vacuum transition.

[10] Here we note that the asymptotic value may be shifted from φ_+ to some new value φ_F which is the thermal and quantum corrected trivial false vacuum stationary point.

potential comes from integrating out the thermal and quantum fluctuations at the loop order of interest (here we take the one-loop order), there is again the one-loop functional determinant for the fluctuation operators in Linde's formula. In order to avoid such double-counting, the finite temperature effective potential $U_{\rm eff}$ should be replaced by one which is obtained by integrating out only the Matsubara modes [11] but leave the spatial fluctuations intact. We will derive such kind of effective potential in a future work.

Here we emphasize that formulae (2.59) and (2.62) should be taken as more fundamental than Linde's formula. If the finite temperature effective potential does not significantly differ from the classical potential, one can still use the classical bounce solution as the stationary point and do the expansion. If the finite temperature effective potential does significantly differ from the classical potential, then the quantum and thermal corrected bounce can be non-perturbatively far away from the classical bounce. In this case, one must use the quantum and thermal corrected bounce in the expansion. In particular, it is well known that there may be symmetry restoration at sufficiently high temperature and in this case, there is no vacuum instability. This symmetry restoration can be viewed as an inverse Coleman-Weinberg (CW) mechanism [12] where SSB is induced by radiative effects. That is, for the classical potential with only one stable vacuum there could be another deeper vacuum generated by the quantum fluctuations, leading to vacuum instability radiatively. False vacuum decay triggered by SSB via the CW mechanism has been studied in Ref. [61].

[11] Matsubara modes are circular harmonic modes along the direction of the periodic Euclidean time

Chapter 3

Correspondence between Quantum and Thermal Vacuum Transitions

Quantum and thermal transitions of vacuum share very similar characteristics. Both kinds of transitions are described by bounce solutions whose actions provide the semi-classical result of the decay rate. The higher order corrections are obtained by fluctuations about the bounce solutions. The only difference is that the bounce solution for false vacuum decay at zero temperature is an $O(4)$-symmetric field configuration while the bounce for thermal transition is a static $O(3)$-symmetric field configuration. The static condition of the bounce solution for thermal transitions can be viewed as an additional symmetry. Actually, the bounce in thermal transition can be made identical to that in the quantum transition when we work in a $1+1$-dimensional spacetime. There the $O(2)$-symmetric bounce in the quantum transition can be viewed as static in the angular direction. This suggests a correspondence for the thermal and quantum transitions of vacuum in $1+1$-dimensional flat spacetime. This correspondence has realistic applications when we study bubble nucleation around black holes.

Bubble nucleation around black holes has attracted comparable interests in recent years because it represents one typical situation where the gravity effects may play an important role in electroweak metastability [13, 14, 15, 16, 62, 63, 64, 65, 66]. Without gravity, the lifetime of the electroweak vacuum in the SM is much longer than the age of the Universe. However, it was shown that the lifetime of the electroweak vacuum can be dramatically reduced for bubble nucleation around black holes and for some parameter space of the coefficients of higher dimensional operators in the Higgs potential that are likely induced by quantum gravity effects [14, 15, 16]. Since such microscopic black holes can be generated via the evaporation of primordial black holes and since our Universe in the electroweak vacuum has enjoyed a very long safe time, the recent results imply that either the Higgs parameters are out of the relevant range or there must be very severe constraints on primordial black holes. Because such primordial black holes can be produced at the post-inflationary matter dominated stage, the absence of them puts severe constraints on inflation [63].

The corresponding false vacuum decay is described by a static bounce solution in the Euclidean Schwarzschild spacetime [13, 15] (see Sec. 3.3). Since the Euclidean Schwarzschild time has a natural periodicity, it is suggested in Refs. [63, 65] that the static bounce should describe a thermal transition of vacuum. It is then suggested that in order to interprete the enchancement of the decay rate induced by black holes, one need to put the black hole in a universe filled with a thermal plasma [63].

In this chapter, we shall show that this doubt is not necessary since these two pictures, quantum tunneling, and thermal transition, are dual with each other for bubble nucleations around horizons. Although we will work in a perturbative regime where the spacetime

background is fixed, the correspondence is sufficient to reveal the following general aspects: the periodicity of the Euclidean Schwarzschild time appears because of the thermal nature of the state observed by the external static observers; and there is no necessity to fill the universe with extra plasma aside from the existing Hawking radiation in order to interpret the static bounce solution. In particular, the probability calculated from the static bounce solution in Refs. [13, 14, 15, 16] gives exactly the thermal transition probability that measured by the external static observers. On the contrary, if one interprets the bounce solution as describing a quantum tunneling, one must extend the Schwarzschild spacetime to the Kruskal-Szekeres spacetime. This point leads to a new theoretical paradox related to black holes as we will discuss in Sec. 3.4. It is clear that the near-horizon spacetime of a black hole is approximately a Rindler spacetime and can be most conveniently modeled in a $1 + 1$-dimensional setting. We, therefore, firstly demonstrate this correspondence for the false vacuum decay in the $1 + 1$-dimensional flat spacetime and then move to the Schwarzschild spacetime. The thermal transition is described by the imaginary-time formalism of thermal field theory which is only valid for equilibrium states. Hence, as long as the nonequilibrium effects do not cause a big deviation at the very late evaporation stage when the enhancement on the vacuum transition probability becomes significant, the calculations in Refs. [13, 14, 15, 16] should be taken as reliable.

3.1 Unruh effect and Hawking radiation

It was first discovered by Parker [67, 68, 69] and Fulling [70] that particles can be generated by expanding universes. In the meantime, Zel'dovich [71] found that the rotating black holes have spontaneous radiation of energy and angular momentum. Based on these results, in 1974 Hawking found that even static black holes can emit particles [72]. The spectrum of the emitted particles appears to be thermal. Together with the four laws of the black hole mechanics [73], the discovery of Hawking radiation finally brought the identification of a black hole with a thermodynamical system.

It was later pointed out by Unruh [57] that the Hawking radiation can be understood by looking into the near-horizon spacetime. The spacetime outside of but near the event horizon can be modeled as a Rindler spacetime as shown in Fig. 3.1. It was shown by Unruh that a vacuum state viewed from an inertial observer in a flat Minkowski spacetime appears to be a thermal state to a uniformly accelerated observer (Rindler observer) [57, 74]. Thus the static observers in the Rindler spacetime can feel a thermal bath. This is called Unruh effect. This effect is due to the non-uniqueness of the concept of particles in quantum field theory. Very like the static observers outside of a black hole, the Rindler observers are associated with a local causal horizon called Rindler horizon. Now the Hawking radiation can be understood as required by the Unruh effect and the equivalence principle. By the equivalence principle, the freely falling observers in curved spacetime are locally in flat spacetime, corresponding to the inertial observers and should be in a vacuum state. While the static observers outside of the black hole are locally in a Rindler spacetime, corresponding to uniformly accelerated observers and should see a thermal bath according to the Unruh effect.

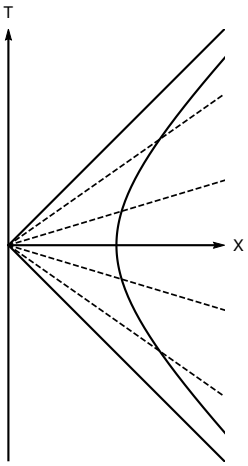

Figure 3.1: The triangle region as a Rindler spacetime. A static observer in the Rindler spacetime corresponds to a uniformly accelerating observer in the Minkowski spacetime, as represented by the solid hyperboloid. The dashed lines are spatial slices of different Rindler times. All the static observers have a past horizon and a future horizon.

The discovery of Hawking radiation and Unruh effect have clearly demonstrated that there are very deep relations between quantum theory and thermodynamics. It is now well known that there can be very different but complementary descriptions on the same physical processes near a horizon [57, 74, 58]. For example, a possible virtual baryon-number-violating process of a falling proton viewed from the comoving falling observers can be a real thermally assisted process viewed from the external static observers. When applied to black hole event horizons, the complementary descriptions have in particular been incorporated into the axioms of black hole complementarity (BHC) [58].

While various local processes have been examined to satisfy BHC via thought experiments [75], non-local processes such as bubble nucleation around the whole event horizon have been overlooked. Imagine there is bubble nucleation around a black hole induced by a quantum vacuum transition observed by the freely falling observers. How would this process be described by the static observers? According to BHC, the external static observers should see a thermal transition because they are in a thermal state. In this chapter, we shall show that this is true up to an unexpected point; in order for the external static observers and the freely falling observers to have the same transition probability, the tunneling interpretation must be given in the extended Kruskal-Szekeres spacetime. Moreover, we will show that there is always a correspondence between thermal and quantum vacuum transitions for bubble nucleations around any horizon, including the Rindler horizon and the de Sitter horizon. From this point of view, the thermal derivation in Ref. [76] of the Coleman-De Luccia tunneling rate [77] is a natural consequence of this correspondence.

3.2 Vacuum transition in $1+1$-dimensional spacetime

In this section, we build the correspondence between thermal and quantum vacuum transitions in $1+1$-dimensional flat spacetime. We begin by presenting the main elements of the

Callan-Coleman description of quantum transitions in $1+1$-dimensional flat spacetime, for the purpose of setting up the notations. We emphasize that this picture of quantum tunneling should be taken by the inertial observers. The same result of the decay rate can be obtained from a thermal description when a Rindler frame is employed. If the spatial dimension is higher than one, the spacetime cannot be foliated in a way such that we have Rindler wedges while still respect the symmetry of the bubble. Only in the $1+1$-dimensional case, this trouble disappears. But the $1+1$-dimensional Rindler spacetime captures the crucial characters of the $t-r$-space outside of a black hole, giving the first support on the correspondence for bubble nucleation around event horizons.

3.2.1 Quantum transitions in $1+1$-dimensional spacetime for inertial observers

We consider a scalar field theory in $1+1$-dimensional flat spacetime

$$S_M[\Phi] = \int \mathrm{d}^2x\sqrt{-\eta}\left[\frac{1}{2}\eta^{\mu\nu}(\partial_\mu\Phi)\partial_\nu\Phi - U(\Phi)\right], \tag{3.1}$$

where η is the determinant of $\eta_{\mu\nu}$. In order to distinguish the inertial coordinates from the Rindler coordinates, we use $\{T, X\}$ to denote the coordinates $\{x_0, x_1\}$ in the inertial frame where the Minkowski metric is $\eta_{\mu\nu} = \mathrm{diag}(1,-1)$. We leave t to denote the time coordinate in the Rindler frame. $U(\Phi)$ is an arbitrary potential that possesses two non-degenerate minima whose details will not enter into the analysis. As we have discussed in Chap. 2, in order to describe such a tunneling process, one can consider the following Euclidean partition function

$$Z_E[0] = \lim_{\mathbb{T}\to\infty}\langle\varphi_+|e^{-H\mathbb{T}}|\varphi_+\rangle = \int \mathcal{D}\Phi\; e^{-S_E[\Phi]}, \tag{3.2}$$

where $\mathbb{T}$ is the amount of the Euclidean time during the transition and

$$S_E[\Phi] = \int \mathrm{d}\mathcal{T}\mathrm{d}X\left[\frac{1}{2}(\partial_\mathcal{T}\Phi)^2 + \frac{1}{2}(\partial_X\Phi)^2 + U(\Phi)\right]. \tag{3.3}$$

Here we have used $\mathcal{T}$ to denote the Euclidean time in the inertial frame and leave τ to denote the Euclidean Rindler time. The decay rate is given as

$$\Gamma_{\mathrm{tunn}} = \frac{2}{\mathbb{T}}\,\mathrm{Im}\; Z_E[0]. \tag{3.4}$$

where it is understood that only the one-bounce configuration (and the trivial false vacuum) need to be considered in evaluating the partition function.

Evaluating Eq. (3.4) within the first quantum corrections gives the tunneling rate per unit volume

$$\Gamma_{\mathrm{tunn}}/V = \left(\frac{B}{2\pi}\right)\left|\frac{\det'[-\Delta^{(2)} + V''(\varphi_B)]}{\det[-\Delta^{(2)} + V''(\varphi_+)]}\right|^{-1/2} e^{-B}, \tag{3.5}$$

where $\Delta^{(2)}$ is the two-dimensional Laplacian. Note the difference in the power of $B/2\pi$ because we now only have two zero modes. The bounce solution φ_B has an $O(2)$ symmetry

and satisfies the EoM

$$-\frac{\mathrm{d}^2\varphi}{\mathrm{d}r^2}-\frac{1}{r}\frac{\mathrm{d}\varphi}{\mathrm{d}r}+U'(\varphi)=0, \tag{3.6}$$

where $r=\sqrt{X^2+\mathcal{T}^2}$.

In the Callan-Coleman formalism, the bounce describes the dominant path for the transition from φ_+ at far past to φ_+ at far future in the Euclidean space. The intermediate configurations at $\mathcal{T}_i$ are given by $\varphi_B(\mathcal{T}_i, X)$ which are apparently time-dependent, as shown by the dashed lines in Fig. 3.2. The Euclidean time $\mathcal{T}$ is open and the bubble nucleation corresponds to a quantum tunneling process from φ_+ to $\varphi_B(\mathcal{T}=0,X)\equiv\varphi_{\mathrm{bubble}}(t=0,X)$. It is, however, possible to do the foliation in another way as shown in Fig 3.3. In this foliation, the spatial slices are the rays while the Euclidean time is given by the angular coordinate which is compact. Apparently, now the intermediate configurations at constant angular values are time-independent. This reminds us of the thermal transition at finite temperature. The observers in the Euclidean spacetime are represented by the circles which can be parameterized as $X=r\cos(\tau), \mathcal{T}=r\sin(\tau)$. If one performs an inverse Wick rotation $\tau\to it$, the circles are mapped to the hyperboloids, corresponding to uniformly accelerated observers in the Minkowski spacetime.

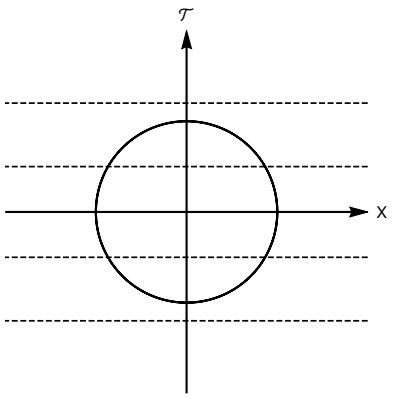

Figure 3.2: The bounce in the thin-wall regime and a foliation of the Euclidean spacetime; the dashed lines represent the space and the field configurations of constant $\mathcal{T}$.

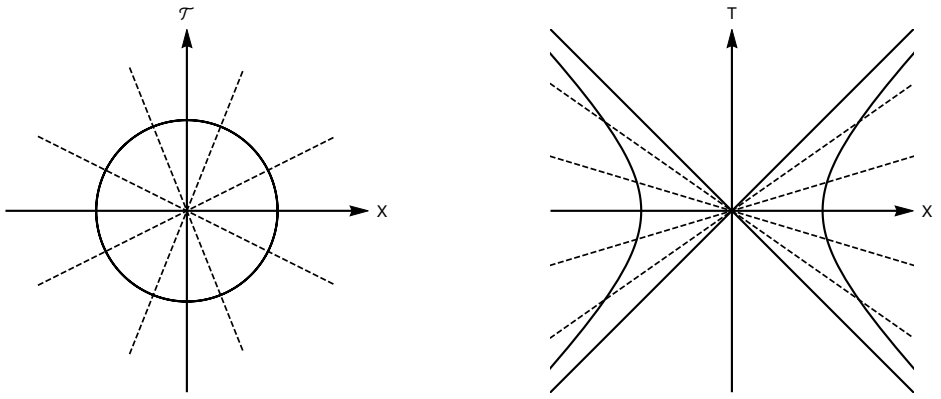

(a) (b)

Figure 3.3: On the left panel is a different way to do the foliation of the Euclidean spacetime; the solid circle can represent a typical worldline of an observer in this foliation; the dashed lines (the rays) represent the intermediate spatial slices. On the right panel is the corresponding foliation in the Minkowski spacetime.

Since the Euclidean time τ has a natural periodicity of 2π, the Euclidean field theory using τ as the Euclidean time can be identified as describing a thermal state. This thermal state is the well-known Unruh effect [57] felt by a uniformly accelerated observer. It should be emphasized that this thermal field theory describes only the right Rinder wedge ($X > 0, -X < T < X$; R-wedge in short) (see Fig. 3.3(b)) or the left Rindler wedge ($X < 0, X < T < -X$; L-wedge in short) but not both. Such kind of identification is due to thermofield dynamics [78]. Thermofield dynamics describes a thermal field system by augmenting the physical Fock space by a fictitious, dual Fock space. In so doing, one can define a pure state in the doubled Fock space with the expectation value of any physical operator agreeing its statistical average in the thermal ensemble. Put in another way, the thermal state in the R-wedge (L-wedge) can be obtained by tracing out the L-wedge (R-wedge) in the pure state of the combined system. The R-wedge (or the L-wedge) is quite similar to the static region outside of a Schwarzschild black hole. We call such kind of a static region a static patch.

In conclusion, we identify two different, complementary interpretations of the Euclidean field theory in the $1+1$-dimensional flat spacetime, depending on the frame we employed.

(I) In the inertial frame: it is a *quantum* field theory analytically continued from the Minkowski quantum field theory via the Wick rotation $T \to -i\mathcal{T}$.

(II) In the Rindler frame: it is a *thermal* field theory[12] for the R-wedge (or another) analytically continued from the Minkowski quantum field theory (formulated also in the Rindler frame) via the Wick rotation $t \to -i\tau$.

In the next subsection, we will derive the decay rate using interpretation (II).

[12]Of course, by "thermal field theory" we actually mean thermal quantum field theory. With a slight ambiguity of the terminology, it is nevertheless clear for the differences in the two field theories interpreted in the inertial frame and the Rindler frame.

3.2.2 Thermal transition in $1+1$-dimensional spacetime for Rindler observers

From the relation $T = r\sinh t,\ X = r\cosh t$ (hence we choose the R-wedge as our physical thermal system), one has the metric in the coordinates $\{t, r\}$ as

$$\mathrm{d}s^2 = r^2\mathrm{d}t^2 - \mathrm{d}r^2. \tag{3.7}$$

The action (3.1) is then expressed as

$$S_M[\Phi] = \int \mathrm{d}t \int_0^\infty \mathrm{d}r\ r\left[\frac{1}{2r^2}(\partial_t\Phi)^2 - \frac{1}{2}(\partial_r\Phi)^2 - U(\Phi)\right]. \tag{3.8}$$

The EoM becomes

$$\frac{1}{r^2}\frac{\partial^2\varphi}{\partial t^2} - \frac{\partial^2\varphi}{\partial r^2} - \frac{1}{r}\frac{\partial\varphi}{\partial r} + U'(\varphi) = 0. \tag{3.9}$$

By a canonical transformation, we can immediately obtain the Hamiltonian in the Rindler coordinates

$$H = \int_0^\infty \mathrm{d}r\ r\left[\frac{1}{2r^2}(\partial_t\Phi)^2 + \frac{1}{2}(\partial_r\Phi)^2 + U(\Phi)\right]. \tag{3.10}$$

Taking the Wick rotation $t \to -i\tau$ and $iS_M \to -S_E$, we get

$$S_E[\Phi] = \int_0^{\beta=2\pi} \mathrm{d}\tau \int_0^\infty \mathrm{d}r\ r\left[\frac{1}{2r^2}(\partial_\tau\Phi)^2 + \frac{1}{2}(\partial_r\Phi)^2 + U(\Phi)\right], \tag{3.11}$$

where we have identified the periodicity of τ. For convenience, we use the global Rindler temperature $T_R = 1/2\pi$ rather than the proper temperature $T_P = 1/(2\pi r)$ measured by the local observers.

The partition function is given as (see Eq. (2.45))

$$\begin{aligned} Z[\beta] &= \mathrm{Tr}[e^{-\beta H}] \\ &= \int_{\Phi(0,r)=\Phi(\beta,r)} \mathcal{D}\Phi\ e^{-\int_0^\beta \mathrm{d}\tau \int_0^\infty \mathrm{d}r\ r\left[\frac{1}{2r^2}(\partial_\tau\Phi)^2 + \frac{1}{2}(\partial_r\Phi)^2 + U(\Phi)\right]}. \end{aligned} \tag{3.12}$$

As explained in the last subsection, we identify Eq. (3.12) as the thermal field theory for Rindler observers in the R-wedge. Once we have a thermal system, we can study thermal transitions whose decay rate formula is given by Eq. (2.59).

As we have discussed in the last chapter, the thermal transition can be described by a time-independent configuration φ_b in the Euclidean spacetime which is simply the solution to Eq. (3.9) subject to the static condition $\partial\varphi/\partial t = 0$ and the boundary conditions $\varphi|_{r\to\infty} = \varphi_+$, $\mathrm{d}\varphi/\mathrm{d}r|_{r=0} = 0$. Note that the EoM for this time-independent configuration φ_b is exactly the one for the bounce (see Eq. (3.6)). This is not surprising since the EoMs are related by a coordinate transformation and the static condition is equivalent to the $O(2)$ symmetry of the bounce. Thus we have $\varphi_b(r) = \varphi_B(r)$ in the polar coordinates for φ_B. The semiclassical result will give us the same exponential suppression $\exp(-S_E[\varphi_b]) =$

$\exp(-S_E[\varphi_B]) \equiv \exp(-B)$. To take the quadratic fluctuations into account, we rewrite the action (3.11) as

$$S_E[\Phi] = \int_0^{\beta=2\pi} \mathrm{d}\tau \int_0^{\infty} \mathrm{d}r \, \left[-\Phi \left(\frac{1}{2r} \partial_\tau^2 \right) \Phi - \Phi \left(\frac{r}{2} \partial_r^2 + \frac{1}{2} \partial_r \right) \Phi + U(\Phi) \right], \tag{3.13}$$

where the integration by parts has been used. The quadratic fluctuations at a stationary point φ then give us the following eigenvalue problem

$$\left[-\frac{\partial^2}{\partial r^2} - \frac{1}{r}\frac{\partial}{\partial r} - \frac{1}{r^2}\frac{\partial^2}{\partial \tau^2} + U''(\varphi) \right] \hat{\Phi}_\lambda(\tau, r) = \lambda \hat{\Phi}_\lambda(\tau, r). \tag{3.14}$$

One can separate the Matsubara modes as

$$\hat{\Phi}_\lambda(\tau, r) = \sum_{n=-\infty}^{n=\infty} \phi_{\lambda,n}(r) e^{i\omega_n \tau}. \tag{3.15}$$

Then we get

$$\left[-\frac{\partial^2}{\partial r^2} - \frac{1}{r}\frac{\partial}{\partial r} + \frac{\omega_n^2}{r^2} + U''(\varphi) \right] \phi_{\lambda,n}(r) = \lambda \, \phi_{\lambda,n}(r). \tag{3.16}$$

The periodic τ (recall $\tau = \tau + 2\pi$) constrains ω_n to be integers. One can recognize Eq. (3.16) as the radial eigenequation of the operator $-\Delta^{(2)} + V''(\varphi)$ appearing in Eq. (3.5) and view Eq. (3.15) as the circular harmonic decomposition. Therefore the full fluctuation spectrum in the thermal field theory $Z[\beta]$ is identical to the one in the quantum field theory $Z_E[0]$ (cf. Eq. (3.2)). It shall be straightforward to show that doing the Gaussian functional integral in $Z[\beta]$ will give us the identical result as in the quantum tunneling case.

The only thing is how to correctly get the factor $B/2\pi$ induced by the zero modes which is not so obvious now. In order to obtain the zero modes, we define the following two independent operators

$$P_X = \cos\tau \frac{\partial}{\partial r} - \frac{1}{r} \sin\tau \frac{\partial}{\partial \tau}; \tag{3.17a}$$

$$P_{\mathcal{T}} = \sin\tau \frac{\partial}{\partial r} + \frac{1}{r} \cos\tau \frac{\partial}{\partial \tau}. \tag{3.17b}$$

Acting on the EoM for φ_b with these operators, one has

$$\left[-\frac{\partial^2}{\partial r^2} - \frac{1}{r}\frac{\partial}{\partial r} + \frac{1}{r^2} + U''(\varphi) \right] (P_{X,\mathcal{T}} \varphi_b) = 0. \tag{3.18}$$

Thus we have two zero modes $B^{-1/2} P_{X,\mathcal{T}} \varphi_b$ with $\omega_n^2 = 1$ where we have included the normalization factor. These zero modes can be traded for the collective coordinates, giving

$$\left(\frac{B}{2\pi} \right) \int \mathrm{d}X \int \mathrm{d}\mathcal{T} = \left(\frac{B}{2\pi} \right) \int \mathrm{d}\tau \int \mathrm{d}r \; r = \left(\frac{B}{2\pi} \right) \beta \tilde{V}, \tag{3.19}$$

where we have defined the effective volume $\tilde{V}$ for the Rindler observers when we use the dimensionless time τ.

Combining all the above analyses, we readily conclude that

$$\Gamma_{\rm tunn}/V = \Gamma_{\rm therm}/\tilde{V}. \tag{3.20}$$

Dividing $\Gamma_{\rm therm}$ by $\tilde{V}$ is related to the fact that the Rindler horizon is not globally unique. One can have an infinite number of Rindler horizons with the light cone apex translated in the X- and T-directions. Mathematically, the result (3.20) is quite natural since the partition function $Z[\beta]$ is related to $Z_E[0]$ simply by a coordinate transformation. Conceptually, this is nontrivial. On the LHS we describe quantum tunneling observed by the inertial observers in the full flat $1+1$-dimensional spacetime while on the RHS we study thermal transition for Rindler observers in a Rindler wedge. For the former case, the nucleated bubble wall is represented by the paired half-hyperboloids. While for the latter case, the bubble wall is only the half-hyperboloid in the R-wedge; the other one in the L-wedge is completely fictitious. Now we have understood that in the correspondence, the Matsubara modes in the thermal field theory are just the circular harmonic modes in the quantum field theory. And only when we sum over all the Matsubara modes can we have agreement on the *exact* results on both sides.

When the finite temperature effective potential differs from the classical potential significantly, we cannot expand around the classical bounce $\varphi_b = \varphi_B$ as we have done above. The correspondence is, however, still valid. In order for the tunneling rate and thermal decay rate to match, one must also expand around the quantum corrected bounce in the partition function $Z_E[0]$. The decay formula (2.62) is mapped to the formula (4.14) that we will discuss in Chap. 4. Note in the formula (2.62), φ_b is understood to be the corrected bounce at the order at which the effective action is evaluated.

3.3 False vacuum decay in Schwarzschild spacetime

Let us now study vacuum transition in Schwarzschild spacetime. We will only consider the perturbative regime where the back-reactions to the spacetime background can be ignored.[13] If the background spacetime changes dramatically during the bubble nucleation, the correspondence between thermal and quantum vacuum transitions has conceptual difficulties. In such a case, the remnant black hole and the original black hole can have different masses, and even worse there may not be a remnant black hole [13]. Therefore it is not clear how to give the definition of the external static observers that simultaneously works before and after the bubble nucleation. Such conceptual problems in the non-perturbative regime, however, are not exclusive for our particular correspondence between thermal and quantum vacuum transitions but are general for correspondences involved in the BHC.

We consider the following action

$$S_M = \int \mathrm{d}^4x\sqrt{-g}\left[\frac{1}{2}g^{\mu\nu}(\partial_\mu\Phi)\partial_\nu\Phi - U(\Phi)\right], \tag{3.21}$$

where the metric $g_{\mu\nu}$ is given as

$$\mathrm{d}s^2 = \left(1-\frac{2GM}{r}\right)\mathrm{d}t^2 - \left(1-\frac{2GM}{r}\right)^{-1}\mathrm{d}r^2 - r^2\mathrm{d}\Omega_2^2, \tag{3.22}$$

[13] The application condition for this perturbative regime is given in Ref. [77].

with $\mathrm{d}\Omega_2^2 \equiv \mathrm{d}\theta^2 + \sin^2\theta \mathrm{d}\phi^2$ being the metric for the unit two-sphere.

We will first consider the thermal description of vacuum transitions given by the external static observers. Denoting the spatial metric as $h_{ij} = -g_{ij}$ and

$$f(r) \equiv \left(1 - \frac{2GM}{r}\right), \tag{3.23}$$

we can rewrite the action as

$$S_M = \int \mathrm{d}t \int \mathrm{d}^3x\sqrt{h}\left[\frac{1}{2\sqrt{f(r)}}\left(\frac{\mathrm{d}\Phi}{\mathrm{d}t}\right)^2 - \frac{1}{2}\sqrt{f(r)}h^{ij}(\partial_i\Phi)\partial_j\Phi - \sqrt{f(r)}U(\Phi)\right], \tag{3.24}$$

where $h = \det(h_{ij})$.

To see that upon the Wick rotation $t \to -i\tau$ the Euclidean Schwarzschild time τ should be periodic, one can move to the Kruskal-Szekeres coordinates through ($r \geq 2GM$)

$$T = \left(\frac{r}{2GM} - 1\right)^{1/2} e^{r/4GM} \sinh\left(\frac{t}{4GM}\right), \tag{3.25a}$$

$$X = \left(\frac{r}{2GM} - 1\right)^{1/2} e^{r/4GM} \cosh\left(\frac{t}{4GM}\right). \tag{3.25b}$$

Note that $X \geq 0$ (since $r \geq 2GM$). The metric now reads

$$\mathrm{d}s^2 = \frac{32G^3M^3}{r}e^{-r/2GM}(\mathrm{d}T^2 - \mathrm{d}X^2) - r^2\mathrm{d}\Omega_2^2, \tag{3.26}$$

where

$$T^2 - X^2 = \left(1 - \frac{r}{2GM}\right)e^{r/2GM}. \tag{3.27}$$

The coordinate transformation (3.25) is analogous to the one from $\{t, r\}$ to $\{T, X\}$ in the $1+1$-dimensional flat spacetime. One can see that, after the Wick rotation $t \to -i\tau$, the Euclidean time τ has a natural periodicity $\beta = 8\pi GM$.

Taking the Wick rotation $t \to -i\tau$; $iS_M \to -S_E$ and the identification $\tau = \tau + 8\pi GM$, we have

$$S_E = \int_0^{\beta=8\pi GM} \mathrm{d}\tau \int \mathrm{d}^3x\sqrt{h}\left[\frac{1}{2\sqrt{f(r)}}\left(\frac{\mathrm{d}\Phi}{\mathrm{d}\tau}\right)^2 + \frac{1}{2}\sqrt{f(r)}h^{ij}(\partial_i\Phi)\partial_j\Phi + \sqrt{f(r)}U(\Phi)\right]. \tag{3.28}$$

We can identify the part of the spatial integral as the Hamiltonian H with τ replaced by t. The thermal field theory is given by the following partition function

$$Z[\beta] = \mathrm{Tr}[e^{-\beta H}]. \tag{3.29}$$

Because of the $O(3)$ symmetry of the spacetime, we expect that the time-independent configuration responsible for the thermal transition has no dependence on θ and ϕ. Then the action (3.28) gives the EoM

$$-\frac{\mathrm{d}^2\varphi}{\mathrm{d}r^2} - \frac{f'(r)}{f(r)}\frac{\mathrm{d}\Phi}{\mathrm{d}r} - \frac{2}{r}\frac{\mathrm{d}\varphi}{\mathrm{d}r} + \frac{U'(\varphi)}{f(r)} = 0. \tag{3.30}$$

To prepare for the construction of the correspondence, we can define a coordinate system $\{\mathcal{T}, X\}$ through the transformation

$$\mathcal{T} = \left(\frac{r}{2GM} - 1\right)^{1/2} e^{r/4GM} \sin\left(\frac{\tau}{4GM}\right), \tag{3.31a}$$

$$X = \left(\frac{r}{2GM} - 1\right)^{1/2} e^{r/4GM} \cos\left(\frac{\tau}{4GM}\right). \tag{3.31b}$$

Note that, once we allow τ to take the whole region from 0 to $8\pi GM$, we have extended the X from $X \geq 0$ to the whole real line. But we still view Eq. (3.29) as describing the thermal ensemble on the original static patch outside of the black hole.[14] This is of course again due to the thermofield dynamics which doubles the Fock space of the thermal field system. The Euclidean metric in the coordinates $\{\mathcal{T}, X\}$ is

$$\mathrm{d}s^2 = \frac{32G^3M^3}{r} e^{-r/2GM}(\mathrm{d}\mathcal{T}^2 + \mathrm{d}X^2) + r^2\mathrm{d}\Omega_2^2. \tag{3.32}$$

On the other hand, we can from the beginning work in the maximally extended Kruskal-Szekeres spacetime with the same metric (3.26) and relation (3.27). In this extended spacetime, there is no particular constraint on X except for that $r > 0$. If one ignores the unphysical white hole region, one can view this spacetime as describing two black holes in two causally uncorrelated spatial regions connected by a wormhole (the Einstein-Rosen bridge [79]); the wormhole is the shared interior of these two black holes, see Fig. 3.4. Now one can study the quantum vacuum transition around the wormhole in the Kruskal-Szekeres spacetime.

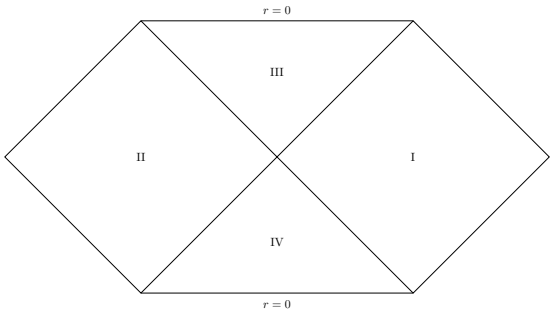

Figure 3.4: Penrose diagram of the Kruskal-Szekeres spacetime which is obtained by a conformal transformation of the metric (3.26). The left and right square regions are two causally uncorrelated universes. The upper and lower triangle regions are the black hole and white hole, respectively. The angular directions (θ and ϕ) are suppressed.

We shall emphasize that there is nothing singular near the wormhole event horizon and in particular, the spacetime curvature can be very small for large black holes. Therefore, the Callan and Coleman's description on false vacuum decay should be still reliable. Now we need to perform the Wick rotation $T \to -i\mathcal{T}$ which gives us the metric (3.32). The

[14] An insignificant point: if the thermal field theory describes the static patch outside of the black hole, i.e., $r > 2GM$, we shall subtract the point $X = \mathcal{T} = 0$ in the Euclidean spacetime. But we can include the horizon $r = 2GM$ into the system to fill this hole.

surprising thing is that after this rotation, the relation (3.27) becomes

$$\mathcal{T}^2 + X^2 = \left(\frac{r}{2GM} - 1\right) e^{r/2GM} \equiv \rho^2 \geq 0. \tag{3.33}$$

That is, the Euclidean Kruskal-Szekeres spacetime has $r \geq 2GM$ and coincides completely with the one where the thermal field theory lives.[15] This point also makes the Euclidean Kruskal-Szekeres spacetime be non-singular in the whole region $-\infty < \mathcal{T} < \infty; -\infty < X < \infty$ and motivates Hawking to propose the Euclidean Kruskal-Szekeres spacetime as the simplest gravitational instanton [80].

Using the coordinates $\{\mathcal{T}, X, \theta, \phi\}$, one can have a Euclidean field theory with an open Euclidean time and the partition function

$$Z_E[0] = \int \mathcal{D}\Phi \; e^{-S_{E,\mathcal{T}}}, \tag{3.34}$$

where we put a subscript $\mathcal{T}$ on S_E to remind us of the Euclidean time we are using. Note that the worldlines with constant $\{X, \theta, \phi\}$ are not geodesics and hence cannot represent the freely falling observers directly. But the Kruskal-Szekeres coordinates provide a very useful global coordinate frame that nevertheless can describe the quantum transition because: (i) the Euclidean Kruskal-Szekeres time is open; (ii) the bounce action, or more generally, the partition function (3.34) is invariant under coordinate transformations. The bubble nucleation around the wormhole can be described by a bounce solution centered at the origin ($\mathcal{T} = X = 0$) in the Euclidean Kruskal-Szekeres spacetime. We would like to emphasize that the coordinates $\{\mathcal{T}, X\}$ here are quite similar to the one in the $1+1$-dimensional Euclidean flat spacetime. In particular, the manifolds described by $\{\mathcal{T}, X\}$ are both $\mathbb{R}^2$ and the metrics possess an $O(2)$ symmetry. This is why the thermal properties of the event horizon can be understood from the Rindler horizon in $1+1$ flat spacetime. Considering the additional $O(3)$ symmetry, we expect that the bounce has an $O(3) \times O(2)$ symmetry and thus only depends on the radial distance ρ (cf. Eq. (3.33)). Such kind of bounce is called *static* and gives the minimal bounce action B [13]. Because there is no dependence on θ and ϕ in the static bounce solution, our tunneling problem is analogous to the one in the $1+1$-dimensional flat spacetime. For instance, it is completely trivial to check that the EoM for this $O(3) \times O(2)$ bounce is exactly the same as Eq. (3.30). And we immediately get the agreement on the semiclassical suppressions in the thermal interpretation and the tunneling interpretation. The "thin-wall" bounce is described in Fig. 3.2 with the extra $O(3)$ symmetry given by the θ- and ϕ-independences. There is one difference compared with the case of $1+1$-dimensional flat spacetime. In the Euclidean Kruskal-Szekeres spacetime, we do not have $\mathcal{T}$- and X-translation symmetries any more since the event horizon is globally unique. Hence we shall consider the total quantum transition probability instead of the transition rate. We have

$$P_{\text{tunn}} = 2\,\text{Im}Z_E[0]. \tag{3.35}$$

[15] Because of this, there is no difference between the *Euclidean* Kruskal-Szekeres spacetime and the *Euclidean* Schwarzschild spacetime (with the Euclidean Schwarzschild time τ taking a full periodicity). Thus these two terms are used interchangeably in this paper. Without the adjective "Euclidean", these two spacetimes are very different.

Similarly we have the thermal transition probability

$$P_{\rm therm} = 2\,{\rm Im}Z[\beta]. \tag{3.36}$$

As before, one can further perform the Gaussian functional integrals in the saddle-point expansions. Since the action in the quantum field theory (Eq. (3.11)) is related to the action in the thermal field theory (Eq. (3.28)) by a coordinate transformation, the fluctuation spectra in both theories must match. The Matsubara modes in the thermal field theory are mapped to the circular harmonic modes (from the $O(2)$ in the $O(3)\times O(2)$) in the quantum field theory. Therefore the thermal transition probability and the quantum transition probability will have identical results: $P_{\rm tunn} = P_{\rm therm}$.

One can easily extend this correspondence between thermal and quantum vacuum transitions to other horizons, e.g., to the de Sitter horizon. The de Sitter spacetime has two causally uncorrelated static patches which are separated by de Sitter horizons, see Fig. 3.5. See also Ref. [81] for more details. Since the de Sitter spacetime is maximally symmetric, one can always choose a Kruskal coordinate system such that the bubble is nucleated around a de Sitter horizon. Viewed from the static observers in this particular coordinate system, the bubble nucleation is thermal. By using a WKB approach, Brown and Weinberg [76] showed the agreement on the semiclassical suppression in the transition rates from a thermal transition description and the Coleman-De Luccia tunneling prescription [77]. However, by repeating the analysis we have given, one can show the exact agreement in the transition rates beyond the semiclassical level.

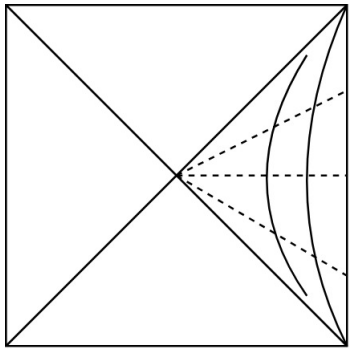

Figure 3.5: Penrose diagram of the de Sitter space. The right triangle region is one of the static patches.

3.4 A New Paradox from Black Holes?

Since the discovery of the black hole evaporation, many questions related to it remain to be answered. For example, we still do not know what are the microscopic degrees of freedom that are responsible for the Bekenstein-Hawking entropy [82, 72]. In particular, by theoretically studying black holes, the famous information paradox [83] was proposed and remains to be one of the deepest mysteries in physics, see Ref. [84] for a pedagogical introduction. The information paradox has been formulated in an extremely sharp version by Almheiri, Marolf, Polchinski and Sully, named as the AMPS firewall paradox [85]. These

paradoxes are intrinsically related to the curious thermal nature of the state observed by the external static observers outside of a black hole.

Here we would like to study a consequence of the correspondence we have constructed so far which may lead to a new paradox related to black holes. The paradox is based on the following assumptions:

(i) The local field theory is valid near the black hole horizon. In particular, the state outside of the horizon is thermal viewed from the external static observers as shown by Hawking.

(ii) The equivalence principle. In particular, the freely falling observers are in a vacuum state at zero temperature.

We consider the following thought experiment. Suppose we have a field system that permits a mild vacuum transition such that the bubble nucleation around a black hole does not change the background spacetime dramatically. We can in principle do experiments to measure the probability of bubble nucleation around evaporating Schwarzschild black holes. By assumption (i), the static observers are in a thermal ensemble and would measure a result $P_{\rm therm}$ for the thermal bubble nucleations. However, by assumption (ii) the freely falling observers are in a vacuum state and thus see tunneling processes of bubble nucleation. Since the experiments are performed outside of the horizon, the static observers and freely falling observers can compare their results. The freely falling observers must observe the same probability, $P_{\rm tunn} = P_{\rm therm}$. But as we have shown, if the freely falling observers calculate the quantum tunneling probability, they can get a correct prediction only with assuming that they are in a Kruskal-Szekeres spacetime. For the single black hole background, the Kruskal-Szekeres coordinate X needs to be constrained as $X \geq 0$, see Fig. 3.6. After the wick rotation $T \to -i\mathcal{T}$, we only have half a Euclidean Kruskal-Szekeres spacetime. In this case, freely falling observers will get a different prediction on the bounce action and the tunneling probability, leading a contradiction between the experimental result and the theoretical prediction.

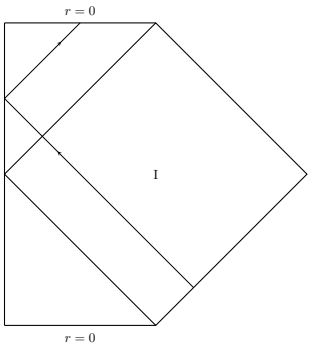

Figure 3.6: Representation of the Schwarzschild spacetime by half of the Kruskal-Szekeres spacetime. The solid line with solid arrows represents a light beam propagating into the black hole. For realistic black holes, the white hole and its event horizon need to be replaced by the collapsing star.

For Rindler and de Sitter horizons, the "freely falling observers" really have another *physical* static patch, although it cannot be seen by the "freely falling observers" from the

patch that our thermal field theory describes. Realizing this, the "freely falling observers" in the Rindler spacetime and the de Sitter spacetime can get a correct prediction for the quantum transition. For black holes, it is very hard to imagine that any Schwarzschild black hole is connected with another black hole as described by the Kruskal-Szekeres metric. Note that in this paradox we do not assume an old black hole (after the Page time [86]) as the information paradox usually does. As long as the event horizon has been formed, we could have such a paradox.

This paradox can be summarized as the following query. The thermal nature that the Rindler and de Sitter horizons present to the static observers on a static patch can be explained by the entanglement between the static patch (say our R-wedge) with another (say our L-wedge) and the tracing out of L-wedge. While the black hole horizon has a similar local structure (such that the static observers outside of the black hole horizon are locally equivalent to uniformly accelerated observers outside of the Rindler horizon) and thus presents the same thermal nature to the external static observers according to the Unruh effect, what is the origin of such thermal character globally?

This paradox may be related to the ER=EPR conjecture [87] proposed by Maldacena and Susskind. The ER=EPR conjectures that any Einstein-Podolsky-Rosen [88] correlated system is connected by some sort of Einstein-Rosen bridge. Thus somehow, the maximally extended Kruskal-Szekeres spacetime may be indeed realized for any evaporating Schwarzschild black hole, perhaps in some exotic way.

Chapter 4

Radiative Effects on False Vacuum Decay I: Motivation and Formalism

4.1 Motivation

As we have mentioned in the introduction, electroweak metastability is among the most important features of the Standard Model (SM) because it could point to its embedding in the framework of more fundamental theories [89, 90, 91, 92, 93]. The beta function had been computed to next-to-leading order (NLO) level before the Higgs boson was discovered [94, 95, 6, 96, 97, 98, 99, 100, 101, 102]. The discovery of 125 GeV Higgs boson [3, 4] has motivated much more precision calculations of the lifetime of the SM electroweak vacuum [7, 8]. With the input from other experimental data, current studies suggest that the Higgs potential turns to be negative at around 10^{11} GeV, leading to an instability of the electroweak vacuum. But the lifetime of the electroweak vacuum is suggested to be much longer than the age of our Universe, leading to the metastability scenario [6, 9, 10, 11].

The conclusion on the lifetime of the electroweak vacuum has uncertainties both from experimental measurements and the theoretical extensions. For the former, the dominant source arises from the measurement of the top-quark mass [103, 104]. For the latter, the lifetime of the electroweak vacuum can be very sensitive to higher-dimensional operators, originating from new physics at around the Planck scale. In certain areas of parameter space, this can dramatically reduce the lifetime of the electroweak vacuum, taking it below the current age of the Universe, leading to strong constraints on physics beyond the SM [105, 106, 107, 108, 109, 110].

Without any extensions of the SM, some aspects in the previous computations nonetheless have been overlooked. Though high precision couplings and renormalization group equations were used in the precision calculations, comparable radiative effects on the tunneling process have not been accounted well. In particular, in false vacuum decay, the bounce is an inhomogeneous background, and the beta functions for the coupling constants do not account for the gradient effects from the inhomogeneous background. Although the one-loop radiative corrections due to fluctuations about the classical bounce, which account for the inhomogeneity of the background, have been calculated using the Gel'fand-Yaglom theorem [111, 42, 112, 113], higher radiative corrections have not been calculated. The Gel'fand-Yaglom method cannot handle the situations where the bounce can only be determined at the quantum level. For instance, in (approximately) scale invariant theories such as the SM [10, 11, 114], the scale of the nucleated bubble depends on radiative effects. Another example is that the true vacuum may emerge radiatively in the first place through the CW mechanism [12, 119, 61]. Furthermore, evaluating the functional determinant using the Gel'fand-Yaglom theorem does not lead to a systematic

method of computing higher-order corrections.

In this chapter, we will introduce a systematic way of addressing these problems by reformulating the vacuum decay rate in terms of the effective action. We will construct Green's functions in the solitonic background, which can then be used to evaluate effective actions [116, 117] and to construct self-consistent equations of motion in perturbation theory or resummed variants thereof [59]. Compared to calculations in homogeneous backgrounds, the reduced symmetry makes it harder, however, to advance calculations to high orders. Nevertheless, problems such as the perturbative improvement of bounce solutions and decay rates [59, 118, 60], and finding bounces in radiatively generated [61] or classically scale invariant potentials [114] can be addressed this way. Here, we will work in a Higgs-Yukawa model in view of the pivotal role played by the top quark in electroweak metastability.

In the next section, we will introduce the general formalism of calculating the radiative effects on false vacuum decay by the use of a Green's function method. As an application, we consider the archetypal model originally analyzed by Coleman and Callan [41, 37] of tunneling between quasi-degenerate vacua in scalar field theory and compute the leading radiative corrections to the bounce, as well as the tunneling action. Referring to the tunneling degree of freedom as the Higgs field, these corrections are induced by the self-interactions of the Higgs boson, as well as its Yukawa couplings to Dirac fermions.

4.2 General formalism

The calculation of scalar-field loops in the case of vacuum decay in field theory, and based on Green's functions evaluated in the inhomogeneous background of the tunneling soliton, has been introduced in Ref. [59] and carried out to two-loop order in the decay rate in Ref. [118]. Here, we extend this methodology to consider the radiative corrections from fermion loops, making a direct comparison with the corresponding effects from scalars. We focus, in particular, on the amplitude for the vacuum transition, as well as the deformations of the classical soliton, and present the main elements of the approach.

4.2.1 Prototypal Higgs-Yukawa model

We consider a Higgs-Yukawa model based on the Euclidean Lagrangian

$$\mathcal{L}_E = \bar{\Psi}\gamma_\mu\partial_\mu\Psi + \kappa\bar{\Psi}\Phi\Psi + \frac{1}{2}(\partial_\mu\Phi)^2 + U(\Phi), \tag{4.1}$$

where κ is the dimensionless Higgs-Yukawa coupling. Since we will work in the Euclidean space throughout chapters 4, 5, we will supress the subscript "E" in these two chapters. The Euclidean gamma matrices are obtained from their Minkowskian counterparts through the replacement $\gamma^k \to i\gamma_k$, for $k = 1, 2, 3$, and $\gamma^0 \to \gamma_4$. For definiteness, we have chosen the same potential as in the archetypal example of tunneling in field theory considered by Coleman and Callan [41, 37], see Eq. (2.26). The leading-order bounce and tunneling rate have been reviewed in Secs. 2.2 and 2.3. In the present work, we will be interested in the thin-wall limit. For convenience, we recall the main results in this regime. We have the classical bounce

$$\varphi_B(\rho) = v\tanh[\gamma(\rho - R)] \equiv vu \tag{4.2}$$

where $\gamma = \mu/\sqrt{2}$ and $R = 12\gamma/(gv)$ with $v = \sqrt{6\mu^2/\lambda}$. The false vacuum $\varphi_+ = v$ and the leading bounce action

$$B = 8\pi^2 R^3 \gamma^3/\lambda. \tag{4.3}$$

The formalism presented below, however, can be applied to general situations beyond the thin-wall approximation.

The Euclidean amplitude for transitions from the false vacuum (at $\tau = -\mathcal{T}/2$) to the false vacuum (at $\tau = +\mathcal{T}/2$) is given in terms of the partition function (cf. Eq. (4.7))

$$\begin{aligned} Z[0,0,0] &= \langle \varphi_+ | e^{-H\mathcal{T}} | \varphi_+ \rangle \\ &= \int \mathcal{D}\Phi\, \mathcal{D}\Psi\, \mathcal{D}\bar{\Psi}\; e^{-S[\Phi,\bar{\Psi},\Psi]}, \end{aligned} \tag{4.4}$$

where H is the full Hamiltonian and $S[\Phi, \bar{\Psi}, \Psi]$ is the Euclidean action. In terms of $Z[0,0,0]$, the decay rate is given by [37]

$$\Gamma \;=\; 2\,|\mathrm{Im}\, Z[0,0,0]|/\mathcal{T}, \tag{4.5}$$

where the partition function is to be evaluated by expanding around the bounce solution and normalized such that $Z^F_{(E)}[0,0,0] = 1$.

4.2.2 Effective action

To account for the quantum corrections, we use the effective action [116, 117] as the main tool. In this section, we present the use of the effective action to calculate the radiative effects for false vacuum decay in Higgs-Yukawa theory. We will see that the effective action can be used not only to derive the corrected bounce but also to obtain the corrected decay rate.

For conciseness, we will now employ the DeWitt notation

$$J_x \Phi_x = \int \mathrm{d}^4 x J(x)\Phi(x), \tag{4.6}$$

in which repeated continuous indices are integrated over. For non-vanishing external sources, the Euclidean partition function is given by

$$Z[J,\bar{\eta},\eta] = \int \mathcal{D}\Phi\mathcal{D}\Psi\mathcal{D}\bar{\Psi}\exp\left\{-\left[S[\Phi,\bar{\Psi},\Psi] - \left(J_x\Phi_x + \bar{\eta}_x\Psi_x + \bar{\Psi}_x\eta_x\right)\right]\right\}. \tag{4.7}$$

It can be used to compute the one-point functions

$$\varphi_x = \langle\Omega|\Phi_x|\Omega\rangle|_{J,\bar{\eta},\eta} = +\frac{\delta \ln Z[J,\bar{\eta},\eta]}{\delta J_x}, \tag{4.8a}$$

$$\bar{\psi}_x = \langle\Omega|\bar{\Psi}_x|\Omega\rangle|_{J,\bar{\eta},\eta} = -\frac{\delta \ln Z[J,\bar{\eta},\eta]}{\delta \eta_x}, \tag{4.8b}$$

$$\psi_x = \langle\Omega|\Psi_x|\Omega\rangle|_{J,\bar{\eta},\eta} = +\frac{\delta \ln Z[J,\bar{\eta},\eta]}{\delta \bar{\eta}_x}. \tag{4.8c}$$

The effective action is defined as the Legendre transform

$$\Gamma[\varphi,\bar{\psi},\psi] = -\ln Z_E[J,\bar{\eta},\eta] + J_x\varphi_x + \bar{\eta}_x\psi_x + \bar{\psi}_x\eta_x. \tag{4.9}$$

It is easy to check that the one-point functions satisfy

$$\frac{\delta\Gamma[\varphi,\bar{\psi},\psi]}{\delta\varphi_x} = J_x, \tag{4.10a}$$

$$\frac{\delta\Gamma[\varphi,\bar{\psi},\psi]}{\delta\psi_x} = -\bar{\eta}_x, \tag{4.10b}$$

$$\frac{\delta\Gamma[\phi,\bar{\psi},\psi]}{\delta\bar{\psi}_x} = \eta_x. \tag{4.10c}$$

Note that we have used the following convention for the Leibniz law for the functional derivative of a functional $F \equiv F[\eta]$ with respect to a Grassmann variable η:

$$\frac{\delta F[\eta]}{\delta\psi_x} = \frac{\delta\eta_y}{\delta\psi_x}\frac{\delta F[\eta]}{\delta\eta_y}. \tag{4.11}$$

From Eqs. (4.10a)–(4.10c), we see that the vacuum expectation values (VEVs) of fields, i.e. the one-point functions in presence of vanishing sources, correspond to the minima of the effective action. Since the VEVs of the fermion fields must vanish, the effective action $\Gamma[\varphi,\bar{\psi},\psi]$ is reduced to $\Gamma[\varphi,\bar{\psi}=\psi=0] \equiv \Gamma[\varphi]$. We can use the effective action to obtain the EoM for the quantum-corrected bounce via

$$\frac{\delta\Gamma^{(n)}[\varphi]}{\delta\varphi_x} = 0, \tag{4.12}$$

where the superscript "(n)" indicates that the effective action is calculated up to n-loop order. The corresponding solution will be denoted as $\varphi^{(n)}$. We shall call $\varphi^{(n)}$ the *quantum bounce* to compare with the classical bounce.

Moreover, when the fields are at the VEVs, one can substitute $J = \bar{\eta} = \eta = 0$ into Eq. (4.9) and have

$$\Gamma[\varphi^{(n)},\bar{\psi}^{(n)}=\psi^{(n)}=0] = -\ln Z_E^B[0,0,0]. \tag{4.13}$$

The decay rate in Eq. (2.23) now can be expressed as

$$\Gamma/V \;=\; 2\,|\mathrm{Im}\, e^{-\Gamma^{(n)}[\varphi^{(n)}]}|/(\mathcal{T}V), \tag{4.14}$$

at the level of the n-th quantum corrections. In this thesis, we aim to calculate $\varphi^{(1)}$ and

$$\Gamma/V \;=\; 2\,|\mathrm{Im}\, e^{-\Gamma^{(1)}[\varphi^{(1)}]}|/(\mathcal{T}V). \tag{4.15}$$

We emphasize that, in the formula (4.15), it is the quantum bounce that enters the formula of the decay rate directly rather than the classical bounce. This point is extremely relevant in the case where a unstable vacuum is entirely induced radiatively via the CW mechanism because the *classical* bounce φ_B does not exist there.

4.2.3 One-loop corrections to the action

In order to obtain the expression $\Gamma^{(1)}[\varphi]$ we proceed by expanding $\Phi(x) = \varphi(x) + \hat{\Phi}(x)$, $\bar{\Psi}(x) = \bar{\psi}(x) + \hat{\bar{\Psi}}(x)$ and $\Psi(x) = \psi(x) + \hat{\Psi}(x)$, such that the action $S[\Phi,\bar{\Psi},\Psi]$ is given to

quadratic order by

$$S[\Phi,\bar{\Psi},\Psi] = S[\varphi,\bar{\psi},\psi] + J_x\hat{\Phi}_x + \bar{\eta}_x\hat{\Psi}_x + \hat{\bar{\Psi}}_x\eta_x + \frac{1}{2}\int \mathrm{d}^4x\mathrm{d}^4y\ \hat{\Phi}(x)G^{-1}(\varphi,\bar{\psi},\psi;x,y)\hat{\Phi}(y) + \frac{1}{2}\int \mathrm{d}^4x\mathrm{d}^4y\ \hat{\bar{\Psi}}(x)\,D^{-1}(\varphi,\bar{\psi},\psi;x,y)\hat{\Psi}(y), \tag{4.16}$$

where the "two-point" operators are defined as

$$G^{-1}(\varphi,\bar{\psi},\psi;x,y) \equiv \left.\frac{\delta^2 S[\Phi,\bar{\Psi},\Psi]}{\delta\Phi_x\delta\Phi_y}\right|_{\Phi=\varphi,\bar{\Psi}=\bar{\psi},\Psi=\psi} = \delta^4(x-y)\big[-\partial^2_{(x)} + U''(\varphi_x)\big], \tag{4.17a}$$

$$D^{-1}(\varphi,\bar{\psi},\psi;x,y) \equiv \left.\frac{\delta^2 S[\Phi,\bar{\Psi},\Psi]}{\delta\Psi_x\delta\bar{\Psi}_y}\right|_{\Phi=\varphi,\bar{\Psi}=\psi,\Psi=\psi} = \delta^4(x-y)\big[\gamma_\mu\partial_\mu + \kappa\varphi_x\big], \tag{4.17b}$$

with $\delta^4(x-y)$ being the four-dimensional Dirac function. The linear terms in the above expressions have been chosen so as to cancel those appearing in the exponent of the partition function (4.7).[16] Since the one-point functions $\bar{\psi}$, ψ are necessarily vanishing, we denote $S[\varphi,\bar{\psi}=0,\psi=0] \equiv S[\varphi]$, $G^{-1}(\varphi,\bar{\psi}=0,\psi=0;x,y) \equiv G^{-1}(\varphi;x,y)$ and, $D^{-1}(\varphi,\bar{\psi}=0,\psi=0;x,y) \equiv D^{-1}(\varphi;x,y)$. Equation (4.16) then defines the tree-level inverse Green's functions

$$G^{-1}(\varphi;x,y) \equiv \left.\frac{\delta^2 S[\Phi,\bar{\Psi},\Psi]}{\delta\Phi_x\delta\Phi_y}\right|_{\Phi=\varphi,\bar{\Psi}=0,\Psi=0} = \delta^4(x-y)\big[-\partial^2_{(x)} + U''(\varphi_x)\big], \tag{4.18a}$$

$$D^{-1}(\varphi;x,y) \equiv \left.\frac{\delta^2 S[\Phi,\bar{\Psi},\Psi]}{\delta\Psi_x\delta\bar{\Psi}_y}\right|_{\Phi=\varphi,\bar{\Psi}=0,\Psi=0} = \delta^4(x-y)\big[\gamma_\mu\partial_\mu + \kappa\varphi_x\big]. \tag{4.18b}$$

The Klein-Gordon and Dirac operators in the background of φ can then be obtained as

$$G^{-1}(\varphi;x) \equiv \int \mathrm{d}^4y\ G^{-1}(\varphi;x,y), \tag{4.19a}$$

$$D^{-1}(\varphi;x) \equiv \int \mathrm{d}^4y\ D^{-1}(\varphi;x,y). \tag{4.19b}$$

Substituting Eq. (4.16) into Eqs. (4.7), (4.9), one obtains the effective action

$$\Gamma^{(1)}[\varphi] = S[\varphi] + \frac{1}{2}\ln\frac{\det G^{-1}(\varphi)}{\det G^{-1}(v)} - \ln\frac{\det D^{-1}(\varphi)}{\det D^{-1}(v)}, \tag{4.20}$$

where we have substituted $\varphi_+ = v$ into the above formula. We now expand the above equation around φ_B, writing $\varphi = \varphi_B + \delta\varphi$. In this way, we obtain

$$\Gamma^{(1)}[\varphi] = S[\varphi] + \frac{i\pi}{2} + B_D^{(1)} + B_S^{(2)} + B_D^{(2)} + \frac{1}{2}\ln\left|\frac{\lambda_0^B\det{}^{(5)}G^{-1}(\varphi_B)}{\frac{1}{4}(VT)^2(\frac{B}{2\pi\hbar})^4\det G^{-1}(v)}\right|, \tag{4.21}$$

where

$$B_D^{(1)} = -\ln\frac{\det D^{-1}(\varphi_B)}{\det D^{-1}(v)}, \tag{4.22}$$

[16] Here the effective action is evaluated using a method with non-vanishing external sources, see Ref. [119].

and

$$B_S^{(2)} = \frac{1}{2}\int \mathrm{d}^4x\ \delta\varphi(x)\ \frac{\delta \ln \det{}^{(5)}\, G^{-1}(\varphi)}{\delta\varphi(x)}\bigg|_{\varphi_B}, \tag{4.23a}$$

$$B_D^{(2)} = -\int \mathrm{d}^4x\ \delta\varphi(x)\ \frac{\delta \ln\ \det\ D^{-1}(\varphi)}{\delta\varphi(x)}\bigg|_{\varphi_B}. \tag{4.23b}$$

The particular $i\pi/2$ is due to the negative mode in the fluctuation spectrum. The determinant of the Dirac operator is understood to be taken over both the coordinate and spinor spaces. The superscript "(5)" indicates that the five lowest eigenvalues are to be omitted when evaluating the functional determinant. We also explicitly extract the five lowest eigenvalues $4\gamma^2$ from the determinant of $G^{-1}(v;x)$ that are not canceled when building the quotient of the determinants [120]; namely,

$$\Big[\det G^{-1}(v)\Big]^{-\frac{1}{2}} = (2\gamma)^{-5}\Big[\det{}^{(5)} G^{-1}(v)\Big]^{-\frac{1}{2}}. \tag{4.24}$$

We denote

$$B_S^{(1)} \equiv \frac{1}{2}\ln\frac{\det{}^{(5)}\, G^{-1}(\varphi_B)}{\det{}^{(5)}\, G^{-1}(v)}. \tag{4.25}$$

The logarithms of these determinants (Eqs. (4.22), (4.25)) appear as additive corrections to the classical action B and, within the present approximations, they can be interpreted as the one-loop contribution to the effective action. Note that these expressions still need to be renormalized which we will carry out in Sec. 5.2.

Functionally differentiating Eq. (4.20) with respect to φ, one can obtain the quantum EoM in the Higgs-Yukawa model

$$-\partial^2\varphi(x) + U'_{\text{eff}}(\varphi;x) = 0, \tag{4.26}$$

where

$$U'_{\text{eff}}(\varphi;x) \equiv U'(\varphi;x) + \Pi_S(\varphi_B;x)\,\varphi_B(x) + \Pi_D(\varphi_B;x)\,\varphi_B(x), \tag{4.27}$$

with Π_S and Π_D being the tadpole contributions from the scalar and Dirac fields, respectively. From Eq. (4.20), we have

$$\Pi_S(\varphi_B;x)\,\varphi_B(x) = \frac{\delta B_S^{(1)}[\varphi]}{\delta\varphi(x)}\bigg|_{\varphi_B} = \frac{\lambda}{2}\,G(\varphi_B;x,x)\,\varphi_B(x), \tag{4.28}$$

where $G(\varphi_B;x,y)$ is the Green's function of the operator $G^{-1}(\varphi_B;x)$. The fermionic contribution Π_D is

$$\Pi_D(\varphi_B;x)\,\varphi_B(x) = \frac{\delta B_D^{(1)}[\varphi]}{\delta\varphi(x)}\bigg|_{\varphi_B} = -\kappa\,\mathrm{tr_S}\,D(\varphi_B;x,x), \tag{4.29}$$

where $\mathrm{tr_S}$ indicates the trace over the spinor indices and $D(\varphi_B;x,y)$ is the Green's function of the operator $D^{-1}(\varphi_B;x)$.

Eq. (4.26) gives us the quantum corrected bounce $\varphi^{(1)}$. Substituting $\varphi^{(1)} = \varphi_B + \delta\varphi$ into Eq. (4.26), one can find

$$\begin{aligned}\delta\varphi(x) &= -\int \mathrm{d}^4y\, G(\varphi_B; x, y)\, \Pi_S(\varphi_B; y)\, \varphi_B(y) - \int \mathrm{d}^4y\, G(\varphi_B; x, y)\, \Pi_D(\varphi_B; y)\, \varphi_B(y) \\ &\equiv -\int \mathrm{d}^4y\, G(\varphi_B; x, y)\, \Pi(\varphi_B; y)\, \varphi_B(y), \end{aligned} \tag{4.30}$$

where we have used Eq. (2.30).

When substituting the quantum corrected bounce into the action $S[\varphi^{(1)}]$, there appear extra contributions at two-loop order. Expanding first the action $S[\varphi^{(1)}]$ about φ_B, we have

$$S[\varphi^{(1)}] = B + \delta S + \mathcal{O}(\hbar^3), \tag{4.31}$$

where

$$\delta S = \frac{1}{2}\int \mathrm{d}^4x\, \delta\varphi(x)\, G^{-1}(\varphi_B; x)\, \delta\varphi(x) = -\frac{1}{2}\int \mathrm{d}^4x\, \delta\varphi(x)\, \Pi(\varphi_B; x)\, \varphi_B(x), \tag{4.32}$$

and where, for the first identity, we have used the fact that the classical bounce φ_B is the stationary point of the classical action and, for the second identity, we have used Eq. (4.30). Comparing Eq. (4.32) with Eqs. (4.23), (4.28) and (4.29), we see that the total correction to the expansion in $\delta\varphi$ is [59]

$$B^{(2)} \equiv \delta S + \delta B_S^{(1)} + \delta B_D^{(1)} = -\delta S = \frac{1}{2}\Big(\delta B_S^{(1)} + \delta B_D^{(1)}\Big). \tag{4.33}$$

Diagrammatically, the contributions to $B^{(2)}$ correspond to (one-particle reducible) dumbbell graphs, cf. Fig. 5.2 (b) for the fermion contributions. They therefore constitute a subset of the two-loop corrections. However, this subset can be the dominant two-loop contribution for theories with a large number of degrees of freedom propagating in the loop [59]. For the numerical examples in Sec. 5.3, we consider such a setup with a large number of fermion and scalar fields coupling to the Higgs degree of freedom Φ.

4.2.4 Radiatively corrected decay rate

We can now summarize all the contributions that we include in the approximation of the tunneling rate per unit volume as

$$\Gamma/V = \left(\frac{B}{2\pi}\right)^2 (2\gamma)^5\, |\lambda_0|^{-\frac{1}{2}} \exp\Big[-\big(B + B_S^{(1)} + B_D^{(1)} + B^{(2)}\big)\Big], \tag{4.34}$$

where B, $B_S^{(1)}$ and $B_D^{(1)}$ are evaluated at the classical bounce.

In summary, given the leading-order approximation φ_B to the bounce and B for the action we apply the following procedure in order to calculate the radiative corrections to the bounce and to the decay rate:

- We first invert Eqs. (4.18a) and (4.18b) to find the Green's functions $G(\varphi_B; x, y)$ and $D(\varphi_B; x, y)$.

- The Green's functions are used in order to calculate $B_S^{(1)}$ and $B_D^{(1)}$ according to Eqs. (4.22) and (4.25) and the discussion in Sec. 5.2.3.
- The Green's functions are also used to obtain the tadpole functions (4.28) and (4.29), which, in turn, yield the corrections to the bounce (4.30).
- When substituted into the tree and one-loop actions, the radiative corrections to the bounce yield the quadratic correction $B^{(2)}$ in Eq. (4.33) by means of Eq. (4.32), corresponding to dumbbell graphs. We account for these contributions in the calculation of the decay rate because they can be relevant when a large number of fields is running in the loops.
- Finally, the pieces B, $B_{S,D}^{(1)}$ and $B^{(2)}$ can be put together to obtain the decay rate per unit volume (4.34).

Chapter 5

Radiative Effects on False Vacuum Decay II: Planar-Wall Limit

In this chapter, we apply the general formalism presented above to the case of the planar-wall limit. In the approximation of a planar wall, it is calculationally simpler to obtain the fermionic functional determinant as well as the tadpole Π_D from the Green's functions of the corresponding Klein-Gordon-like operators, obtained from "squaring" the Dirac operator, as we discuss below. We, therefore, calculate the Green's functions of all these Klein-Gordon and Klein-Gordon-like operators in the background of the planar-wall bounce. A method of calculating the Green's function of the Dirac operator in a hyperspherically symmetric background is worked out in Appendix B.

5.1 Green's functions, functional determinants and bounce correction in the planar-wall approximation

5.1.1 Green's function and functional determinants in the planar-wall limit

The scalar Green's function satisfies

$$(-\partial^2 + U''(\varphi_B; x))G(\varphi_B; x, x') = \delta^4(x - x'). \tag{5.1}$$

In a hyperspherically symmetric background, this equation can be solved by separating the angular part using a partial-wave decomposition. This reduces the problem to one of finding the hyperradial function $G_j(\varphi_B; r, r')$, where j is the quantum number of angular momentum, see, e.g., Ref. [59]. However, to make things simple, we will restrict to the planar-wall approximation as described below. When the radius of the bubble wall R is very large compared to μ^{-1}, i.e. when $g \ll \sqrt{\lambda}\mu$, we can essentially view the bubble wall as planar. The bounce then is a function of only the perpendicular coordinate $z_\perp$ and has no dependence on the parallel coordinates $\mathbf{z}_\parallel$ on the three-dimensional hypersurface as explained in Fig. 5.1. In the remainder of this chapter, we will employ this planar-wall approximation.

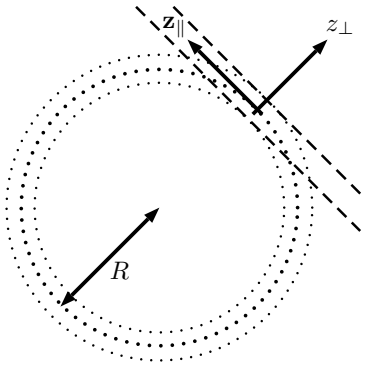

Figure 5.1: Planar-wall approximation to the bounce. Dotted: lines of constant values of the bounce φ, where the middle line indicates the center of the bounce $\varphi = 0$. We choose the coordinates $z_\perp \equiv z$ perpendicular and $\mathbf{z}_\parallel$ parallel to the three-dimensional planar hypersurface tangential to the bubble wall.

Without loss of generality, we take $z_\perp \equiv z = x_4 - R$ and $\mathbf{z}_\parallel = \mathbf{x}$, i.e., we take the perpendicular direction as that of x_4 (or τ). Then the effective squared mass term in Eq. (5.1) is independent of $\mathbf{x}$. One can Fourier-transform the Green's function with respect to the coordinates $\mathbf{x}$,

$$G(\varphi_B; x, x') = \int \frac{\mathrm{d}^3\mathbf{k}}{(2\pi)^3}\, e^{i\mathbf{k}\cdot(\mathbf{x}-\mathbf{x}')}\, G(\varphi_B; z, z', \mathbf{k}). \tag{5.2}$$

The three-momentum-dependent Green's function $G(\varphi_B; z, z', \mathbf{k})$ satisfies the one-dimensional inhomogeneous Klein-Gordon equation

$$(-\partial_z^2 + \mathbf{k}^2 + U''(\varphi_B; z)\, G(\varphi_B; z, z', \mathbf{k}) = \delta(z - z'). \tag{5.3}$$

We refer to $G(\varphi_B; z, z', \mathbf{k})$ as the *three-plus-one representation*. Equation (5.3) can be solved analytically or numerically. The analytical result is given in Refs. [59, 114].

Starting from the representation of the Green's function as a spectral sum, one can show [121, 122, 123, 124] that it can be used to calculate the functional determinant directly. We review this method in Appendix A. Specifically, the functional determinant can be evaluated as

$$\begin{aligned} B_S^{(1)} \;=\; & -\frac{1}{2}\int_{-\infty}^{\infty} \mathrm{d}z \int \mathrm{d}^3\mathbf{x} \int_0^{\infty} \mathrm{d}s \int_0^{\Lambda} \frac{\mathbf{k}^2\, \mathrm{d}|\mathbf{k}|}{2\pi^2} \\ & \times \Big[G\big(\varphi_B; z, z, \sqrt{\mathbf{k}^2 + s}\big) - G\big(\varphi_+; z, z, \sqrt{\mathbf{k}^2 + s}\big) \Big], \end{aligned} \tag{5.4}$$

where Λ is a three-momentum cutoff. Here we have written the coincident Green's function $G(\varphi_B; z, z, |\mathbf{k}|) \equiv G(\varphi_B; z, z, \mathbf{k})$ because of the isotropy parallel to the bubble wall. Note that, in these integrals, the negative and zero modes correspond to $|\mathbf{k}| = 0$ and therefore lead to a vanishing contribution.

In analogy with the scalar case, the Green's function for the Dirac operator in a hyperspherically symmetric background can be solved by a separation ansatz. The angular solutions in this approach are spin hyperspherical harmonics of definite total angular

momentum, as is explained in detail in Appendix B. Considerable simplifications are, however, possible in the planar-wall approximation.

Since φ_B depends on z (or x_4) only in the planar-wall approximation, one defines the local Dirac mass $m_D(z) \equiv \kappa\,\varphi_B(z)$. It turns out that one can generalize the well-known method of "squaring" in evaluating the determinant of the Dirac operator to the situation where the mass varies in one direction of spacetime. Noticing that the determinant

$$I = \ln\det D^{-1}(\varphi_B; x) = \ln\det\big(\gamma_\mu\partial_\mu + m_D(z)\big) \tag{5.5}$$

is invariant under chiral conjugation, we multiply by γ_5 from the left and right of the inhomogeneous Dirac operator. This yields

$$\det\big(\gamma_\mu\partial_\mu + m_D(z)\big) = \det\big[\gamma_5\big(\gamma_\mu\partial_\mu + m_D(z)\big)\gamma_5\big] = \det\big(-\gamma_\mu\partial_\mu + m_D(z)\big), \tag{5.6}$$

where we have used the anticommutation relations between γ_5 and γ_μ and the multiplicativity property of the determinant. We can thus express

$$\begin{aligned} I &= \frac{1}{2}\big[\ln\det\big(\gamma_\mu\partial_\mu + m_D(z)\big) + \ln\det\big(-\gamma_\mu\partial_\mu + m_D(z)\big)\big] \\ &= \frac{1}{2}\ln\det\big[-\partial^2 + m_D^2(z) + \gamma_4\big(\partial_4 m_D(z)\big)\big]. \end{aligned} \tag{5.7}$$

Now, after employing the representation of gamma matrices

$$\gamma_4 \;=\; \begin{bmatrix} 0 & 1 \\ 1 & 0 \end{bmatrix}, \quad \gamma_i \;=\; \begin{bmatrix} 0 & i\sigma_i \\ -i\sigma_i & 0 \end{bmatrix}, \tag{5.8}$$

where σ_i are the Pauli matrices, we obtain

$$I \;=\; \frac{1}{2}\ln\left\| \begin{matrix} \big(-\partial^2 + m_D^2(z)\big)\cdot\mathbb{I}_2 & \big(\partial_4 m_D(z)\big)\cdot\mathbb{I}_2 \\ \big(\partial_4 m_D(z)\big)\cdot\mathbb{I}_2 & \big(-\partial^2 + m_D^2(z)\big)\cdot\mathbb{I}_2 \end{matrix} \right\|. \tag{5.9}$$

This is a determinant in block form, and we can make use of the relation

$$\det\begin{bmatrix} A & B \\ B & A \end{bmatrix} \;=\; \det(A-B)\det(A+B), \tag{5.10}$$

which applies even when A and B do not commute with each other, provided A and B are square matrices of the same dimensions. We are led to

$$\begin{aligned} I &= \frac{1}{2}\ln\big\{\det\big[\big(-\partial^2 + m_D^2(z) - \partial_z m_D(z)\big)\cdot\mathbb{I}_2\big]\det\big[\big(-\partial^2 + m_D^2(z) + \partial_z m_D(z)\big)\cdot\mathbb{I}_2\big]\big\} \\ &= \ln\det\big[-\partial^2 + m_D^2(z) - \partial_z m_D(z)\big] + \ln\det\big[-\partial^2 + m_D^2(z) + \partial_z m_D(z)\big], \end{aligned} \tag{5.11}$$

where, in the second step, the determinant over the remaining 2×2 block has been performed. When m_D is constant, this reduces to the well-known result for the fermion determinant. The result of this computation can be substituted into Eq. (4.34) for the decay rate.

With the above results, we can now rewrite the fermion radiative correction (4.22) to the tunneling action as

$$B_D^{(1)} \;=\; B_{D+}^{(1)} \;+\; B_{D-}^{(1)}, \tag{5.12}$$

where

$$B^{(1)}_{D\pm} = -\,\ln\,\frac{\det\,D^{-1}_{\pm}(\varphi_B)}{\det\,D^{-1}_{\pm}(v)}, \tag{5.13a}$$

$$D^{-1}_{\pm}(\varphi_B\,;x) = -\,\partial^2\,+\,\kappa^2\varphi_B^2(z)\,\pm\,\kappa\,\partial_z\varphi_B(z). \tag{5.13b}$$

The problem has thus been reduced to one of evaluating the determinants of scalar fluctuation operators. This can be accomplished by first calculating the Green's functions $D_\pm(\varphi_B;x)$, as well as their Fourier transforms with respect to the coordinates parallel to the bubble wall, as in Eq. (5.2). From these, the quantities $B^{(1)}_{D\pm}$ can be obtained in analogy with the determinant for the scalar field in Eq. (5.4), i.e.

$$\begin{aligned} B^{(1)}_{D\pm} = &\int\limits_{-\infty}^{\infty}\mathrm{d}z\int\mathrm{d}^3\mathbf{x}\int\limits_0^\infty\mathrm{d}s\int\limits_0^\Lambda\frac{\mathbf{k}^2\,\mathrm{d}|\mathbf{k}|}{2\pi^2}\\ &\times\Big[D_\pm\big(\varphi_B;z,z,\sqrt{\mathbf{k}^2+s}\big)\;-\;D_\pm\big(v;z,z,\sqrt{\mathbf{k}^2+s}\big)\Big]. \end{aligned} \tag{5.14}$$

The fermionic tadpole is now most straightforwardly obtained by functionally differentiating the one-loop determinant as in Eq. (4.29):

$$\Pi_D(\varphi_B;x)\,\varphi_B(x) = \left.\frac{\delta B^{(1)}_{D+}[\varphi]}{\delta\varphi(x)}\right|_{\varphi_B}\;+\;\left.\frac{\delta B^{(1)}_{D-}[\varphi]}{\delta\varphi(x)}\right|_{\varphi_B}. \tag{5.15}$$

We emphasize that $\delta/\delta\varphi$ denotes the functional derivative and, after making use of the Jacobi formula, we obtain from Eq. (5.13) that

$$\left.\frac{\delta B^{(1)}_{D\pm}[\varphi]}{\delta\varphi(x)}\right|_{\varphi_B} = -\,2\,\kappa^2 D_\pm(\varphi_B;x)\,\varphi_B\pm\,\kappa\,\partial_z D_\pm(\varphi_B;x). \tag{5.16}$$

These expressions can be substituted into Eqs. (4.30) and (4.29) in order to obtain the fermion contribution to the one-loop correction $\delta\varphi$ to the bounce. We also note from Eqs. (4.29), (5.15) and (5.16) that there follows the identity for the spinor trace:

$$\mathrm{tr_S}D(\varphi_B;x,x) = \sum_\pm\Big(2\,\kappa D_\pm(\varphi_B;x)\,\varphi_B\;\mp\;\partial_z D_\pm(\varphi_B;x)\Big). \tag{5.17}$$

In the homogeneous limit $\varphi_B = \text{const.}$, D_+ and D_- coincide, and we quickly recover the familiar result for the one-loop fermion determinant — including the factor of 4 from the spinor trace — after summing over $\pm$.

It is also possible to compute $D(\varphi_B;x,x')$ and all of its spinor components directly by solving the equations derived in Appendix B which can be applied to more general situations. While this is calculationally more cumbersome, we have checked the analytical and numerical results for the fermion loop effects reported on below using both methods.

5.1.2 One-loop correction to the bounce in the planar-wall limit

Acting on Eq. (4.30) with the tree-level Klein-Gordon operator, we obtain the EoM for the one-loop corrections to the bounce

$$\left[\frac{\mathrm{d}^2}{\mathrm{d}z^2}\,+\,\mu^2\,-\,\frac{\lambda}{2}\,\varphi_B^2\right]\,\delta\varphi\;=\;\Pi(\varphi_B;x)\,\varphi_B. \tag{5.18}$$

The operator in front of $\delta\varphi$ is simply $G^{-1}(\varphi_B; z, z', \mathbf{k})$ for $\mathbf{k} = \mathbf{0}$ (see Eq. (5.3)) whose Green's function has an analytic expression [59]:

$$\begin{aligned} G(\varphi_B; z, z', \mathbf{k}) \equiv G(u, u', \nu) = \frac{1}{2\gamma\,\nu} \Bigg[& \theta(u-u') \left(\frac{1-u}{1+u}\right)^{\frac{\nu}{2}} \left(\frac{1+u'}{1-u'}\right)^{\frac{\nu}{2}} \\ & \times \left(1 - 3\frac{(1-u)(1+\nu+u)}{(1+\nu)(2+\nu)}\right) \\ & \times \left(1 - 3\frac{(1-u')(1-\nu+u')}{(1-\nu)(2-\nu)}\right) + (u \leftrightarrow u') \Bigg], \end{aligned} \tag{5.19}$$

where $\nu = 2\sqrt{1 + \mathbf{k}^2/(4\gamma^2)}$ and u is defined in Eq. (4.2). Convoluting Eq. (5.18) with the above Green's function, we obtain

$$\delta\varphi(u) \;=\; -\frac{v}{\gamma} \int_{-1}^{1} \mathrm{d}u' \; \frac{u'\, G(u, u', 2)\, \Pi(\varphi_B; u')}{1 - u'^2}. \tag{5.20}$$

As can be seen from Eq. (5.19), $G(u, u', \nu)$ is singular as $\nu \to 2$, i.e. $|\mathbf{k}| \to 0$. However, since $\Pi(u')$ is an even function, the part of the integrand multiplied by $G(u, u', 2)$ is an odd function in u'. The integral remains finite because the singularity of $G(u, u', 2)$ turns out to reside in the even part. We can therefore replace $G(u, u', 2)$ in Eq. (5.20) with the odd part of the Green's function [59]

$$G^{\mathrm{odd}}(u, u') \;\equiv \frac{1}{2}\left(G(u, u', 2) \;-\; G(u, -u', 2)\right), \tag{5.21}$$

which can be expressed as [59]

$$G^{\mathrm{odd}}(u, u') = \vartheta(u-u') \frac{1}{32\gamma} \frac{1-u^2}{1-u'^2} \left[2u'(5 - 3\,u'^2) + 3(1-u'^2)^2 \ln\frac{1+u'}{1-u'}\right] + (u \leftrightarrow u') \tag{5.22}$$

in the domain $0 \le u, u' \le 1$. For given $\Pi(u)$, we can thus compute the first correction to the bounce.

5.2 Renormalization

It is well known that the loop calculations bring ultraviolet divergences and need renormalization. We therefore add the following counterterms to the Lagrangian in Eq. (4.1):

$$\mathcal{L} \;\to\; \mathcal{L} + \frac{1}{2}\delta Z (\partial_\mu \varphi)^2 + \frac{1}{2}\delta\mu^2\varphi^2 + \frac{1}{4!}\delta\lambda\varphi^4. \tag{5.23}$$

The absence of a counterterm corresponding to the Yukawa interaction is due to the fact that the fermionic fields Ψ and $\bar{\Psi}$ cannot possess non-vanishing background field values. The ultraviolet divergences come from the scalar and fermion loops due to the quartic scalar and Yukawa interactions. They appear when we perform the loop integrals in momentum space in, e.g., Eqs. (5.2) and (5.4). Since we use the mixed three-plus-one representation of momentum space parallel to the three-dimensional hypersurface and position space in the perpendicular direction, we introduce a three-momentum cutoff Λ.

We must specify the counterterms with certain renormalization conditions, such that the physical results are independent of the cutoff Λ. For the problem of false vacuum decay, it is very convenient to impose these conditions on the derivatives of the effective action evaluated at the false vacuum. The effective action is given by Eq. (4.20) in the one-loop approximation. When ignoring derivative operators, the effective action in the false vacuum coincides with the Coleman-Weinberg (CW) potential [12]. We therefore use the derivatives of the latter to define the renormalization conditions for μ^2 and λ, and these are worked out in Sec. 5.2.1.

The radiative effects also lead to corrections to the wave-function normalization which are logarithmically divergent for the fermion loops and finite for the scalar loops. In Sec. 5.2.2, we extract these terms analytically by a gradient expansion of the Green's functions. The gradient expansion of the Green's functions then gives the leading gradient corrections to the CW potential which can then be identified with the wave-function normalization. We impose the standard unit residue at the single-particle pole as a wave-function renormalization condition. Combining the counterterms with the one-loop determinants and tadpole functions, we then summarize these results in Sec. 5.2.3. In this way, renormalized results for $B^{(1)}$, $B^{(2)}$ and the tadpole function are obtained, which lead directly to the renormalized decay rate and the correction $\delta\varphi$ to the bounce.

5.2.1 Renormalization of the mass and the quartic coupling constant using the Coleman-Weinberg potential

The CW potential is obtained by evaluating the effective action (4.20) for configurations φ that are constant throughout spacetime. It is given by

$$\begin{aligned}\Gamma_{\mathrm{CW}}[\varphi] = S[\varphi] &+ \frac{1}{2}\int \mathrm{d}^4x \int \frac{\mathrm{d}^4k}{(2\pi)^4} \ln\frac{k^2+U''(\varphi)}{k^2+U''(v)} \\ &- 2\int \mathrm{d}^4x \int \frac{\mathrm{d}^4k}{(2\pi)^4} \ln\frac{k^2+\kappa^2\varphi^2}{k^2+\kappa^2 v^2}.\end{aligned} \tag{5.24}$$

It can be directly read from the above expression that

$$B_S^{(1)\mathrm{hom}}[\varphi] = \frac{1}{2}\int \mathrm{d}^4x \int \frac{\mathrm{d}^4k}{(2\pi)^4} \ln\frac{k^2+U''(\varphi)}{k^2+U''(v)}, \tag{5.25a}$$

$$B_D^{(1)\mathrm{hom}}[\varphi] = -2\int \mathrm{d}^4x \int \frac{\mathrm{d}^4k}{(2\pi)^4} \ln\frac{k^2+\kappa^2\varphi^2}{k^2+\kappa^2 v^2}, \tag{5.25b}$$

where the superscript "hom" means that the quantities are obtained assuming the background field φ is constant. These quantities can also be calculated from the Green's functions in the three-plus-one representation for the limit of a constant background field, using Eqs. (5.4) and (5.14) (cf. Eqs. (5.44) and (5.48) later). Factoring out the integral over the spacetime four-volume, one gets the CW potential

$$U_{\mathrm{CW}}(\varphi) = U(\varphi) + \frac{1}{2}\int \frac{\mathrm{d}^4k}{(2\pi)^4} \ln\frac{k^2+U''(\varphi)}{k^2+U''(v)} - 2\int \frac{\mathrm{d}^4k}{(2\pi)^4} \ln\frac{k^2+\kappa^2\varphi^2}{k^2+\kappa^2 v^2}. \tag{5.26}$$

Considering the planar-wall approximation and the corresponding three-plus-one representation that we have employed, we make a three-plus-one decomposition of momentum

space in the four-dimensional momentum integral. Carrying out the integral over k_0, we obtain

$$U_{\rm CW}(\varphi) = U(\varphi) + \frac{1}{2}\int\frac{{\rm d}^3\mathbf{k}}{(2\pi)^3}\Big(\sqrt{\mathbf{k}^2+U''(\varphi)}-\sqrt{\mathbf{k}^2+U''(v)}\Big) - 2\int\frac{{\rm d}^3\mathbf{k}}{(2\pi)^3}\Big(\sqrt{\mathbf{k}^2+\kappa^2\varphi^2}-\sqrt{\mathbf{k}^2+\kappa^2 v^2}\Big). \tag{5.27}$$

Evaluating the remaining integral up to a cutoff Λ, this yields

$$U_{\rm CW}(\varphi) = U(\varphi) + \bigg\{\bigg[\frac{\Lambda^2}{16\pi^2}\Big(-\mu^2+\frac{\lambda}{2}\varphi^2\Big)+\frac{1}{64\pi^2}\Big(-\mu^2+\frac{\lambda}{2}\varphi^2\Big)^2\Big(\ln\frac{-\mu^2+\frac{\lambda}{2}\varphi^2}{4\Lambda^2}+\frac{1}{2}\Big) - \frac{\Lambda^2\kappa^2\varphi^2}{4\pi^2}-\frac{\kappa^4\varphi^4}{16\pi^2}\Big(\ln\frac{\kappa^2\varphi^2}{4\Lambda^2}+\frac{1}{2}\Big)\bigg]-(\varphi\to v)\bigg\}. \tag{5.28}$$

The renormalized CW potential is obtained when adding the counterterms $\delta\mu^2$ and $\delta\lambda$ in accordance with Eq. (5.23) as

$$U_{\rm CW} \;\to\; U_{\rm CW} + \delta\mu^2(\varphi^2-v^2)/2 + \delta\lambda(\varphi^4-v^4)/4!, \tag{5.29}$$

where $\delta\mu^2$ and $\delta\lambda$ are specified by the following renormalization conditions:

$$\frac{\partial^2 U_{\rm CW}(\varphi)}{\partial\varphi^2}\Big|_{\varphi=v} = -\mu^2+\frac{\lambda}{2}v^2 = 2\mu^2, \tag{5.30a}$$

$$\frac{\partial^4 U_{\rm CW}(\varphi)}{\partial\varphi^4}\Big|_{\varphi=v} = \lambda. \tag{5.30b}$$

These counterterms are given explicitly in Eq. (5.51) below, along with the remaining one for the wave-function renormalization.

5.2.2 Wave-function renormalization through adiabatic expansion of the Green's functions

While the counterterms for the coupling constants can be obtained conveniently from the effective potential, the latter does not lead to conditions on the renormalization of the derivative operator, i.e. the wave-function normalization. Our objective is to express this additional counterterm in an analytic form. This can be achieved by performing a gradient expansion of the Green's functions around a constant background field configuration. We refer this calculation as an adiabatic or WKB expansion.

We first construct the adiabatic expansion of the scalar Green's function, which satisfies

$$\big(-\partial_z^2+M^2(z)\big)\,G(\varphi_B;z,z',\mathbf{k}) = \delta(z-z'), \tag{5.31}$$

with

$$M^2(z) = \mathbf{k}^2 + U''(\varphi_B(z)). \tag{5.32}$$

This can be solved by the ansatz

$$G(\varphi_B;z,z',\mathbf{k}) = \theta(z-z')A^>(z')f^>(z)+\theta(z'-z)A^<(z')f^<(z), \tag{5.33}$$

where

$$\big(-\partial_z^2 + M^2(z) \big) f^{\gtrless}(z) = 0 \tag{5.34}$$

and where we impose

$$f^{>}(z) \to 0, \text{ for } z \to +\infty, \tag{5.35a}$$
$$f^{<}(z) \to 0, \text{ for } z \to -\infty. \tag{5.35b}$$

The latter enforce the boundary condition that the Green's function vanishes at infinity.

In order to isolate the leading gradient effects, we make the WKB ansatz

$$f^{\gtrless}(z) = \frac{1}{\sqrt{2W(z)}}\, e^{\mp \int^z \mathrm{d}z'\, W(z')}. \tag{5.36}$$

When substituted into Eq. (5.34), this leads to

$$W^2 = M^2 - \frac{3}{4}\frac{W'^2}{W^2} + \frac{1}{2}\frac{W''}{W}, \tag{5.37}$$

where the prime $'$ used in this subsection denotes a derivative with respect to z. In the gradient expansion, the zeroth-order approximation to W is given by ${W^{(0)}}^2 = M^2$. Substituting this back into Eq. (5.37), one obtains

$${W^{(1)}}^2 = -\frac{3}{4}\frac{{W^{(0)}}'^2}{{W^{(0)}}^2} + \frac{1}{2}\frac{{W^{(0)}}''}{W^{(0)}}. \tag{5.38}$$

Demanding continuity and the correct jump in the first derivative to reproduce the delta function in Eq. (5.31) at the coincident point $z = z'$, we obtain the matching conditions

$$A^{>}(z) f^{>}(z) = A^{<}(z) f^{<}(z), \tag{5.39a}$$
$$A^{>}(z) f^{>\prime}(z) - A^{<}(z) f^{<\prime}(z) = -1, \tag{5.39b}$$

such that

$$G(\varphi_B; z, z, \mathbf{k}) = \frac{f^{>}(z) f^{<}(z)}{W[f^{>}(z), f^{<}(z)]}, \tag{5.40}$$

where

$$W[f^{>}(z), f^{<}(z)] = f^{>}(z) f^{<\prime}(z) - f^{>\prime}(z) f^{<}(z) \tag{5.41}$$

is the Wronskian. Putting these results together, we find that the Green's function is approximated to second order in gradients by

$$G(\varphi_B; z, z, \mathbf{k}) \approx \frac{1}{2}\frac{1}{M(z)} + \frac{3}{16}\frac{M'^2(z)}{M^5(z)} - \frac{1}{8}\frac{M''(z)}{M^4(z)}. \tag{5.42}$$

In terms of the local squared mass $m_S^2(z) = U''(\varphi_B(z))$, this reads

$$G(\varphi_B; z, z, \mathbf{k}) \approx \frac{1}{2}\frac{1}{\sqrt{\mathbf{k}^2 + m_S^2(z)}} + \frac{5}{16}\frac{m_S^2(z) \cdot m_S'^2(z)}{(\mathbf{k}^2 + m_S^2(z))^{\frac{7}{2}}} - \frac{1}{8}\frac{m_S(z) \cdot m_S''(z) + m_S'^2(z)}{(\mathbf{k}^2 + m_S^2(z))^{\frac{5}{2}}}. \tag{5.43}$$

The first term on the RHS can be identified with the Green's function in the three-plus-one representation and for a homogeneous background. We explicitly define this as

$$G^{\text{hom}}(\varphi_B; z, z', \mathbf{k}) = \frac{1}{2}\frac{1}{\sqrt{\mathbf{k}^2 + m_S^2(z)}}\Big(\vartheta(z-z')\mathrm{e}^{\sqrt{\mathbf{k}^2+m_S^2(z)}(z'-z)} + \vartheta(z'-z)\mathrm{e}^{\sqrt{\mathbf{k}^2+m_S^2(z)}(z-z')}\Big), \tag{5.44}$$

where we show the general expression that also holds away from the coincident points in order to highlight the exponentially decaying behavior of the Green's functions for large separations. G^{hom} can be used to compute the loop contributions without gradient effects which then can be compared with those that include gradient corrections.

The last two terms in Eq. (5.43) are the leading gradient corrections. These corrections are $\sim 1/|\mathbf{k}|^5$ and therefore the three-momentum integral leads to a finite correction to the derivative operators of the field Φ, i.e. the wave-function normalization, in the effective action. It is most straightforward to determine this correction by substituting the result (5.43) into Eq. (5.4):

$$B_S^{(1)} \supset \int_{-\infty}^{\infty} \mathrm{d}z \int \mathrm{d}^3\mathbf{x}\, \frac{1}{384\,\pi^2}\, \frac{\lambda^2\varphi^2\varphi'^2}{-\mu^2 + \frac{\lambda}{2}\varphi^2}, \tag{5.45}$$

where we recall that $B_S^{(1)}$ is related to the functional determinants through the definitions (4.25) and to the effective action through Eq. (4.20). While this result is finite, i.e. independent of the momentum cutoff, the corresponding contribution $B_D^{(1)}$ from the Dirac field is not, as we will see below.

The fermionic contributions to the wave-function normalization can be computed analogously. The propagators $D_\pm(\varphi_B; z, z', \mathbf{k})$ satisfy the same equation as $G(\varphi_B; z, z', \mathbf{k})$, i.e. Eq. (5.31), but with

$$M^2(z) = \mathbf{k}^2 + \kappa^2\varphi_B^2(z) \pm \kappa\partial_z\varphi_B(z). \tag{5.46}$$

Solving that equation in the WKB approximation, we find

$$D_+(\varphi_B; z, z, \mathbf{k}) + D_-(\varphi^{(0)}; z, z, \mathbf{k}) \approx \frac{1}{\sqrt{\mathbf{k}^2 + m_D^2(z)}} + \frac{5}{8}\frac{m_D^2(z)\, m_D'^2(z)}{(\mathbf{k}^2 + m_D^2(z))^{\frac{7}{2}}} + \frac{1}{8}\frac{m_D'^2(z) - 2m_D(z)\, m_D''(z)}{(\mathbf{k}^2 + m_D^2(z))^{\frac{5}{2}}}. \tag{5.47}$$

Again, in order to isolate the gradient effects in Sec. 5.3, we define the contributions that arise in homogeneous backgrounds without gradients as

$$D_\pm^{\text{hom}}(\varphi_B; z, z, \mathbf{k}) = \frac{1}{2\sqrt{\mathbf{k}^2 + m_D^2(z)}}. \tag{5.48}$$

We note that, while the three-momentum integrals over the derivative terms in Eq. (5.47) are finite, the trace of the coincident Dirac propagator (5.17), and therefore the tadpole

correction, cf. Eqs. (4.29), (5.15) and (5.16), contains an extra derivative with respect to z. This generates a logarithmically divergent contribution that can be identified with the divergent part of the wave-function renormalization. Computing the corrections to the derivative operators in the effective action using Eq. (5.14), we find

$$B_D^{(1)} \supset \int_{-\infty}^{\infty} \mathrm{d}z \int \mathrm{d}^3\mathbf{x}\, \frac{\kappa^2\varphi'^2}{8\pi^2}\bigg(- \ln\frac{\kappa^2\varphi^2}{\Lambda^2} + 2\ln 2 - \frac{8}{3}\bigg). \tag{5.49}$$

We use this result along with Eq. (5.45) in order to specify the renormalization condition

$$\frac{\partial^2}{\partial(\partial_\nu\varphi)^2}\bigg[\mathcal{L} + \frac{1}{384\,\pi^2}\frac{\lambda^2\varphi^2(\partial_\mu\varphi)^2}{-\mu^2+\frac{\lambda}{2}\varphi^2} + \frac{\kappa^2}{8\pi^2}(\partial_\mu\varphi)^2\bigg(- \ln\frac{\kappa^2\varphi^2}{\Lambda^2} + 2\ln 2 - \frac{8}{3}\bigg)\bigg]_{\varphi\,=\,v} = 1, \tag{5.50}$$

where the Lagrangian is implied to contain the counterterms as per the definition (5.23). This relation fixes the counterterm δZ.

5.2.3 Renormalized bounce, effective action and decay rate

We can now summarize the one-loop counterterms as

$$\delta Z = \frac{\kappa^2}{8\pi^2}\bigg(\ln\frac{\kappa^2 v^2}{\Lambda^2} - 2\ln 2 + \frac{8}{3}\bigg) - \frac{\lambda}{64\pi^2}, \tag{5.51a}$$

$$\delta\mu^2 = -\frac{\lambda\mu^2}{32\pi^2}\bigg(\frac{2\Lambda^2}{\mu^2} - \ln\frac{\mu^2}{2\Lambda^2} - 31\bigg) + \frac{\Lambda^2\kappa^2}{2\pi^2}\bigg(- \frac{27\kappa^2\mu^2}{\lambda\Lambda^2} + 1\bigg), \tag{5.51b}$$

$$\delta\lambda = -\frac{3\lambda^2}{32\pi^2}\bigg(\ln\frac{\mu^2}{2\Lambda^2} + 5\bigg) + \frac{3\kappa^4}{2\pi^2}\bigg(\ln\frac{3\kappa^2\mu^2}{2\lambda\Lambda^2} + \frac{14}{3}\bigg). \tag{5.51c}$$

The renormalized tadpole correction can then be defined as

$$\Pi^{\mathrm{ren}}\,\varphi_B = \Pi\,\varphi_B + \delta\mu^2\,\varphi_B + \frac{\delta\lambda}{3!}\,\varphi_B^3 - \delta Z\,\partial_z^2\varphi_B, \tag{5.52}$$

which should replace $\Pi\,\varphi_B$ in the equation of motion (4.26) for the bounce. Finally, to the one-loop contributions to the effective action [i.e. to the exponent of Eq. (2.7)], we consistently add

$$\delta B^{(1)} = \int \mathrm{d}^4x\,\bigg[\frac{1}{2}\,\delta\mu^2\,(\varphi_B^2 - v^2) + \frac{1}{4!}\,\delta\lambda\,(\varphi_B^4 - v^4) + \frac{1}{2}\,\delta Z\,(\partial_z\varphi_B)^2\bigg], \tag{5.53}$$

and the renormalized result for $B^{(2)}$ is obtained when replacing Π with Π^{ren} in Eq. (4.33).

5.3 Numerical studies

In this section, we apply the methods elaborated above in a specific numerical study. We will focus on, in particular, the comparison between the quantum corrections with and without the gradient effects from the background inhomogeneity. We also isolate the contributions from the scalar and the fermion loops in presenting the results.

To enhance the corrections to the bounce and decay rate compared to the other quantum effects that appear at second order in perturbation theory, we will extend the fermion field Ψ to N_Ψ copies. The fermions may be referred to as *spectators* since their vacuum expectation values do not change through the bubble wall, in contrast to the Higgs field Φ. In order to directly compare effects from fermion and scalar loops, we introduce additional scalar spectator fields χ_i with $i = 1, \ldots, N_\chi$ that also couple to the Higgs field. In this setup, the Lagrangian without counterterms is

$$\begin{aligned}\mathcal{L} = &\sum_{i=1}^{N_\Psi} \left\{ \bar{\Psi}_i \gamma_\mu \partial_\mu \Psi_i + \kappa\, \bar{\Psi}_i \Phi \Psi_i \right\} \; + \; \frac{1}{2}(\partial_\mu \Phi)^2 \; + \; U(\Phi) \\ &+ \sum_{i=1}^{N_\chi} \left\{ \frac{1}{2}(\partial_\mu \chi_i)^2 + \frac{1}{2} m_{\chi_i}^2 \chi_i^2 + \frac{\alpha}{4} \Phi^2 \chi_i^2 \right\}. \end{aligned} \tag{5.54}$$

For simplicity and in order to have the scalar and fermionic spectators have similar properties, we take $m_{\chi_i} = 0$. The developments for the effective action and the tadpole corrections of the previous sections generalize straightforwardly to loops of the fields χ_i, yielding one-loop corrections $B_\chi^{(1)}$ to the action and tadpole functions Π_χ.

When enhanced by N_Ψ copies of the fermion fields, the term $B_D^{(2)}$ then contains the dominant two-loop contributions from fermions to the effective action. To illustrate this, we present a diagrammatic representation of the fermionic corrections to the bounce action in Fig. 5.2. Diagram (a) is the one-loop term $B_D^{(1)}$ of order $(\kappa^4/\lambda^2)N_\Psi$. Note that the dependence on λ comes from the background bounce $\varphi_B \sim 1/\sqrt{\lambda}$ appearing in the Dirac operator. Diagram (b) is the main contribution to $B_D^{(2)}$, which is of order $(\kappa^6/\lambda^2)N_\Psi^2$, cf. Eqs. (4.33) and (5.20). In addition to diagram (b), there is also a contribution of order $(\kappa^6/\lambda^2)N_\Psi$ represented by diagram (c), which we do not calculate. Diagram (c) is therefore suppressed by a relative factor of $1/N_\Psi$ compared to diagram (b) and hence may be neglected, cf. also Ref. [59].

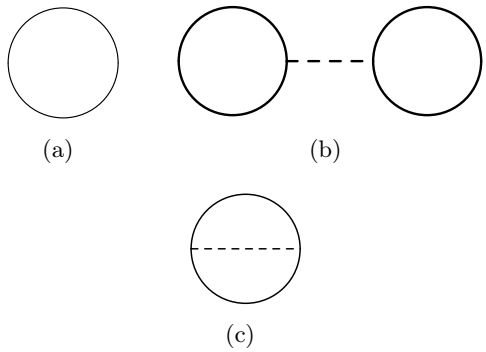

Figure 5.2: Diagrammatic representation of the fermionic contributions to the effective action: (a) is the one-loop term $B_D^{(1)}$, of order $\mathcal{O}[(\kappa^4/\lambda^2)N_\Psi]$, (b) is the $\mathcal{O}[(\kappa^6/\lambda^2)N_\Psi^2]$ contribution to $B_D^{(2)}$ and (c) is the term of $\mathcal{O}[(\kappa^6/\lambda^2)N_\Psi]$. Solid lines denote the Dirac propagator $D(\varphi_B; x, x')$; dashed lines denote the scalar propagator $G(\varphi_B; x, x')$.

We decompose the tadpole function and the one-loop corrections to the action as

$$\Pi \;=\; \Pi_S \,+\, \Pi_D \,+\, \Pi_{\rm spec}\;, \tag{5.55}$$

$$B^{(1)} \;=\; B_S^{(1)} \,+\, B_D^{(1)} \,+\, B_{\rm spec}^{(1)} \tag{5.56}$$

in order to compare the loop contributions from the various species. Here the subscript S, D and "spec" indicate the Higgs scalar field Φ, the Dirac fermion spectators Ψ_i and the scalar spectator fields χ_i, respectively. It shall be understood that all results presented in this section for the tadpole corrections Π, as well as the corrections to the effective action $B^{(1,2)}$, are renormalized, i.e. include contributions from counterterms.

The Green's functions $G(\varphi_B; x, x)$ and $D(\varphi_B; x, x)$ are to be replaced by $G^{\rm hom}(\varphi_B; x, x)$ and $D^{\rm hom}(\varphi_B; x, x)$ in Eqs. (5.4) and (5.14) to compute the one-loop action terms in the homogeneous background. Including the corresponding spectator corrections, we thus have

$$B^{(1)\rm hom} \;=\; B_S^{(1)\rm hom} \,+\, B_D^{(1)\rm hom} \,+\, B_{\rm spec}^{(1)\rm hom}\;. \tag{5.57}$$

Accordingly, substituting the homogeneous Green's functions in Eqs. (4.28), (4.29) (and analogously for the scalar spectators), we also obtain

$$\Pi^{\rm hom} \;=\; \Pi_S^{\rm hom} \,+\, \Pi_D^{\rm hom} \,+\, \Pi_{\rm spec}^{\rm hom}\;. \tag{5.58}$$

5.3.1 Tadpoles and corrections to the bounce

Before we present the numerical results, we choose the parameters

$$\begin{aligned} &\mu = 1\;,\;\; \lambda = 2\;,\;\; \kappa = 0.5, \\ &\alpha = 0.5\;,\;\; N_\Psi = N_\chi = 10, \end{aligned} \tag{5.59}$$

as a benchmark point in the following. The above parameters have been chosen such that there is a substantial amount of accidental cancellation between the fermion and scalar loop contributions as can be seen from the plot of the total tadpole correction Π in Fig. 5.3. In such a situation, the relative impact of the gradient corrections can be of order one. All tadpole corrections Π are even functions about the center of the bubble wall, as expected. We note that it is the combination $\varphi_B \Pi(\varphi_B; y)$ that acts as a source for the radiative correction to the bounce as can be seen from Eq. (4.30). While the tadpole functions are largest around the point $u = 0$, the classical bounce φ_B, which is an odd function, takes zero value at $u = 0$. We therefore expect that the relative impact on the radiative correction $\delta\varphi$ to the bounce is suppressed.

Due to a transition to the tachyonic region in the classical potential, which causes a divergence in the derivative of Π_S, there are bumps around $u = \pm 0.4$ in the graph of Π_S without gradient contributions. While in the graph of the full one-loop result for Π_S, which accounts for gradient corrections, these bumps are absent because the field gradients counteract the tachyonic instability. There is of course still a particular negative mode that represents the vacuum instability even for the inhomogeneous bounce background. But it has no impact on the full one-loop result for Π_S since the negative mode corresponds

to $\mathbf{k} = 0$ and makes no contribution as commented below Eq. (5.4).[17] For the fermionic and scalar spectator fields, there are no tachyonic regions across the bubble wall.

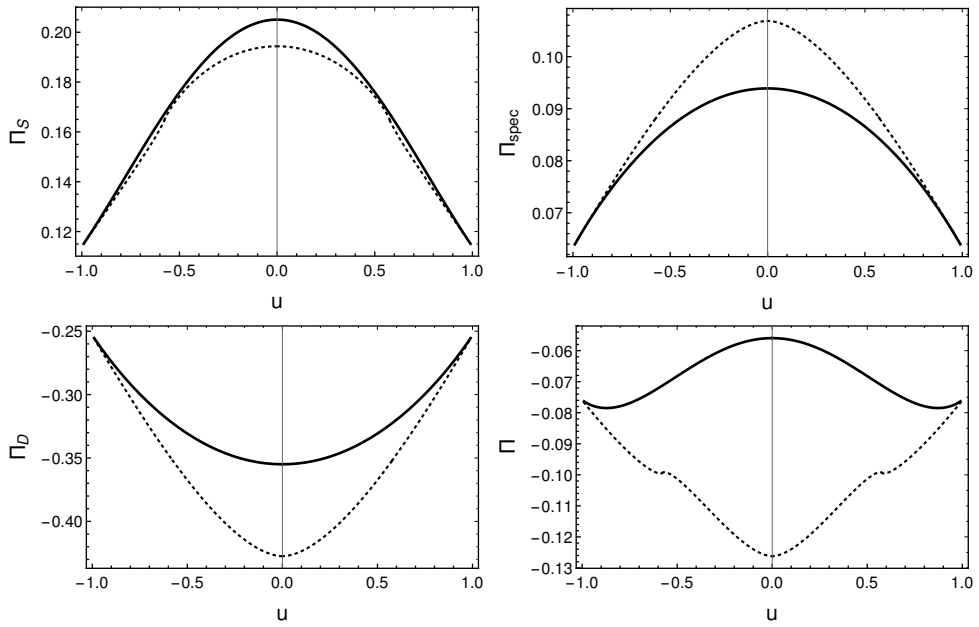

Figure 5.3: The renormalized tadpole contributions Π as a function of u. The tadpole Π is the total result, Π_S is the contribution from the scalar field Φ, $\Pi_{\rm spec}$ is from scalar spectator fields χ_i and Π_D is from Dirac spectator fields Ψ_i. Graphs with solid lines show the tadpole corrections Π that include gradient effects; dotted graphs show the corrections $\Pi^{\rm hom}$, where these effects are ignored.

We focus in particular on the comparison between the full one-loop results with the tadpole functions without gradient corrections. The latter are calculated by assuming a constant background $\varphi = \varphi_B(u)$ for each value of u. For the field Φ, the squared mass may become negative for a certain range of u such that the resulting tadpole function acquires an imaginary part that we do not show in the diagrams. This imaginary part arises if we assume a constant field configuration, because there is a continuum of negative modes contributing to the Gaussian integrals in the tachyonic region where $-\mu^2 + (\lambda/2)\varphi^2 < 0$. The imaginary part is an artifact because constant configurations do not correspond to extremal points (or stationary points) of the effective action away from the minima of the potential at $\pm v$. As explained in Ref. [59], imaginary parts, except for the one associated with the negative mode, do not appear when calculating the loop diagrams for fluctuations around the full bounce solutions that account for gradients, i.e. when expressing the loops in terms of the Green's function solutions in the bounce background.

We can see from Fig. 5.3 that the gradient effects suppress the tadpole corrections when compared with the corrections without gradients for the fermionic and scalar spectator fields. While for the Higgs field, the tadpole correction appears to be enhanced compared to the real part of the loop correction without gradients. This enhancement shall not be

[17] The fact that the negative mode contribute an imaginary part in the effective action has been taken into account by the $i\pi/2$ in Eq. (4.21).

directly compared with corrections from the spectator fields because the tachyonic modes and the imaginary part in the CW potential arising from the Higgs field have no direct physical interpretation.

We compare the radiative corrections to the bounce with and without gradient effects in Figs. 5.4 and 5.5. They are calculated by substituting $\Pi_{S,D,\mathrm{spec}}$ and $\Pi^{\mathrm{hom}}_{S,D,\mathrm{spec}}$ into Eq. (5.20). We find that the turning points in the functions $\delta\varphi_{D,\mathrm{spec}}$ are softened relative to those in $\delta\varphi^{\mathrm{hom}}_{D,\mathrm{spec}}$, see Fig. 5.5. That means for the Dirac spectator fields Ψ_i (subscript "D") and the scalar spectators χ_i (subscript "spec"), the gradient effects tend to smooth the field profile. While for the correction $\delta\varphi_S$ from Higgs loops, there appears to be an opposite effect. However, since we have dropped the imaginary parts from Π^{hom}_S, this opposite effect is not directly comparable with the one from the spectator fields. We note that the correction from the Dirac spectators is larger than that from the scalar spectators by roughly a factor of minus four. This factor is accounted for by the number of Dirac spinor degrees of freedom and the opposite sign of the fermion loop. [The squared mass of the Dirac spectator fields across the wall is $\kappa^2\varphi^2(z)$, for the scalar spectators it is $\alpha\,\varphi^2(z)/2$. For the values of α and κ chosen in Eq. (5.59), these are therefore coincident, such that the relative factor of minus four is actually exact when ignoring gradients.] The relative impact of the gradient corrections on $\delta\varphi$ from the Dirac spectators turns out to be about twice as that from the scalar spectators.

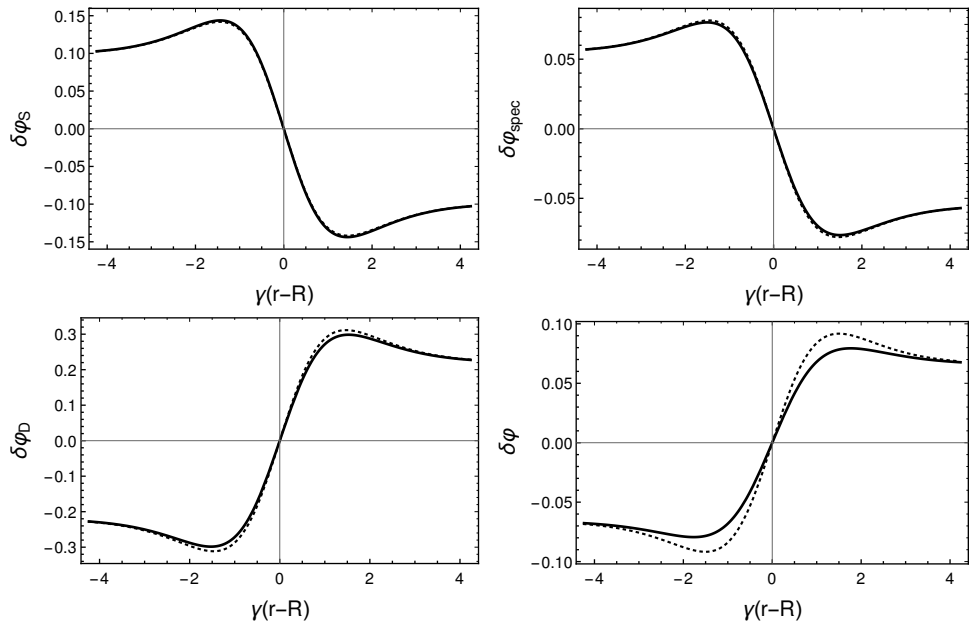

Figure 5.4: The correction $\delta\varphi$ to the bounce as a function of $\gamma(r-R)$ with ($\delta\varphi$, solid) and without ($\delta\varphi^{\mathrm{hom}}$, dotted) gradients in separate panels for the contributions $\delta\varphi_S$ from the Higgs field, $\delta\varphi_{\mathrm{spec}}$ from the scalar spectators, $\delta\varphi_D$ from the Dirac spectators and for the total correction $\delta\varphi$.

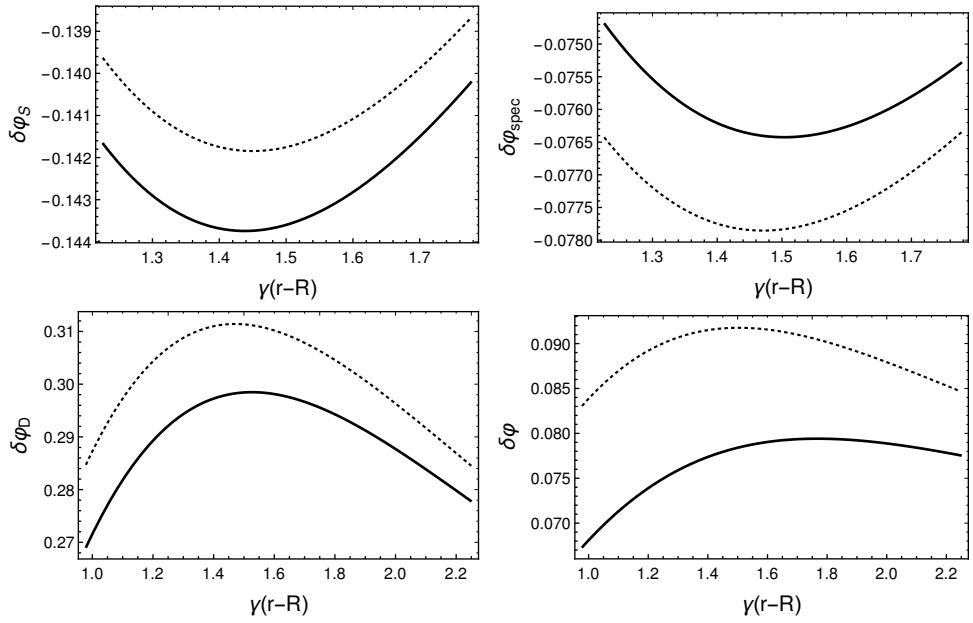

Figure 5.5: Same as Fig. 5.4, showing the detail around the point where the radiative correction to the bounce is maximal.

5.3.2 Corrections to the action

In this subsection, we investigate the gradient effects on the action and the tunneling rate. Since in the action there is an integral over the four-dimensional space which gives an infinite value, we therefore define the contributions to the action *per unit area of bubble surface*

$$\bar{B} \;=\; \frac{B}{2\pi^2 R^3}\,, \qquad \bar{B}^{(1,2)} \;=\; \frac{B^{(1,2)}}{2\pi^2 R^3}\,, \tag{5.60}$$

and accordingly for the individual contributions from the Higgs, Dirac and scalar spectator fields, as well as for the loop corrections $\bar{B}^{(1,2)\mathrm{hom}}$ derived from the Green's functions in the homogeneous background.

For the benchmark parameters (5.59), the results for the various corrections to the action are compared in Table 5.1. With or without gradient effects, we see that the corrections $B^{(1)}$ for the scalar loops are negative (leading to an enhanced decay rate) and for fermion loops, these are positive (leading to a suppressed decay rate). Since our renormalization conditions fix λ at the false vacuum, fermion loops lead to a running toward smaller $|\lambda|$ and scalar loops toward larger $|\lambda|$ around the center of the bounce, where $\varphi = 0$. From the tree-level action (4.3), we see that larger (smaller) λ lead to a faster (slower) decay rate, which qualitatively explains this numerical observation. As for the relative contributions from field gradients to $B^{(1)}$ shown in Table 5.1, we note that for Dirac spectators, these are larger by a factor of about four in comparison with the contribution from scalar spectators.

	(i) no gradients	(ii) gradients	[(ii)-(i)]/(i)
$\bar{B}^{(1)}_{\mathrm{S}}$	-0.583	-0.585	0.34%
$\bar{B}^{(1)}_{\mathrm{spec}}$	-0.320	-0.324	1.25%
$\bar{B}^{(1)}_{\mathrm{D}}$	1.278	1.345	5.24%
$\bar{B}^{(1)}$	0.375	0.436	16.3%
$\bar{B}^{(2)}$	5.085×10^{-4}	-5.719×10^{-3}	

Table 5.1: Comparison of $\bar{B}^{(1)}$ and $\bar{B}^{(2)}$ (i) without gradients (i.e. based on the Green's functions in homogeneous backgrounds) and (ii) with gradients (i.e. based on the Green's function in the background of the tree-level soliton). These quantities are computed for the benchmark point (5.59). We draw attention to the fact that the values of $\bar{B}^{(2)}$ differ in sign for cases (i) and (ii), leading to a relative increase in the tunneling rate when the gradients are included. For completeness, the value of $\bar{B}$ — which does not differ between cases (i) and (ii) — is approximately 2.828.

To avoid accidental conclusions specific to our benchmark parameters, in Figs. 5.6, 5.7 and 5.8, we show the results of varying the dimensionless couplings λ, κ and α separately about the benchmark point given in Eq. (5.59).

Since a change in the self-coupling λ of the Higgs field changes the shape of the bounce, λ-dependence is expected to exist for all three types of one-loop corrections: $\bar{B}^{(1)}_S$, $\bar{B}^{(1)}_D$, and $\bar{B}^{(1)}_{\mathrm{spec}}$. From Fig. 5.6, we see, however, that $\bar{B}^{(1)}_S$ is insensitive to the value of λ. This is because, in our perturbation expansion, one loop corresponds to one power in λ, such that $\bar{B}^{(1)}_S$ is one order higher in λ compared to $\bar{B}$, which itself scales as $1/\lambda$, cf. Eq. (4.3). In principle, there are further logarithmic dependencies on λ [cf., e.g., the effective potential (5.28)] but these turn out to cancel when performing the integral over $\mathrm{d}z$, as is shown analytically in Refs. [120, 59, 118].

Only the Dirac spectator correction $\bar{B}^{(1)}_D$ depends on κ and only the scalar spectator correction $\bar{B}^{(1)}_{\mathrm{spec}}$ depends on α and the corresponding dependences are presented in Figs. 5.7 and 5.8. When comparing the Dirac and scalar spectator contributions in Figs. 5.7 and 5.8, one should bear in mind that the squared masses depend on the couplings as $\kappa^2\varphi^2(z)$ and $\alpha\,\varphi^2(z)/2$, respectively. This explains the stronger curvature in the plot for Dirac spectators, that is, the stronger dependence on κ.

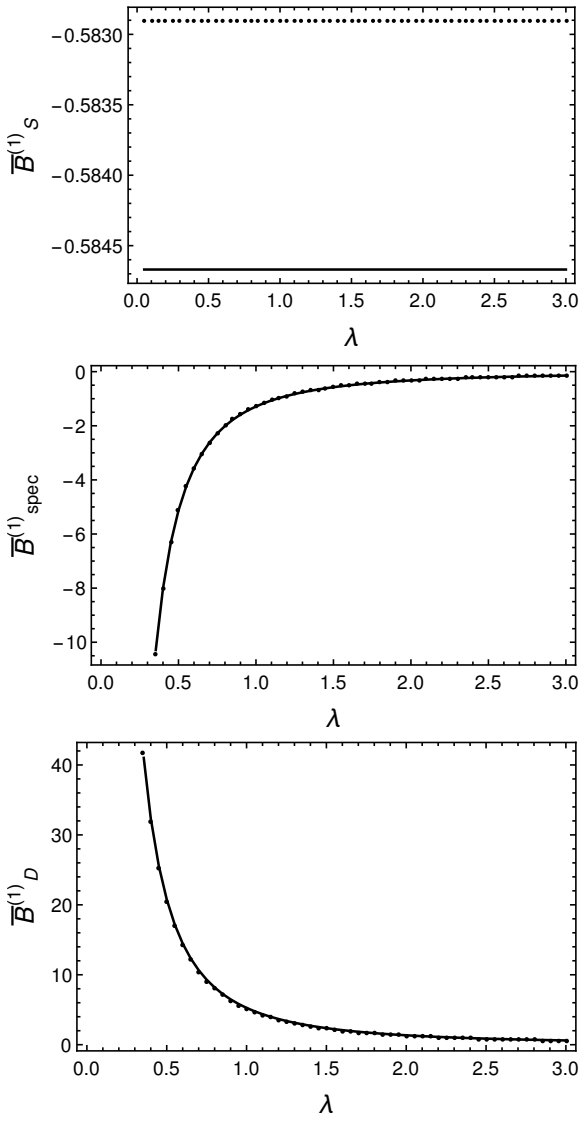

Figure 5.6: Dependence of the one-loop corrections to the bounce action on λ. Solid: $\bar{B}^{(1)}$ (i.e. with gradients). Dotted: $\bar{B}^{(1)\rm hom}$ (i.e. without gradients). The remaining parameters besides λ are given in Eq. (5.59).

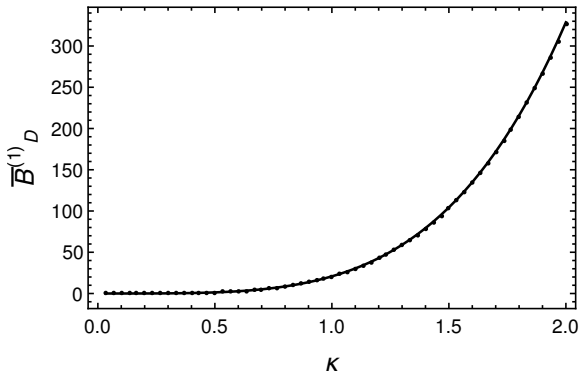

Figure 5.7: Dependence of the one-loop corrections to the bounce action on κ. Solid: $\bar{B}_D^{(1)}$ (i.e. with gradients). Dotted: $\bar{B}_D^{(1)\mathrm{hom}}$ (i.e. without gradients). The remaining parameters besides κ are given in Eq. (5.59).

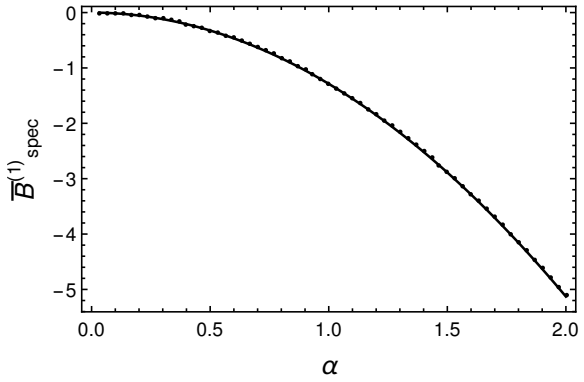

Figure 5.8: Dependence of the one-loop corrections to the bounce action on α. Solid: $\bar{B}_{\mathrm{spec}}^{(1)}$ (i.e. with gradients). Dotted: $\bar{B}_{\mathrm{spec}}^{(1)\mathrm{hom}}$ (i.e. without gradients). The remaining parameters besides α are given in Eq. (5.59).

In accordance with the above remarks on the effect of fermion and scalar loops on the decay rate, we can understand the dependence of $\bar{B}_{\mathrm{D}}^{(1)}$ on κ and of $\bar{B}_{\mathrm{spec}}^{(1)}$ on α in Figs. 5.7 and 5.8. As κ increases, $\bar{B}_D^{(1)}$ increases and therefore the decay rate decreases. This is due to a higher barrier from fermion fluctuations in the effective potential for larger Yukawa couplings. Similarly, as α increases, $\bar{B}_{\mathrm{spec}}^{(1)}$ decreases and therefore the decay rate increases. This implies that there is a lower barrier in the effective potential for larger couplings α. To illustrate this point, the dependence of the barrier in the CW potential (5.28) on κ and α is shown in Fig 5.9. We emphasize, however, that, while the CW potential can be used in order to interpret the leading effects from radiative corrections, it does not include the subleading gradient effects on the particles running in the loops. In Fig. 5.10, we explicitly isolate the gradient effects by plotting $\delta\bar{B}^{(1)} = \bar{B}^{(1)} - \bar{B}^{(1)\mathrm{hom}}$ for the one-loop contributions from the particular species.

In Fig. 5.11, we compare the dependence of $B^{(2)}$ on the various coupling constants with and without gradient effects. The relative difference between the cases with and without gradient effects is of order one. When recalling the dependence of $B^{(2)}$ on the tadpole

functions given in Eq. (4.33), we see that this sizable difference is because of the large relative impact of gradient effects on Π due to the cancellation from fermion and scalar loop effects, cf. Fig. 5.3. We reiterate, however, that this cancellation is coincidental due to the parameter choices in Eq. (5.59).

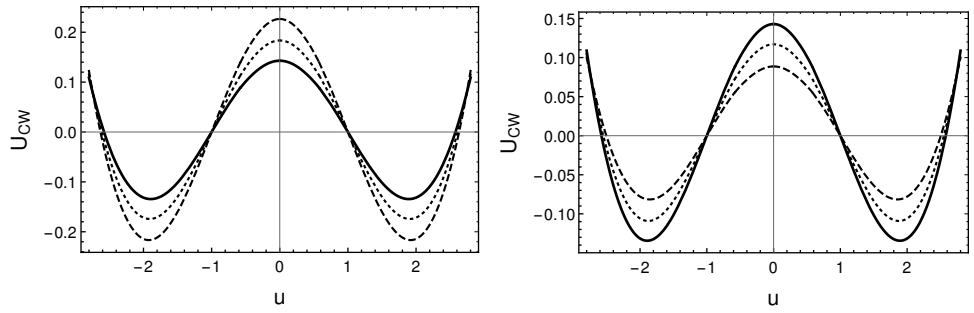

Figure 5.9: The left plot shows the shape of the barrier in the CW potential $U_{\rm CW}$ for $\kappa = 0.5$ (solid), $\kappa = 0.51$ (dotted) and $\kappa = 0.52$ (dashed), while the right is for $\alpha = 0.5$ (solid), $\alpha = 0.55$ (dotted) and $\alpha = 0.6$ (dashed). In both cases, the remaining parameters not being varied are chosen as in Eq. (5.59).

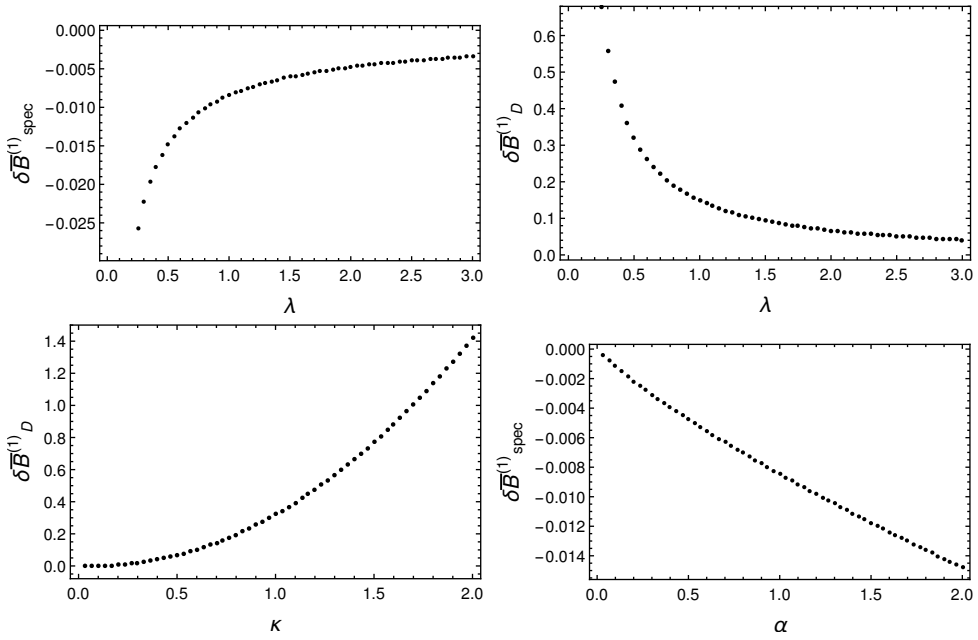

Figure 5.10: The differences $\delta\bar{B}^{(1)} \equiv \bar{B}^{(1)} - \bar{B}^{(1)\rm hom}$, which isolate the gradient contributions to the one-loop action. The remaining parameters besides those varied on the horizontal axes are chosen as in Eq. (5.59).

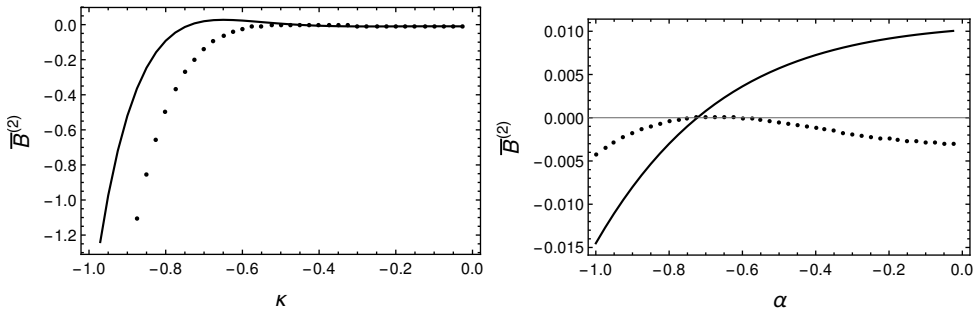

Figure 5.11: Parametric dependencies of $\bar{B}^{(2)}$ when varied about the benchmark point (5.59). Solid: $\bar{B}^{(2)}$ with gradient effects. Dotted: $\bar{B}^{(2)\mathrm{hom}}$ without gradient effects.

Chapter 6

Real-time Picture of Quantum Tunneling I: Optical Theorem

It is believed that there occurs the nucleation of *classical* critical bubbles during false vacuum decay, which could play an important role in a number of cosmological processes. The picture of nucleation of a classical critical bubble, however, has never been rigorously justified. For quantum tunneling of a particle, one shall expect a non-vanishing wave function outside of the barrier after the tunneling instead of position eigenstate at the exit point. To understand the situation in quantum field theory, we need to obtain a real-time picture of quantum tunneling that can be generalized to false vacuum decay.

So far, the standard description of false vacuum decay is the Callan-Coleman method that makes use of the Euclidean path integral, see Sec. 2.1. In this chapter, we base our discussion on a simple particle tunneling problem which however also captures the essential features of false vacuum decay. In the Callan-Coleman formalism, one considers the following Euclidean transition amplitude

$$Z_E[\mathcal{T}] \equiv \langle x_f | e^{-H\mathcal{T}} | x_i \rangle = \int \mathcal{D}x \, e^{-S_E[x]}. \tag{6.1}$$

In the case of quantum tunneling, x_i and x_f are chosen to be the metastable minimum. As we described in Chap. 2, one can evaluate Eq. (6.1) through the method of steepest descent by first finding out all the stationary points. One particular stationary point is the bounce. The fluctuation operator (the generalization of the Hessian matrix) evaluated at the bounce contains a negative eigenvalue. It is argued in Ref. [37] that performing the Gaussian functional integral around the bounce gives an imaginary part in the Euclidean transition amplitude which is further related to the decay rate. However Eq. (6.1) is apparently real. If one takes the method of steepest descent seriously, one will find that the imaginary result obtained from the fluctuations about the bounce will be canceled by an imaginary contribution from the fluctuations about the shot [47], see Sec. 6.1. The extraction of the particular imaginary part given in Ref. [37] relies upon the so-called potential deformation which leaves open questions since it is not defined clearly. Normally, the analytic continuation is taken over, e.g., Mandelstam variables which are parameters describing the physical process we study. It is strange that one needs to analytically continue the parameters of a theory in order to describe a process described by this theory rather than to compare this theory with another, for instance, to study the dualities between different theories.

Apart from the above issues, the Euclidean path integral does not provide a clear picture of how the tunneling proceeds in a real-time path-integral formulation. In particular, the Euclidean instantons generally do not have correspondences in real configurations in Minkowski spacetime. One way to justify that instantons do describe quantum tunneling

is comparing the results obtained from instanton techniques with those from the WKB expansion in solving the static Schrödinger Equation. But this again tells us little about the real-time picutre of tunneling. One may therefore wish to compute directly the Minkowski transition amplitude

$$Z_M[T] \equiv \langle x_f|e^{-iHT}|x_i\rangle = \int \mathcal{D}x\, e^{iS_M[x]}. \tag{6.2}$$

Since in Minkowski spacetime, we generally have no real classical solutions that would correspond to the quantum tunneling process, we do not have real stationary points which give the dominant contribution to tunneling in the Minkowski path integral. It is even not clear how to perform perturbative calculations for quantum tunneling in the real-time Feynman path integral. Recently, however, it has been understood that one can analytically continue the path integral over real paths to one over complex paths and evaluate the original path integral via Picard-Lefschetz theory [125, 126, 48, 49]. Therefore we may aim to find in a deformed but equivalent integral contour *complex* stationary points which can be identified as correspondences of the Euclidean instantons. Then the expansion of the Minkowski path integral around these complex saddle points[18] will give the dominated contributions in the Minkowski transition amplitude and could generate the same results as those obtained from the expansion around instantons in the Euclidean path integral. Based on these new developments, some attempts to understand quantum tunneling in the real-time formalism have been pursued in Refs. [127, 128].

Complex saddle points now have become a very useful concept in the study of perturbative series around the perturbative vacuum [129]. Even when the complex saddles are not located on the integration contour, they could still encode very important information on physical observables as a consequence of resurgence [130, 131, 132]. The resurgence theory states that the perturbative expansion around the perturbative vacuum encodes the information of all non-perturbative saddles. In this chapter, we shall discuss complex saddles which lie on the (deformed) integration contour and directly describe the non-perturbative quantum tunneling phenomenon. The idea that such complex saddles may recover the results obtained from the instanton techniques was suggested in Ref. [127] for the double-well model. We work it out in a very detailed and concrete way for the general case. In particular, we transfer the original problem of solving the gradient equations to one of solving ordinary eigenequations and therefore we successfully carry out the path integral on the Lefschetz thimble which passes through the complex saddle point of relevance. We shall show that, under plausible assumptions, the particle tunneling rate and the false vacuum decay rate can be derived from the unitarity of the evolution operator.

6.1 Euclidean path integral revisited: Picard-Lefschetz theory

In Sec. 2.1, we have mentioned that the direction associated with the negative mode is not the steepest descent direction but a steepest ascent direction. To correctly make use of the method of steepest descent, one needs to complexify the paths $x(\tau)$ to $z(\tau)$ and then

[18] When the paths are complexified, all the stationary points are saddle points due to the complex structure.

perform the path integral on a middle-dimensional contour. The general way to do this for the multiple-dimensional integral and even the generalization to Feynman path integrals is given by Picard-Lefschetz theory that we will now review (see e.g., Refs. [48, 49]).

To provide the discussion in a general context, we denote the holomorphic function appearing in the exponential of the integrand as $-S_E[z] \equiv \mathcal{I}[z]$ and we define $h[z] = \mathrm{Re}(\mathcal{I}[z])$ which is called Morse function. The saddle points are given by the equation of motion $\delta\mathcal{I}[z] = 0$ subject to the boundary conditions of interest. For a saddle point z_σ of $\mathcal{I}[z]$, one can find a downward flow (the steepest descent path) according to the gradient flow equation [48]

$$\frac{\partial z(\tau;u)}{\partial u} = -\overline{\left(\frac{\delta\mathcal{I}[z(\tau;u)]}{\delta z(\tau;u)}\right)}\,,\ \frac{\partial\overline{z(\tau;u)}}{\partial u} = -\frac{\delta\mathcal{I}[z(\tau;u)]}{\delta z(\tau;u)}, \tag{6.3}$$

where $u \in \mathbb{R}$ and the boundary condition is $z(\tau; u = -\infty) = z_\sigma$. One can easily check that

$$\frac{\partial h}{\partial u} = \frac{1}{2}\left(\frac{\delta\mathcal{I}}{\delta z}\cdot\frac{\partial z}{\partial u} + \frac{\delta\overline{\mathcal{I}}}{\delta\overline{z}}\cdot\frac{\partial\overline{z}}{\partial u}\right) = -\left|\frac{\partial z(\tau;u)}{\partial u}\right|^2 \leq 0. \tag{6.4}$$

That is, the real part of $\mathcal{I}[z]$ is always decreasing when we move away from the saddle point along the contour given by $z(\tau; u)$. Further, one can show that $\partial\mathrm{Im}\mathcal{I}[z(\tau;u)]/\partial u = 0$, meaning that the phase is constant on that contour.

Substituting the Euclidean action into Eq. (6.3), we have

$$\frac{\partial z(\tau;u)}{\partial u} = -\frac{\partial^2\overline{z}(\tau;u)}{\partial\tau^2} + U'(\overline{z}(\tau;u)). \tag{6.5}$$

Expanding $z(\tau; u)$ around the saddle point $z(\tau;u) = z_\sigma(\tau) + \Delta z_\sigma(\tau;u)$, one obtains

$$\frac{\partial\Delta z_\sigma(\tau;u)}{\partial u} = \left(-\frac{\partial^2}{\partial\tau^2} + U''(\overline{z_\sigma}(\tau))\right)\overline{\Delta z_\sigma}(\tau;u), \tag{6.6}$$

subject to the boundary condition $\Delta z_\sigma(\tau; u = -\infty) = 0$. The downward flows generate from every saddle point a middle-dimensional manifold with a stationary phase called Lefschetz thimble [48]. In our case, we denote the Lefschetz thimble associated with x_F, x_B, and x_S as $\mathcal{J}_F$, $\mathcal{J}_B$, and $\mathcal{J}_S$. Generically, the deformed contour $\mathcal{C}$ can be expressed as

$$\mathcal{C} = \sum_{\sigma\in\Sigma} n_\sigma\,\mathcal{J}_\sigma \tag{6.7}$$

where Σ is the moduli space of all the Lefschetz thimbles. The intersection numbers n_σ can be either zero or positive integer numbers. If the saddle points are not connected by the flows, the thimbles end at convergent regions for the integration at infinity. One has an independent perturbation series

$$Z_E^\sigma = e^{\mathcal{I}[z_\sigma]}\int\mathcal{D}\Delta z_\sigma e^{\frac{1}{2}\int\mathrm{d}\tau_1\mathrm{d}\tau_2\,\Delta z_\sigma(\tau_1)\cdot\frac{\delta^2\mathcal{I}[z]}{\delta z(\tau_1)\delta z(\tau_2)}\Big|_{z_\sigma}\cdot\Delta z_\sigma(\tau_2)+\ldots}. \tag{6.8}$$

In this case, one may view every Lefschetz thimble that contributes to the contour $\mathcal{C}$ as a single perturbative theory. Those saddle points then generate the vacua of the theory.

Two saddle points z_{σ_1}, z_{σ_2} may be connected with each other by the flows when $\mathrm{Im}\mathcal{I}[z_{\sigma_1}] = \mathrm{Im}\mathcal{I}[z_{\sigma_2}]$, as will happen in our quantum tunneling problem. In that case, the expansion around one saddle point may not be independent of another and one of the saddle points could describe the non-perturbative phenomena relating to different vacua.

The contour $\mathcal{C}$ is not unique. Suppose we consider a general integral $\int_{\Omega_n} \mathrm{d}\omega$ where Ω_n is a n-dimensional contour in a $2n$-dimensional manifold and $\mathrm{d}\omega$ is a holomorphic differential n-form. Then any two contours Ω_n^1, Ω_n^2 that differ by an exact manifold Ω_n^3, i.e., $\Omega_n^3 = \partial\Omega_{n+1}$ for some $n+1-$dimensional manifold Ω_{n+1} with ∂ here denoting the boundary operator, give identical integration result because of the Cauchy theorem. This defines an equivalence relation. To ensure convergence, the integration contour is either compact or its infinite ends lie in the "convergent regions" where $h[z]$ is sufficiently small such that the integral is convergent. In this sense, we say that all the contours that ensure a convergent integration are closed and are called integration cycles. Together with their equivalent relations, all the integration cycles give a relative homology group. In our situation, we are just looking for a contour that is homologous to the original one.

Determining all the saddle points and the integers n_σ is generally difficult. Fortunately, it is not necessary to do such a complicated analysis in our tunneling problem. In the original expansion, all the directions except for the one associated with the negative eigenvalue λ_0^B at the bounce generate correctly the steepest descent paths. Along with this special direction, the three saddle points are actually related to each other as explained in Fig. 2.3. It was first pointed out in Ref. [47] that, it is exactly the shot that is essential to understand how an imaginary part can emerge from a purely real Euclidean path integral, as we will see below.

It is easy to find the missed steepest descent direction. We simply let the variable ζ (cf. Fig (2.3)) be complex and deform the contour as follows. We let ζ start from minus infinity and flow on the real axis towards to the point $\zeta = b$ where it turns upward[19] to the imaginary axis and ends at $+i\infty$. That is, we have the first path $\mathcal{J}_{FB}^{\zeta} : -\infty \to b \to b+i\infty$. After that, the contour will flow on the imaginary axis from $b+i\infty$ to the point $\zeta = b$ again and rushes on the real axis to the shot $\zeta = s$, ending finally at positive infinity on the real axis. That is, we have a second path $\mathcal{J}_{SB}^{\zeta} : b+i\infty \to b \to \infty$. In so doing, we are still using the previous three real saddle points but with the one-dimensional subset path slightly deformed from the real line to $\mathcal{C}_\zeta \equiv \mathcal{J}_{FB}^{\zeta} + \mathcal{J}_{SB}^{\zeta}$. Compared with the original one, $\mathcal{C}_\zeta$ contains, in addition, a compact line: $b \to b+i\infty \to b$ and is therefore equivalent to the original one.

From the above analysis, we see, however, the trivial false vacuum solution $x_F(\tau)$ is connected with the bounce by the flow $\mathcal{J}_{FB}^{\zeta}$ and the shot is connected with the bounce by the flow $\mathcal{J}_{SB}^{\zeta}$. Therefore we expect that the bounce does not give a single perturbative sector but rather describes the non-perturbative phenomena between the false vacuum and the shot (which actually corresponds to the true vacuum). The integral from the one-dimensional contour $\mathcal{C}_\zeta$ is

$$Z_E^{\zeta} = Z_E^{FB(\zeta)} + Z_E^{SB(\zeta)} \equiv \int_{\mathcal{J}_{FB}^{\zeta}} \mathrm{d}\zeta\, e^{\mathcal{I}[\zeta]} + \int_{\mathcal{J}_{SB}^{\zeta}} \mathrm{d}\zeta\, e^{\mathcal{I}[\zeta]}. \tag{6.9}$$

[19]The path can turn either upward or downward. We take the "upward direction" in order to have a positive imaginary part in the false vacuum energy.

Both $Z_E^{FB(\zeta)}$ and $Z_E^{SB(\zeta)}$ contain an imaginary part but with opposite sign, leading a *purely real* and also finite result as expected. We will denote $\mathcal{J}_F + \mathcal{J}_B$ but with a one-dimensional contour deformed to $\mathcal{J}_{FB}^{\rho}$ as described above as $\mathcal{J}_{FB}$. Similarly we define $\mathcal{J}_{SB}$. Note that, though with a bit amuse of notations here, $\mathcal{J}_{FB}$ or $\mathcal{J}_{SB}$ shall not be understood as one thimble. They are combinations of two thimbles with a slight deformation. We denote the path integral on $\mathcal{J}_{FB}$ as Z_E^{FB}; accordingly we define Z_E^{SB}.

In Ref. [37], only Z_E^{FB} is picked in the Euclidean transition amplitude $\langle x_+|e^{-H\mathcal{T}}|x_+\rangle$, leading the authors to claim an imaginary energy for the false vacuum. Our explanation for this is the following. The energy, as eigenvalues of the Hermitian Hamiltonian, must be real. Indeed, the dominant real part in the full $\langle x_+|e^{-H\mathcal{T}}|x_+\rangle$, residing in Z_E^{SB}, gives the truly lowest energy and the corresponding wave function. A complex energy can only emerge if we look at a subsystem. In this sense, we may think of Z_E^{FB} and Z_E^{SB} as the theories describing the subsystems or sectors—the false vacuum and the true vacuum—isolatedly. The imaginary parts from both Z_E^{FB} and Z_E^{SB} indicate that both the false vacuum and the true vacuum are open systems.[20] Since the whole system is closed, the imaginary parts from Z_E^{FB} and Z_E^{SB} must cancel with each other. In this understanding, there is no so-called potential deformation. Note that the factor $1/2$ comes naturally when we only study the subsystem represented by $\mathcal{J}_{FB}$. In the next section, we will explain from another point of view why we need to exclude the perturbative expansion from the shot. There, we will show that what we actually aim to study is the Minkowski false vacuum to false vacuum transition amplitude which describes the false vacuum decay via an optical theorem. And the perturbative expansion around the shot contributes instead to the true vacuum to true vacuum transition amplitude.

Now, Z_E^{FB} can readily be evaluated directly since only the modification on the one-dimensional contour $\mathcal{C}_\zeta$ needs to be taken into account, as we have analyzed in Chap. 2. However, we shall give a general analysis of how to evaluate Z_E^{FB} from the point of view of the flow equation. This can be done by solving the linearized flow equation (6.6) around the relevant saddle points $x_a(\tau)$. We make the separation $\Delta z_{a,n}(\tau;u) = g_n^a(u)\chi_n^a(\tau)$ where $g_n^a(u) \in \mathbb{R}$ and the subscript "n" denotes a specific direction. Eq. (6.6) becomes

$$\left(-\partial_\tau^2 + U''(\overline{x_a}(\tau))\right)\overline{\chi_n^a}(\tau)g_n^a(u) = \chi_n^a(\tau)\frac{\mathrm{d}g_n^a(u)}{\mathrm{d}u}. \tag{6.10}$$

Eq. (6.10) leads to

$$\left(-\partial_\tau^2 + U''(\overline{x_a}(\tau))\right)\overline{\chi_n^a}(\tau)/\chi_n^a(\tau) = \kappa_n^a = \frac{1}{g_n^a(u)}\frac{\mathrm{d}g_n^a(u)}{\mathrm{d}u}, \tag{6.11}$$

where $\kappa_n^a \in \mathbb{R}$. The first equation gives us

$$\left(-\partial_\tau^2 + U''(\overline{x_a}(\tau))\right)\overline{\chi_n^a}(\tau) = \kappa_n^a\chi_n^a(\tau) \tag{6.12}$$

with Dirichlet boundary conditions $\chi_n^a(\tau = \pm\mathcal{T}/2) = 0$. We refer to Eq. (6.12) as the *flow eigenequation* to distinguish it from the ordinary eigenequation and κ_n^a, $\chi_n^a(\tau)$ as

[20] In the context of quantum mechanics, "open system" is easy to be understood since the false vacuum or true vacuum is defined only in a subregion in space—the left well or the right well. In quantum field theory, "subsystem" should be understood in the sense of field space.

the *flow eigenvalue* and *flow eigenfunction*, respectively. Further, the normalized flow eigenfunctions have the following relations

$$\int_{-\mathcal{T}/2}^{\mathcal{T}/2} \mathrm{d}\tau\ \overline{\chi_m^a}(\tau)\chi_n^a(\tau) = \delta_{mn}. \tag{6.13}$$

One important property of Eq. (6.12) is that κ_n^a is always paired with $-\kappa_n^a$, which is associated with the flow eigenfunction $i\chi_n^a(\tau)$, as can be checked easily. Another equation derived from Eq. (6.10) gives us $g_n^a(u) = a_n^a \exp(\kappa_n^a u)$ where $a_n^a \in \mathbb{R}$. Recalling the boundary condition $g_n^a(u = -\infty) = 0$, we have $\kappa_n^a > 0$.[21]

The complex conjugate of Eq. (6.12) gives us

$$\left(-\partial_\tau^2 + U''(x_a(\tau))\right)\chi_n^a(\tau) = \kappa_n^a \overline{\chi_n^a}(\tau). \tag{6.14}$$

Since $x_a(\tau)$ is real, $\overline{\chi_n^a}(\tau)$ is the flow eigenfunction associated with the same flow eigenvalue. Thus one has $\overline{\chi_n^a}(\tau) = \pm\chi_n^a(\tau)$, assuming there is no degeneracy for the non-zero modes as it is the case in general. Therefore, Eq. (6.12) has purely real or purely imaginary flow eigenfunctions and it can be reduced to the ordinary eigenequation

$$(-\partial_\tau^2 + U''(x_a(\tau)))f_n^a(\tau) = \lambda_n^a f_n^a(\tau). \tag{6.15}$$

For $\lambda_n^a > 0$, we simply have $\chi_n^a(\tau) = f_n^a(\tau)$ and $\kappa_n^a = \lambda_n^a$. For the negative mode $f_0^B(\tau)$, we have $\chi_0^B(\tau) = if_0^B(\tau)$ in order to have positive α_0^B.

Now let us look at the integrand $\exp(I[z])$ in the path integral by substituting $z(\tau; u) = z_a(\tau) + \sum_n g_n^a(u)\chi_n^a(\tau)$ into $I[z]$. One has up to $\mathcal{O}(\Delta z^2)$

$$\begin{aligned} I[z] &= I[z_a] - \frac{1}{2}\int \mathcal{D}\tau\, \Delta z_a(\tau; u)\left(-\partial_\tau^2 + U''(x_a(\tau))\right)\Delta z_a(\tau; u) \\ &= I[z_a] - \frac{1}{2}\sum_n \kappa_n^a \left(g_n^a(u)\right)^2, \end{aligned} \tag{6.16}$$

where in the second equality, we have used the complex conjugate of Eq. (6.12) and the orthogonal normalization relations Eq. (6.13). Since $g_n^a(u)$ are real and κ_n^a are real and positive, the last line in Eq. (6.16) tells us that the path integral on the Lefschetz thimble $\mathcal{J}_a$ is a Wiener integration at the Gaussian level, hence it is convergent.

From $\Delta z_a(\tau; u) = \sum_n g_n^a(u)\chi_n^a(\tau)$, we define the path integral measure as

$$\mathcal{D}\Delta z_a = J_a \prod_n \frac{1}{\sqrt{2\pi}} \mathrm{d}g_n^a, \tag{6.17}$$

where J_a is the Jacobian due to the transformation from the original real basis to the new basis $\{\chi_n^a(\tau)\}$. At the Gaussian level, we have (again, the zero mode will be considered separately)

$$J_a \prod_n \int \mathrm{d}g_n^a\ \frac{1}{\sqrt{2\pi}}\ e^{-\frac{1}{2}\sum_n \kappa_n^a {g_n^a}^2} = J_a \prod_n \frac{1}{\sqrt{\kappa_n^a}} = J_a |\det(-\partial_\tau^2 + U''(x_a))|^{-1/2}. \tag{6.18}$$

[21] It is possible to have a zero mode in the limit $\mathcal{T} \to \infty$ which has to be handled separately.

Without the the deformation of the contour, the path integral measure is defined from the decomposition of $\Delta z_a(\tau;u)$ into the real eigenfunctions of $-\partial_\tau^2+U''(x_a)$, $\Delta z_a(\tau;u)=\sum_n c_n^a f_n^a(\tau)$, as

$$\mathcal{D}\Delta z_a=\prod_n\frac{1}{\sqrt{2\pi}}\mathrm{d}c_n^a. \tag{6.19}$$

Since for the saddle point x_F, the basis $\{\chi_n^F(\tau)\}$ is the same as $\{f_n^F(\tau)\}$, we have $J_F=1$. For the bounce, since $\chi_0^B(\tau)=if_0^B(\tau)$, we have $\mathrm{d}c_0^B=i\mathrm{d}g_0^B$ as can be seen from $\Delta z_{B,0}=g_0^B\chi_0^B(\tau)=c_0^Bf_0^B(\tau)$. Since for the other modes, $\chi_{n\neq0}^B$ are the same as $f_{n\neq0}^B$, we finally arrive at $J_B=i$. Thus the Jacobian can be identified as the exponential of minus half of the phase of the determinant of $-\partial_\tau^2+U''(x_a)$. This claim as well as the second equility of Eq. (6.18) are actually quite general and we will give the proof in the next chapter.

Recall that the bounce is connected with the false vacuum via the flow generated by the negative flow eigenmode $\chi_0^B(\tau)$, leading the integral over g_0^B cut by half in Z_E^{FB}. We account this fact by introducing a modified path integral measure around the bounce

$$\mathcal{D}\Delta z_B\to\widetilde{\mathcal{D}\Delta z_B}=\frac{J_B}{2}\prod_n\frac{1}{\sqrt{2\pi}}\mathrm{d}g_n^B. \tag{6.20}$$

We finally have

$$Z_E^{FB}=Z_E^F+\tilde{Z}_E^B, \tag{6.21}$$

where

$$\tilde{Z}_E^B=e^{-B}\int\widetilde{\mathcal{D}\Delta z_B}\,e^{-\int_{-\mathcal{T}/2}^{\mathcal{T}/2}d\tau\left[\Delta z_B\left(-\frac{1}{2}\frac{d^2}{d\tau^2}+\frac{1}{2}U''(x_B)\right)\Delta z_B+\frac{1}{3!}(g+\lambda\,x_B(\tau))\Delta z_B^3+\frac{\lambda}{4!}\Delta z_B^4\right]}. \tag{6.22}$$

With additional care about the zero mode and evaluating the partition function with proper normalization, one can finally get

$$\frac{\tilde{Z}_E^B}{Z_E^F}=\frac{i\mathcal{T}}{2}\sqrt{\frac{B}{2\pi}}\left|\left(\frac{\det'[-\partial_\tau^2+U''(x_B)]}{\det[-\partial_\tau^2+U''(x_+)]}\right)\right|^{-1/2}e^{-B}, \tag{6.23}$$

which can then be related to the decay rate as discussed in Chap. 2.

6.2 Optical theorem for unstable vacuum

We have argued in the last section why the false ground state, or false vacuum in field theory, can possess a complex energy and how the imaginary part emerges from the purely real Euclidean path integral. This analysis, however, does not tell us much about the dynamical process in the Minkowski spacetime. We therefore aim to study particle tunneling and false vacuum decay in the Minkowski path integral. We shall obtain the tunneling rate or the decay rate from the unitarity of the S matrix. In the following, we use "false vacuum" to generally denote the "false ground state" either in quantum mechanics or in field theory.

To prepare for the derivation, we first recall the optical theorem. For the S-matrix, we have the unitarity $S^\dagger S = \mathbf{1}$. Inserting $S = \mathbf{1} + iM$[22] to $S^\dagger S = \mathbf{1}$, we have

$$-i(M - M^\dagger) = M^\dagger M. \tag{6.24}$$

We can take the matrix element of this equation between particle states, say $|\mathbf{p}_1\mathbf{p}_2\rangle$ and $|\mathbf{k}_1\mathbf{k}_2\rangle$ for a 2-to-2 scattering for simplicity. To evaluate the RHS, insert a complete set of intermediate states:

$$\langle \mathbf{p}_1\mathbf{p}_2|M^\dagger M|\mathbf{k}_1\mathbf{k}_2\rangle = \sum_n \langle \mathbf{p}_1\mathbf{p}_2|M^\dagger|\{\mathbf{q}_n\}\rangle\langle\{\mathbf{q}_n\}|M|\mathbf{k}_1\mathbf{k}_2\rangle, \tag{6.25}$$

where $\{\mathbf{q}_n\}$ is an arbitrary complete set of intermediate states normalized properly. Thus Eq. (6.24) gives us

$$-i\left[\langle \mathbf{p}_1\mathbf{p}_2|M|\mathbf{k}_1\mathbf{k}_2\rangle - \langle \mathbf{p}_1\mathbf{p}_2|M^\dagger|\mathbf{k}_1\mathbf{k}_2\rangle\right] = \sum_n \langle \mathbf{p}_1\mathbf{p}_2|M^\dagger|\{\mathbf{q}_n\}\rangle\langle\{\mathbf{q}_n\}|M|\mathbf{k}_1\mathbf{k}_2\rangle. \tag{6.26}$$

Further, letting the initial and final states be the same, i.e., taking $\mathbf{p}_i = \mathbf{k}_i$, we obtain

$$-i\left[\langle \mathbf{k}_1\mathbf{k}_2|M|\mathbf{k}_1\mathbf{k}_2\rangle - \langle \mathbf{k}_1\mathbf{k}_2|M^\dagger|\mathbf{k}_1\mathbf{k}_2\rangle\right] = \sum_n \langle \mathbf{k}_1\mathbf{k}_2|M^\dagger|\{\mathbf{q}_n\}\rangle\langle\{\mathbf{q}_n\}|M|\mathbf{k}_1\mathbf{k}_2\rangle. \tag{6.27}$$

Therefore the imaginary part of the M-matrix corresponds to the decay probability from the initial state to the intermediate states.

The crucial ingredient to the above construction is the unitarity of the S-matrix. Since in our case we need to keep T finite (but still large microscopically) to study the exponential decay law, we cannot use the normal S-matrix defined at the limit of $T = \infty$. But the optical theorem does not rely on the condition $T = \infty$, and therefore we can define a time-dependent S-matrix

$$\langle \mathrm{F}|S(T)|\mathrm{I}\rangle = {}_{\mathrm{out}}\langle \mathrm{F}|\mathrm{I}\rangle_{\mathrm{in}}, \tag{6.28}$$

where $|\mathrm{I}\rangle_{\mathrm{in}}$, $|\mathrm{F}\rangle_{\mathrm{out}}$ are the in and out states respectively. Note that we use the Heisenberg picture where states are time-independent while the name of a state depends on the eigenvalues or expectation values of time-dependent operators. Apparently, such a time-dependent $S-$matrix is still unitary and the above argument for the optical theorem still applies.

Now let us construct an optical theorem for false vacuum decay. We consider the following element of $S(T)$:

$${}_{\mathrm{out}}\langle \mathrm{FV}|\mathrm{FV}\rangle_{\mathrm{in}} = \langle \mathrm{FV}|S(T)|\mathrm{FV}\rangle, \tag{6.29}$$

where "FV" denotes the false vacuum state. Or in common reference time,

$$\langle \mathrm{FV}|S(T)|\mathrm{FV}\rangle = \langle \mathrm{FV}|e^{-iHT}|\mathrm{FV}\rangle. \tag{6.30}$$

Obviously, the false vacuum state should be taken as a resonant state. It is not the unique time-translation-invariant vacuum state (the true vacuum); otherwise, it would

[22] To avoid a mixed-use of notations, we use M instead of T to denote the so-called "T-matrix" because we reserve T as the Minkowski time period.

never decay. For this reason, we do not have the simple normalization ${}_{\rm out}\langle {\rm FV}|{\rm FV}\rangle_{\rm in} = 1$ (see later). Inserting $S(T) = \mathbf{1} + iM(T)$ into $S(T)^\dagger S(T) = \mathbf{1}$ for the above matrix element, we have

$$-i\left[\langle {\rm FV}|M(T)|{\rm FV}\rangle - \langle {\rm FV}|M(T)^\dagger|{\rm FV}\rangle\right] = \sum_n \langle {\rm FV}|M(T)^\dagger|\{\mathbf{q}_n\}\rangle\langle\{\mathbf{q}_n\}|M(T)|{\rm FV}\rangle, \tag{6.31}$$

where we choose the complete set $\{\mathbf{q}_n\}$ to be position eigenstates in the case of particle tunneling, or the field configuration eigenstates in the case of vacuum decay. Eq. (6.31) gives

$$2\,{\rm Im}\langle {\rm FV}|M(T)|{\rm FV}\rangle = \sum_n \langle {\rm FV}|M(T)^\dagger|\{\mathbf{q}_n\}\rangle\langle\{\mathbf{q}_n\}|M(T)|{\rm FV}\rangle. \tag{6.32}$$

We are close to achieving our purpose if we can find out the imaginary part in Eq. (6.32). Since we cannot solve the system exactly, we do not know what exactly the false vacuum is. But we know that the false vacuum state should be approximately a Gaussian centered at x_+. For the moment, let us pretend that $|{\rm FV}\rangle$ is globally stable. Then we can get $|{\rm FV}\rangle$ through the usual trick:

$$e^{-iHT}|x_+\rangle = e^{-iE_0T}|{\rm FV}\rangle\langle {\rm FV}|x_+\rangle + \sum_{n\neq 0} e^{-iE_nT}|n\rangle\langle n|x_+\rangle, \tag{6.33}$$

and

$$|{\rm FV}\rangle = \lim_{T\to\infty(1-i\epsilon)} (e^{-iE_0T}\langle {\rm FV}|x_+\rangle)^{-1}\, e^{-iHT}|x_+\rangle \equiv \mathcal{N} \lim_{T\to\infty(1-i\epsilon)}\, e^{-iHT}|x_+\rangle, \tag{6.34}$$

where $\epsilon = 0^+$ is a positive infinitesimal number. That is, the position eigenstate $|x_+\rangle$ is projected onto the vacuum state through the $i\epsilon$-prescription and large T. Now we have

$$\langle {\rm FV}|e^{-iHT}|{\rm FV}\rangle = \mathcal{N}^2\langle x_+|e^{-iHT(1-i\epsilon)}|x_+\rangle \ \text{ for large } T. \tag{6.35}$$

The normalization factor $\mathcal{N}$ will be fixed later. Since the false vacuum is not the global ground state, Eq. (6.35) cannot be true. However, if we consider only small oscillations around x_+, Eq. (6.35) is correct since the false vacuum appears to be the *locally* lowest-energy state. But if we consider large oscillations around x_+, the RHS actually contributes to

$$\langle {\rm TV}|e^{-iHT}|{\rm TV}\rangle \tag{6.36}$$

where $|{\rm TV}\rangle$ represents the true vacuum state; the large oscillations detect the *global* lowest-energy state rather than the false vacuum in Eq. (6.34). To exclude this contribution, we need to constrain the paths that are to be integrated. This is perhaps the deep reason why we discard Z_E^{SB} in the Euclidean path integral.

These physical intuitions can be made more precise via Picard-Lefschetz theory. Small oscillations and large oscillations simply correspond to different Lefschetz thimbles. Thus, we have

$$\begin{aligned}\langle {\rm FV}|e^{-iHT}|{\rm FV}\rangle = \mathcal{N}^2\langle x_+|e^{-iHT(1-i\epsilon)}|x_+\rangle \ \text{ for large } T \\ \text{and on } \textit{constrained} \text{ Lefschetz thimbles.}\end{aligned} \tag{6.37}$$

We will specify the particular constraint on the Lefschetz thimbles later.

6.3 Minkowski path integral and complex bounce

Now we need to find out the relevant saddle points and the corresponding Lefschetz thimbles in the Minkowski path integral. We begin with a more general transition amplitude

$$U_\theta(x_+, T/2; x_+, -T/2) \equiv \langle x_+|e^{-iHTe^{i\theta}}|x_+\rangle = \int \mathcal{D}x(t)\, e^{iS_M^\theta[x(t)]} \equiv Z_{M,\theta}[T], \tag{6.38}$$

where

$$S_M^\theta[x] = e^{-i\theta}\int_{-T/2}^{T/2} \mathrm{d}t \left[\frac{1}{2}\left(\frac{\mathrm{d}x}{\mathrm{d}t}\right)^2 \cdot e^{+2i\theta} - U(x)\right]. \tag{6.39}$$

Here $\theta \in [\epsilon, 2\pi]$. We obtain the Euclidean and Minkowski transition amplitudes and path integrals for $\theta = \pi/2$ and $\theta = \epsilon$, respectively. All the paths in the path integral in Eq. (6.38) are understood to have the boundary conditions $x(-T/2) = x_i$ and $x(T/2) = x_f$.

The saddle points are given by the solutions to the EoM

$$e^{+2i\theta} \cdot \frac{\mathrm{d}^2x(t)}{\mathrm{d}t^2} + U'(x(t)) = 0 \tag{6.40}$$

subject to the Dirichlet boundary conditions $x(-T/2) = x(T/2) = x_+$. If we work in the real paths and take the limit $\theta \to 0^+$ and $T \to \infty$, one can deduce from the potential that we may have two solutions; the first one is the trivial false vacuum solution $x_F(t)$ and the second one is similar to the shot in the Euclidean case but the particle arrives instead at $x = 0$ at $t = 0$. The second solution, however, only describes a classical solution with sufficient initial energy for the particle. The expansion around it cannot describe quantum tunneling. To extract the dominant contribution in the Minkowski path integral to quantum tunneling, one needs to complexify $x(t)$ to $z(t)$.

In the limit $T \to \infty$, we can quickly obtain the complex solutions to Eq. (6.40) in the following way. Comparing Eq. (6.40) with Eq. (2.8), one has solutions from substituting $\tau \to ie^{-i\theta}t$ into the Euclidean saddle points and have

$$\tilde{x}_a^\theta(t) = x_a(\tau \to ie^{-i\theta}t). \tag{6.41}$$

Although we keep the general values θ, the quantities in the following shall be understood to be of ultimate interest for $\theta = \epsilon$. Apparently, when applying Eq. (6.41) to the trivial false vacuum solution $x_F(\tau)$, we still obtain a trivial false vacuum solution $\tilde{x}_F^\theta(t) \equiv x_+$. For other Euclidean saddles, if $\tilde{x}_a^\theta(t)$ is a holomorphic function at infinity with $\epsilon \leq \theta \leq \pi/2$, then it will still converge to x_+ as $t \to \pm\infty$, satisfying the boundary conditions. This is indeed the case for the kink solution [127]. The bounce solution in field theory, as an instanton, actually takes the form of the kink solution in the thin-wall limit when the vacua become quasi-degenerate (see Sec. 2.3). In the quantum mechanics case, the bounce can be viewed as an antikink-kink pair in the "thin-wall" limit. We, therefore, expect that when applying Eq. (6.41) to the bounce, we obtain a complex saddle point $\tilde{x}_B^\theta(t)$ which we refer to as the *complex bounce*.

The parameter θ in $\tilde{x}_a^\theta(t)$ can be visualised as a continuous deformation starting from the original Euclidean saddle points $x_a(\tau)$. Similarly, we shall have a continuous deformation of the original Lefschetz thimbles, giving $\tilde{\mathcal{J}}_{FB}^\theta$ and $\tilde{\mathcal{J}}_{SB}^\theta$. Though this looks plausible,

we do not have a rigorous proof. We assume this is true. We shall show that the above assumption can give the same NLO result as the one obtained from the Euclidean path integral. From Eq. (6.37), we propose

$$\langle \mathrm{FV}|e^{-iHT}|\mathrm{FV}\rangle = \mathcal{N}^2 \int_{\tilde{\mathcal{J}}^{\epsilon}_{FB}} \mathcal{D}z\, e^{iS^{\epsilon}_M[z]} \equiv \mathcal{N}^2 Z^{FB}_{M,\epsilon}. \tag{6.42}$$

That is, we specify $\tilde{\mathcal{J}}^{\epsilon}_{FB}$ as the constrained Lefschetz thimbles.

It is remarkable that the complex bounce gives us the same exponential suppression as in the Euclidean formalism, first observed for the kink instanton in Ref. [127]. To see this, we write the action S^{θ}_M as

$$S^{\theta}_M[z] = e^{-i\theta} \int_{-T/2}^{T/2} \mathrm{d}t \left(\frac{1}{2} \left[\left(\frac{\mathrm{d}z}{\mathrm{d}t} \right) e^{+i\theta} \pm i\sqrt{2U(z)} \right]^2 \mp i \left(\frac{\mathrm{d}z}{\mathrm{d}t} e^{i\theta} \sqrt{2U(z)} \right) \right). \tag{6.43}$$

The complex bounce $\tilde{x}^{\theta}_B$ is simply the solution to

$$\left(\frac{\mathrm{d}z}{\mathrm{d}t} \right) e^{+i\theta} + i\sqrt{2U(z)} = 0, \text{ for } -T/2 \le t \le 0, \tag{6.44a}$$

$$\left(\frac{\mathrm{d}z}{\mathrm{d}t} \right) e^{+i\theta} - i\sqrt{2U(z)} = 0, \text{ for } 0 \le t \le T/2. \tag{6.44b}$$

For $\theta = \pi/2$, Eq. (6.44) is the EoM of the Euclidean bounce. Substituting Eq. (6.44) into Eq. (6.43), we have

$$\mathcal{I}[\tilde{x}^{\theta}_B] \equiv iS^{\theta}_M[\tilde{x}^{\theta}_B] = -ie^{-i\theta} \int_{-T/2}^{T/2} \mathrm{d}t\; 2U(\tilde{x}^{\theta}_B(t)). \tag{6.45}$$

The potential U is polynomial at tree level and hence holomorphic. Also, $\tilde{x}^{\theta}_B(t)$ should be analytic because it is the analytic continuation of the Euclidean bounce $x_B(\tau)$. Then starting from the expression of iS^{θ}_M above and rotating the integration contour $t \to -ie^{i\theta}\tau$, one gets *minus* the Euclidean bounce action, $-S_E[x_B]$. Note here, since at the infinity boundary of interest, the complex bounce will always converge to x_+, where the potential is zero, the integral (6.45) at the infinity boundary does not contribute when we deform the contour from t to $-ie^{i\theta}\tau$.

Chapter 7

Real-time Picture of Quantum Tunneling II: Flow Equations

The complex bounce that we have identified as a complex saddle point already gives correctly the semiclassical suppression in the decay rate. In order to verify the one-loop result of the decay rate, we need further to perform the path integral on the Lefschetz thimbles $\tilde{\mathcal{J}}^{\epsilon}_{FB}$. This forces us to solve the flow equations.

7.1 Flow equations and flow eigenequations

For $\mathcal{I}[z] = iS^{\theta}_{M}[z]$, the flow equation is

$$\frac{\partial z(t;u)}{\partial u} = e^{+i(\theta-\pi/2)}\left(\frac{\partial^2 \overline{z}(t;u)}{\partial t^2}\cdot e^{-2i\theta} + U'(\overline{z}(t;u))\right). \tag{7.1}$$

Expanding $z(t;u) = \tilde{x}^{\theta}_{a}(t) + \Delta z_a(t;u)$ with $a = F, B$, one obtains the linearized flow equation

$$\frac{\partial \Delta z_a(t;u)}{\partial u} = e^{+i(\theta-\pi/2)}\left(e^{-2i\theta}\cdot\frac{\partial^2}{\partial t^2} + U''(\overline{\tilde{x}^{\theta}_{a}}(t))\right)\overline{\Delta z}_a(t;u). \tag{7.2}$$

The expansion of the path integral around the saddle point is

$$Z^{a}_{M,\theta} = e^{I[\tilde{x}^{\theta}_{a}]} \times \int \mathcal{D}\Delta z_a\, e^{ie^{-i\theta}\int_{-T/2}^{T/2}\mathrm{d}t\left[-\frac{1}{2}\Delta z_a(t)\left(e^{+2i\theta}\cdot\frac{\mathrm{d}^2}{\mathrm{d}t^2}+U''(\tilde{x}^{\theta}_{a}(t))\right)\Delta z_a(t)-\frac{1}{3!}(g+\lambda\tilde{x}^{\theta}_{a}(t))\Delta z^3_a(t)-\frac{1}{4!}\lambda\Delta z^4_a(t)\right]}. \tag{7.3}$$

To obtain $\Delta z_a(t)$, we write $\Delta z_{a,n} = \sqrt{-i}e^{i\theta/2}\tilde{g}^{a}_{n}(u)\tilde{\chi}^{a}_{n}(t)$ with $\tilde{g}^{a}_{n}(u) \in \mathbb{R}$. Substituting the separation ansatz into Eq. (7.2), one has

$$\left(e^{-2i\theta}\cdot\frac{\partial^2}{\partial t^2} + U''(\overline{\tilde{x}^{\theta}_{a}}(t))\right)\overline{\tilde{\chi}^{a}_{n}}(t) = \tilde{\kappa}^{a}_{n}\tilde{\chi}^{a}_{n}(t) \tag{7.4}$$

and

$$\tilde{\kappa}^{a}_{n}\tilde{g}^{a}_{n}(u) = \frac{\mathrm{d}\tilde{g}^{a}_{n}(u)}{\mathrm{d}u} \tag{7.5}$$

with $\tilde{\chi}^{a}_{n}(t)$ having the orthogonal normalization relations

$$\int_{-T/2}^{T/2}\mathrm{d}t\overline{\tilde{\chi}^{a}_{m}}(t)\tilde{\chi}^{a}_{n}(t) = \delta_{mn}. \tag{7.6}$$

Repeating the analysis in Sec. 6.1, one has $\tilde{g}_n^a(u) = \tilde{a}_n^a \exp(\tilde{\kappa}_n^a u)$ with $\tilde{a}_n^a \in \mathbb{R}$ and $\tilde{\kappa}_n^a \in \mathbb{R}^+$. This is the ansatz used in Ref. [128]. Using the above orthogonal normalization relations and Eq. (7.4), one can check that the quadratic term in the exponential of the integrand of the path integral becomes negative definite (except for the zero mode), giving again a Wiener integration. From $\Delta z_a = \sum_n \sqrt{-i} e^{i\theta/2} \tilde{g}_n^a \tilde{\chi}_n^a(t)$, we define the path integral measure as

$$\mathcal{D}\Delta z_a = \tilde{J}_a \prod_n \frac{\sqrt{-i} e^{i\theta/2}}{\sqrt{2\pi}} \mathrm{d}\tilde{g}_n^a. \tag{7.7}$$

At the Gaussian level, the path integral gives

$$\tilde{J}_a \prod_n \sqrt{-i} e^{i\theta/2} \frac{1}{\sqrt{\tilde{\kappa}_n^a}}. \tag{7.8}$$

One might hope to obtain the solutions to Eq. (7.4) and $\tilde{\kappa}_n^a$ from the analytic continuation $\tau \to i e^{-i\theta} t, \mathcal{T} \to i e^{-i\theta} T$ of the Euclidean flow eigenequation (6.12). But this is impossible due to the complex conjugates appearing in the flow eigenequations. We leave the problem of solving the flow eigenequations to the next section.

7.2 Mapping flow eigenequations to ordinary eigenequations

In this section, we discuss how to relate the flow eigenequations to the ordinary eigenequations and derive the Jacobian induced by the basis transformation when the path integral is performed on the Lefschetz thimbles. Although we work with the path integral (7.3) in the following, the discussion is general for Picard-Lefschetz theory.

Consider a general flow equation

$$\frac{\partial \Delta z_a(t;u)}{\partial u} = \hat{L}_a^* \overline{\Delta z_a}(t;u), \tag{7.9}$$

where

$$\hat{L}_a = -\int \mathrm{d}t' \frac{\delta^2 \mathcal{I}[z]}{\delta z(t') \delta z(t)}\bigg|_{z_a} \equiv -\frac{\delta^2 \mathcal{I}}{\delta z^2}\bigg|_{z_a(t)}. \tag{7.10}$$

Following the analysis in Sec. 6.1, one can make the ansatz [128] $\Delta z_a(t;u) = \sum_n e^{i\psi} \tilde{a}_n^a \exp(\tilde{\kappa}_n^a u) \tilde{\chi}_n^a(t)$ $\equiv \sum_n e^{i\psi} \tilde{g}_n^a(u) \tilde{\chi}_n^a$ where $\tilde{a}_n^a \in \mathbb{R}$, $\tilde{\kappa}_n^a \in \mathbb{R}^+$ and $\psi = \theta/2 - \pi/4$. As it is understood, when there is a zero mode, it needs to be handled separately. In the following, the discussion is only about the non-zero modes. We therefore have

$$e^{-2i\psi} \hat{L}_a^* \overline{\tilde{\chi}_n^a}(t) = \tilde{\kappa}_n^a \tilde{\chi}_n^a(t) \tag{7.11}$$

with Dirichlet boundary conditions $\tilde{\chi}_n^a(t = \pm T/2) = 0$. The orthogonal normalization relations are

$$\int_{-T/2}^{T/2} \mathrm{d}t \, \overline{\tilde{\chi}_m^a}(t) \tilde{\chi}_n^a(t) = \delta_{mn}. \tag{7.12}$$

To distinguish, we use $\{\tilde{f}_n^a(t)\}$ to denote the ordinary eigenfunctions with corresponding eigenvalues $\tilde{\lambda}_n^a$ satifying the following eigenequation

$$e^{2i\psi}\hat{L}_a\,\tilde{f}_n^a(t) = \tilde{\lambda}_n^a \tilde{f}_n^a(t). \tag{7.13}$$

From $\Delta z_a(t;u) = \sum_n e^{i\psi}\tilde{g}_n^a(u)\tilde{\chi}_n^a(t)$, we define the path integral measure as

$$\mathcal{D}\Delta z_a = \tilde{J}_a \prod_n \frac{e^{i\psi}}{\sqrt{2\pi}} \mathrm{d}\tilde{g}_n^a, \tag{7.14}$$

where $\tilde{J}_a$ is the Jacobian. At the Gaussian level, we have

$$\tilde{J}_a \prod_n \int \mathrm{d}\tilde{g}_n^a \, \frac{e^{i\psi}}{\sqrt{2\pi}} \, e^{-\frac{1}{2}\sum_n \tilde{\kappa}_n^a (\tilde{g}_n^a)^2} = \tilde{J}_a \prod_n \frac{e^{i\psi}}{\sqrt{\tilde{\kappa}_n^a}}. \tag{7.15}$$

To relate the infinite product of the flow-eigenvalues to the determinant of $\hat{L}_a$, we consider the complex conjugate of Eq. (7.11) and write the combined equation in an ordinary eigenequation form:

$$\begin{pmatrix} \mathbf{0} & e^{-2i\psi}\hat{L}_a^* \\ e^{2i\psi}\hat{L}_a & \mathbf{0} \end{pmatrix} \begin{pmatrix} \tilde{\chi}_n^a(t) \\ \overline{\tilde{\chi}_n^a}(t) \end{pmatrix} = \tilde{\kappa}_n^a \begin{pmatrix} \tilde{\chi}_n^a(t) \\ \overline{\tilde{\chi}_n^a}(t) \end{pmatrix}. \tag{7.16}$$

This equation is associated with another equation

$$\begin{pmatrix} \mathbf{0} & e^{-2i\psi}\hat{L}_a^* \\ e^{2i\psi}\hat{L}_a & \mathbf{0} \end{pmatrix} \begin{pmatrix} i\tilde{\chi}_n^a(t) \\ -i\overline{\tilde{\chi}_n^a}(t) \end{pmatrix} = -\tilde{\kappa}_n^a \begin{pmatrix} i\tilde{\chi}_n^a(t) \\ -i\overline{\tilde{\chi}_n^a}(t) \end{pmatrix}. \tag{7.17}$$

Now $\tilde{\kappa}_n^a$ and $-\tilde{\kappa}_n^a$ are true eigenvalues for the extended operator on the LHS of Eq. (7.16). Then we have

$$\prod_n \left[-(\tilde{\kappa}_n^a)^2\right] = \det \begin{pmatrix} \mathbf{0} & e^{-2i\psi}\hat{L}_a^* \\ e^{2i\psi}\hat{L}_a & \mathbf{0} \end{pmatrix} \tag{7.18}$$

which gives $\prod_n (\tilde{\kappa}_n^a)^2 = |\det(\hat{L}_a^*\hat{L}_a)|$ for the particular block structure. We therefore arrive at

$$\prod_n \tilde{\kappa}_n^a = |\det(\hat{L}_a)| = \left|\prod_n \tilde{\lambda}_n^a\right|, \tag{7.19}$$

where we recall $\tilde{\kappa}_n^a > 0$.

We still need to work out the Jacobian $\tilde{J}_a$. This Jacobian appears because of the relative phase between the original real contour and the rotated Lefschetz thimble. To find its explicit form, we pick an arbitrary orthonormal *real* basis $\{\varphi_n(t)\}$ such that

$$\int \mathrm{d}t \; \varphi_m(t)\varphi_n(t) = \delta_{mn}. \tag{7.20}$$

In this basis, we have

$$\Delta z_a(t) = \sum_n \Delta z_{a,n}\varphi_n(t), \tag{7.21}$$

where

$$\Delta z_{a,n} = \int \mathrm{d}t\ \varphi_n(t)\Delta z_a(t) = \sum_m \int \mathrm{d}t\ \varphi_n(t) e^{i\psi}\tilde{\chi}^a_m(t)\tilde{g}^a_m \equiv \sum_m R_{nm}(e^{i\psi}\tilde{g}^a_m). \tag{7.22}$$

Thus

$$\mathrm{d}\Delta z_{a,n} = \sum_m R_{nm} e^{i\psi}\mathrm{d}\tilde{g}^a_m. \tag{7.23}$$

With the real basis, the path integral is given as

$$Z_a = \int_{\tilde{\mathcal{J}}_a} \frac{\mathrm{d}\Delta z_{a,1}}{\sqrt{2\pi}} \frac{\mathrm{d}\Delta z_{a,2}}{\sqrt{2\pi}} \cdots e^{\mathcal{I}[z]}. \tag{7.24}$$

Making use of the relation (7.23), one immediately obtain

$$Z_a = \int_{\tilde{\mathcal{J}}_a} \frac{e^{i\psi}\mathrm{d}\tilde{g}_1}{\sqrt{2\pi}} \frac{e^{i\psi}\mathrm{d}\tilde{g}_2}{\sqrt{2\pi}} \cdots \det R\, e^{\mathcal{I}[z]} \tag{7.25}$$

Comparing the above equation with Eq. (7.14), we obtain $\tilde{J}_a = \det R$.

As a function, $\tilde{\chi}^a_n(t)$ can also be expanded in the φ-basis such that we have

$$\tilde{\chi}^a_n(t) = \sum_m Q_{nm}\varphi_m(t). \tag{7.26}$$

Substituting the above expression into the definition of R-matrix, one obtains

$$R_{nm} = \int \mathrm{d}t\ \varphi_n(t) \left(\sum_i Q_{mi}\,\varphi_i(t) \right) = Q_{mn}. \tag{7.27}$$

Therefore $\det R = \det Q$. Now, we multiply the conjugate of Eq. (7.11) by $\tilde{\chi}^a_m(t)$ on both sides and performing the integral over t and obtain

$$\int \mathrm{d}t\ \tilde{\chi}^a_m(t)(e^{2i\psi}\hat{L}_a)\tilde{\chi}^a_n(t) = \tilde{\kappa}^a_n\delta_{mn} \quad (n \text{ is not summed}), \tag{7.28}$$

where we have used Eq. (7.12). Using Eq. (7.26), one thus has

$$\int \mathrm{d}t\ Q_{mi}(\varphi_i(t)e^{2i\psi}\hat{L}_a\varphi_j(t))Q_{nj}\varphi_j(t) = \tilde{\kappa}^a_n\delta_{mn} \text{ (n is not summed)}. \tag{7.29}$$

This is simply the matrix relation

$$Q_{mi}(e^{2i\psi}\hat{L}_{a,ij})Q^T_{jn} = \tilde{\kappa}^a_n\delta_{mn} \text{ (n is not summed)}. \tag{7.30}$$

Taking the determinant, one obtains

$$(\det Q)^2 \det(e^{2i\psi}\hat{L}_a) = \prod_n \tilde{\kappa}^a_n = |\det \hat{L}_a| = |\det(e^{2i\psi}\hat{L}_a)|. \tag{7.31}$$

Therefore one has

$$\tilde{J}_a = \det R = \det Q = \sqrt{\frac{|\det \mathcal{M}^\theta_a|}{\det \mathcal{M}^\theta_a}}, \tag{7.32}$$

where we have defined the operator $\mathcal{M}_a^\theta = e^{2i\psi}\hat{L}_a$. We therefore conclude that the Jacobian is the exponential of minus half of the phase of $\det \mathcal{M}_a^\theta$.

The relation (7.19) is particularly useful because we can relate the original flow eigenequation (7.11) to the ordinary eigenequation (7.13). In our tunneling problem in the Minkowski spacetime, we only need to solve

$$\mathcal{M}_a^\theta \tilde{f}_n^a(t,T) \equiv \left(e^{+2i\theta}\cdot\frac{\partial^2}{\partial t^2} + U''(\tilde{x}_a^\theta(t))\right)\tilde{f}_n^a(t,T) = \tilde{\lambda}_n^a(T)\tilde{f}_n^a(t,T). \tag{7.33}$$

And this equation can readily be analytically continued from the Euclidean ordinary eigenequation as we will show in the next section.

7.3 Analytic continuation of functional determinants

We want to carry out analytic continuation from Eq. (6.15) to Eq. (7.33). For convenience we copy these eigenequations here:

$$(-\partial_\tau^2 + U''(x_a(\tau)))f_n^a(\tau,\mathcal{T}) = \lambda_n^a(\mathcal{T})f_n^a(\tau,\mathcal{T}), \tag{7.34a}$$

$$\left(e^{+2i\theta}\cdot\frac{\partial^2}{\partial t^2} + U''(\tilde{x}_a^\theta(t))\right)\tilde{f}_n^a(t,T) = \tilde{\lambda}_n^a(T)\tilde{f}_n^a(t,T), \tag{7.34b}$$

where $f_n^a(-\mathcal{T}/2) = f_n^a(\mathcal{T}/2) = 0$ and $\tilde{f}_n^a(-T/2) = \tilde{f}_n^a(T/2) = 0$. Here, we note that, due to the Dirichlet boundary conditions, the eigenfunctions and eigenvalues in general have $\mathcal{T}$- or T-dependence.

7.3.1 Finite $\mathcal{T}$ and T

To get some intuition on Eq. (7.34), we first look at the trivial false vacuum saddle point $x_F(\tau) = x_+$. Denoting $U''(x_+) \equiv m^2$, Eq. (7.34a) becomes

$$\left(-\partial_\tau^2 + m^2\right) f_n^F(\tau,\mathcal{T}) = \lambda_n^F(\mathcal{T})q_n^F(\tau,\mathcal{T}). \tag{7.35}$$

The normalized solutions satisfying the boundary conditions are

$$\begin{aligned} f_n^F(\tau,\mathcal{T}) &= \sin\left(\frac{2n\pi\tau}{\mathcal{T}}\right)/\sqrt{\mathcal{T}/2}, \text{ or} \\ &= \cos\left(\frac{(2n+1)\pi\tau}{\mathcal{T}}\right)/\sqrt{\mathcal{T}/2}, \end{aligned} \tag{7.36}$$

with the eigenvalues

$$\lambda_n^F(\mathcal{T}) = \left(\frac{2n\pi}{\mathcal{T}}\right)^2 + m^2, \text{ or } \left(\frac{(2n+1)\pi}{\mathcal{T}}\right)^2 + m^2. \tag{7.37}$$

In this example, we see explicitly how the eigenfunctions and eigenvalues can depend on the time interval due to the Dirichlet boundary conditions.

The functional determinant that will appear in the Euclidean path integral is

$$\begin{aligned}\det(-\partial_\tau^2+m^2) &= \prod_{n=1}^{\infty}\left[\left(\frac{n\pi}{\mathcal{T}}\right)+m^2\right] \\ &= \left(\prod_{n=1}^{\infty}\left(\frac{n\pi}{\mathcal{T}}\right)^2\right)\left(\prod_{p=1}^{\infty}\left[1+\left(\frac{\mathcal{T}m}{p\pi}\right)^2\right]\right) \\ &= \left(\prod_{n=1}^{\infty}\left(\frac{n\pi}{\mathcal{T}}\right)^2\right)\frac{\sinh(m\mathcal{T})}{m\mathcal{T}}. \end{aligned} \tag{7.38}$$

The remaining infinite product should be canceled when we consider the functional determinant ratio. The functional determinant has an analytical expression in terms of $\mathcal{T}$.

By inspection, the normalized solutions to Eq. (7.34b) satisfying the boundary conditions are

$$\begin{aligned}\tilde{f}_n^F(t) &= \sin\left(\frac{2n\pi t}{T}\right)/\sqrt{T/2},\ \text{or} \\ &= \cos\left(\frac{(2n+1)\pi t}{T}\right)/\sqrt{T/2}. \end{aligned} \tag{7.39}$$

Hence we have the eigenvalues

$$\begin{aligned}\tilde{\lambda}_n^F(T) &= -e^{+2i\theta}\left(\frac{2n\pi}{T}\right)^2+m^2=\left(\frac{2n\pi}{ie^{-i\theta}T}\right)^2+m^2,\ \text{or} \\ &= \left(\frac{(2n+1)\pi}{ie^{-i\theta}T}\right)^2+m^2 \end{aligned} \tag{7.40}$$

The functional determinant that will appear in the Minkowski path integral is

$$\begin{aligned}\det(e^{2i\theta}\partial_t^2+m^2) &= \prod_{n=1}^{\infty}\left[\left(\frac{n\pi}{ie^{-i\theta}T}\right)^2+m^2\right] \\ &= \left(\prod_{n=1}^{\infty}\left(\frac{n\pi}{ie^{-i\theta}T}\right)^2\right)\left(\prod_{p=1}^{\infty}\left[1+\left(\frac{ie^{-i\theta}Tm}{p\pi}\right)^2\right]\right) \\ &= \left(\prod_{n=1}^{\infty}\left(\frac{n\pi}{ie^{-i\theta}T}\right)^2\right)\frac{\sinh(ie^{-i\theta}mT)}{ie^{-i\theta}mT}. \end{aligned} \tag{7.41}$$

The Minkowski functional determinant can be obtained from the Euclidean one by the replacement $\mathcal{T}\to ie^{-i\theta}T$.

Actually, we do not need to solve the Minkowski eigenequations. Recalling $\tilde{x}_a(t)=x_a(\tau\to ie^{-i\theta}t)$ and comparing Eq. (7.34b) with Eq. (7.34a), one can obtain $\tilde{f}_n^a(t,T)$ and $\tilde{\lambda}_n^a(T)$ from $f_n^a(\tau,\mathcal{T})$ and $\lambda_n^a(\mathcal{T})$ through the analytic continuations: $\tau\to ie^{-i\theta}t$, $\mathcal{T}\to ie^{-i\theta}T$. Thus we immediately know that the continuation $\mathcal{T}\to ie^{-i\theta}T$ in the determinant works also for the bounce.

7.3.2 Taking the limit $\mathcal{T}$,$\mathbf{T}\to\infty$

What will happen if we take the limit $\mathcal{T}\to\infty$ before carrying out the analytic continuation? We discuss this one by one, for the false vacuum and the bounce.

7.3.2.1 a=F

When taking $\mathcal{T}\to\infty$, it is sufficient to take only the sine functions or cosine functions in order to analyze the continuum spectrum. In the continuum case, the eigenvalues (taking the sine functions for the sake of clarity)

$$\lambda_n^F = \left(\frac{2n\pi}{\mathcal{T}}\right)^2 + m^2 \to \omega^2 + m^2, \tag{7.42}$$

where we identify the correspondence

$$\frac{2n\pi}{\mathcal{T}} \leftrightarrow \omega \tag{7.43}$$

between discrete and continuum cases.

Now let us ask whether the argument of the previous section still applies in the continuum case. First, it seems that, the functions $\sin(\omega\tau)$ and eigenvalues λ_ω^F have no dependence on $\mathcal{T}$. But this is not true, because ω is implicitly a function of $\mathcal{T}$. Whenever we go back to the finite time interval, we will have the quantization condition (7.43) and the $\mathcal{T}$-dependence shows up explicitly in ω. To calculate the functional determinant, we consider instead $\log\det$ which enjoys the identity $\log\det = \mathrm{Tr}\log$. Thus

$$\begin{aligned}\log\det(-\partial_\tau^2 + m^2) &= \sum_\omega \log(\omega^2 + m^2) \\ &= \mathcal{T}\int_{-\infty}^{\infty}\frac{d\omega}{2\pi}\log(\omega^2+m^2).\end{aligned} \tag{7.44}$$

where we have used

$$\sum_n \frac{2\pi}{\mathcal{T}} \leftrightarrow \int \mathrm{d}\omega. \tag{7.45}$$

Now let us consider the continuation to the Minkowski formalism. The eigenequation is

$$(e^{2i\theta}\partial_t^2 + m^2)\tilde{f}_{\tilde{\omega}}^F(t) = \tilde{\lambda}_{\tilde{\omega}}^F \tilde{f}_{\tilde{\omega}}^F(t). \tag{7.46}$$

The eigenfunctions are $\tilde{f}_{\tilde{\omega}}^F(t) = \sin(\tilde{\omega}t)$ (or cosine functions) with eigenvalues $\tilde{\lambda}_{\tilde{\omega}}^F = -e^{2i\theta}\tilde{\omega}^2 + m^2$. These can be obtained by directly substituting $\tau \to ie^{-i\theta}t, \mathcal{T}\to ie^{-i\theta}T$ into the Euclidean eigenfunctions and eigenvalues. One shall remember that the original ω is implicitly a function of $\mathcal{T}$, and thus under the continuation, takes

$$\omega \to -ie^{i\theta}\tilde{\omega}. \tag{7.47}$$

Note that both ω and $\tilde{\omega}$ are real as for the usual Wick rotation.

The Minkowski functional determinant is

$$\begin{aligned}\log\det(e^{2i\theta}\partial_t^2+m^2) &= \sum_{\tilde{\omega}}(-e^{2i\theta}\tilde{\omega}^2+m^2)\\ &= T\int_{-\infty}^{\infty}\frac{d\tilde{\omega}}{2\pi}\log(-e^{2i\theta}\tilde{\omega}^2+m^2)\\ &= (ie^{-i\theta}T)\int_{-\infty}^{\infty}\frac{d\omega}{2\pi}\log(\omega^2+m^2). \end{aligned} \tag{7.48}$$

Thus we see how, in the continuum case, the Minkowski functional determinant can be obtained directly by continuation $\mathcal{T}\to ie^{-i\theta}T$ from the Euclidean one, in agreement with the argument given in the last section.

Actually, the continuation of the parameter in Eq. (7.47) can be understood without reference to the quantization condition. The parameter ω in the eigenfunctions $\sin(\omega\tau)$ must be real because we need $\sin(\omega\tau)$ to be normalizable in the improper sense. When the functions $\sin(\omega\tau)$ are analytically continued via $\tau\to ie^{-i\theta}t$, the parameter ω must be also rotated accordingly as in Eq. (7.47) to ensure the normalization in the improper sense.

7.3.2.2 a=B

Now, let us consider a nontrivial background. We will only consider the kink instanton as the saddle point, mimicking the bounce. For a general argument for saddle point solutions, see Appendix. C.

The kink solution is (cf. Eq. (2.37))

$$\bar{x}(\tau) = v\tanh[\gamma(\tau-\tau_0)]\equiv vu, \tag{7.49}$$

where $v=\sqrt{6\mu^2/\lambda}$, $\gamma=\mu/\sqrt{2}$. This kink solution has boundary conditions $\bar{x}(-\infty)=-v, \bar{x}(\infty)=v$ and therefore is *not* the bounce $x_B(\tau)$ in the quantum mechanical tunneling problem. The bounce $x_B(\tau)$, in the limit $g\to 0$, should be an antikink-kink pair which has the correct boundary condition $x_B(\tau=\pm\infty)=v$. Since we only want to see how the analytic continuation from Eq. (7.34a) to Eq. (7.34b) works for a nontrivial saddle point, we therefore use the kink as an example. The analysis for the quantum mechanical bounce $x_B(\tau)$ should be straightforward. (The argument in Appendix. C shows this in generality.) Without loss of generality, we set $\tau_0=0$.

Using the variable u, we have

$$\frac{\mathrm{d}u}{\mathrm{d}\tau}=\gamma(1-u^2), \tag{7.50}$$

thus

$$\frac{\mathrm{d}}{\mathrm{d}\tau}=\gamma(1-u^2)\frac{\mathrm{d}}{\mathrm{d}u}. \tag{7.51}$$

The Euclidean eigenequation takes the form

$$\left[-\gamma^2(1-u^2)\frac{\mathrm{d}}{\mathrm{d}u}\left((1-u^2)\frac{\mathrm{d}}{\mathrm{d}u}\right)-\mu^2+\frac{\lambda}{2}v^2u^2\right]f_\varpi^K(u)=\lambda_\varpi^K f_\varpi^K(u), \tag{7.52}$$

where the superscript "K" indicates that the saddle point is the kink instanton. Since $-\mu^2 + \frac{\lambda}{2}v^2u^2 = \mu^2(3u^2-1)$, we have

$$\left[\frac{\mathrm{d}}{\mathrm{d}u}(1-u^2)\frac{\mathrm{d}}{\mathrm{d}u} - \frac{\varpi^2}{1-u^2} + 6\right] f_\varpi^K(u) = 0, \tag{7.53}$$

where

$$\varpi^2 = 4 - \lambda_\varpi^K/\gamma^2. \tag{7.54}$$

This is the associated Legendre differential equation and the solutions are the associated Legendre functions of degree 2 and order ϖ, $P_2^\varpi(u)$. The explicit expression for $P_2^\varpi(u)$ is

$$P_2^\varpi(u) = \frac{1}{\cos(\varpi\pi/2)}\left(\frac{u+1}{u-1}\right)^{\frac{\varpi}{2}} (3-\varpi)_\varpi \, P_2^{(-\varpi,+\varpi)}(u), \tag{7.55}$$

where $(z)_\varpi$ is the Pochhammer symbol, defined as

$$(z)_\varpi = \frac{\Gamma(z+\varpi)}{\Gamma(z)} \tag{7.56}$$

and $P_2^{(-\varpi,+\varpi)}$ is the Jacobi polynomial with the following explicit expression

$$P_2^{(-\varpi,+\varpi)} = \frac{1}{2}\left[(1-\varpi)(2-\varpi) - 3(2-\varpi)(1-u) + 3(1-u)^2\right]. \tag{7.57}$$

To understand what the eigenvalues λ_ϖ^K, or equivalently, the ϖ are, we can consider the asymptotic behaviour of $P_2^\varpi(u)$ at $u \to \pm 1$. We have

$$P_2^\varpi(u) \to (-1)^{\frac{\varpi}{2}} e^{\gamma\varpi\tau}\frac{1}{\cos(\varpi\pi/2)}(3-\varpi)_\varpi \, \frac{(1-\varpi)(2-\varpi)}{2}, \quad \text{as u} \to \ 1; \tag{7.58a}$$

$$P_2^\varpi(u) \to (-1)^{\frac{\varpi}{2}} e^{\gamma\varpi\tau}\frac{1}{\cos(\varpi\pi/2)}(3-\varpi)_\varpi \, \frac{(1+\varpi)(2+\varpi)}{2}, \quad \text{as u} \to \ -1; \tag{7.58b}$$

Now as commented in the previous section, the continuous modes $P_2^\varpi(u)$ must be normalized in the improper sense which requires ϖ to be imaginary such that the solutions become oscillating functions for large τ instead of exponential explosions.

For the Minkowski case, we have the saddle point

$$\tilde{\tilde{x}}(t) = v\tanh(ie^{-i\theta}\gamma t) \equiv v\tilde{u}(t). \tag{7.59}$$

We have

$$\frac{\mathrm{d}\tilde{u}}{\mathrm{d}t} = ie^{-i\theta}\gamma(1-\tilde{u}^2) \tag{7.60}$$

and thus

$$\frac{\mathrm{d}}{\mathrm{d}t} = ie^{-i\theta}\gamma(1-u^2)\frac{\mathrm{d}}{\mathrm{d}u}. \tag{7.61}$$

One can find that the Minkowski eigenequation becomes identical in form with the Euclidean eigenequation

$$\left[\frac{\mathrm{d}}{\mathrm{d}\tilde{u}}(1-\tilde{u}^2)\frac{\mathrm{d}}{\mathrm{d}\tilde{u}} - \frac{\varpi^2}{1-\tilde{u}^2} + 6\right] \tilde{f}^K_{\varpi}(\tilde{u}) = 0. \tag{7.62}$$

One can immedaitely obtain the solutions to Eq. (7.62) which are $P_2^{\varpi}(\tilde{u})$. Now the requirement of that $P_2^{\varpi}(\tilde{u})$ must be normalized in the improper sense enforces the rotation of the parameter ϖ:

$$\varpi \to -ie^{i\theta}\tilde{\varpi}, \tag{7.63}$$

with $\tilde{\varpi}$ being imaginary, as can be seen from the asymptotic behaviour (7.58).

As in the case for $a = F$, when we compute the determinants we will have a contribution from the continuum of eigenvalues associated with the improperly normalized functions. This will be an integral over ϖ or $\tilde{\varpi}$. The rotation (7.63), together with the rotation Eq. (7.47), gives us the continuation $\mathcal{T} \to ie^{-i\theta}T$ between Euclidean result and Minkowski result.

As we know, for the bounce saddle point, we have an additional discrete negative mode. But discrete modes in Euclidean case and Minkowski case should, however, match independently of the rotation. In Euclidean space, the discrete modes are normalizable in the proper sense, and they decay exponentially for large $|\tau|$, going as $\exp(-c\tau)$, with $c > 0$ for $\tau > 0$, and negative for $\tau < 0$. After continuation to $\tau \to ie^{-i\theta}t$, the analytically continued solutions for large t are proportional to $e^{-ct\sin\theta}e^{-ict\cos\theta}$. Therefore the real and imaginary parts still decay exponentially due to the first factor, as long as $\theta > 0$. Therefore for the discrete modes, one does not need to complexify other parameters of the Euclidean solutions, meaning that the discrete eigenvalues are preserved under rotations of the time contour, see Appendix C for details.

7.4 The decay rate

As we have shown in Sec. 7.2, the infinite product of the flow eigenvalues can be expressed as

$$\prod_n \tilde{\kappa}^a_n = \left|\det\left(e^{+2i\theta}\cdot\frac{\partial^2}{\partial t^2} + U''(\tilde{x}^{\theta}_a(t))\right)\right|, \tag{7.64}$$

and the Jacobian $\tilde{J}_a$ is the minus half of the phase of the above determinant. Through this, one transfers the problem of solving the flow eigenequations to that of solving the ordinary eigenequations. Together with the analytic continuation between the Euclidean and Minkowski functional determinants that we have proved in the last section, we therefore have

$$\tilde{J}_a \prod_n \sqrt{-i}e^{i\theta/2}\frac{1}{\sqrt{\tilde{\kappa}^a_n}} = \left[\left(\det(-\partial_\tau^2 + U''(x_a))|\right)_{\mathcal{T}\to ie^{-i\theta}T}\right]^{-1/2} \prod_n \sqrt{-i}e^{i\theta/2}. \tag{7.65}$$

The particular zero mode around the complex bounce is

$$\tilde{f}^B_1(t) = \frac{1}{\sqrt{-i}e^{i\theta/2}\sqrt{B}}\left.\frac{\mathrm{d}x_B(\tau)}{\mathrm{d}\tau}\right|_{\tau\to ie^{-i\theta}t} = -ie^{+i\theta}\frac{1}{\sqrt{-i}e^{i\theta/2}\sqrt{B}}\frac{\mathrm{d}\tilde{x}^{\theta}_B(t)}{\mathrm{d}t}. \tag{7.66}$$

Using Eqs. (6.44), (6.45), one can check that

$$\int_{-T/2}^{T/2} \mathrm{d}t\ \tilde{f}_1^B(t)\tilde{f}_1^B(t) = 1. \tag{7.67}$$

Therefore we have

$$\sqrt{-i}e^{i\theta/2}\tilde{f}_1^B(t)\,\mathrm{d}\tilde{c}_1^B = \mathrm{d}\Delta z_B = \frac{\mathrm{d}\tilde{x}_B}{\mathrm{d}t}\mathrm{d}t = \sqrt{-i}e^{i\theta/2}\sqrt{B}\tilde{f}_1^B(t)(ie^{-i\theta}\mathrm{d}t). \tag{7.68}$$

Hence, the integral measure over the zero mode has the following replacement

$$\frac{\sqrt{-i}e^{i\theta/2}}{\sqrt{2\pi}}\,\mathrm{d}\tilde{c}_1^B \to \sqrt{-i}e^{i\theta/2}\sqrt{\frac{B}{2\pi}}(ie^{-i\theta}\mathrm{d}t). \tag{7.69}$$

Upon integration, the zero mode gives us

$$\sqrt{-i}e^{i\theta/2}\sqrt{\frac{B}{2\pi}}(ie^{-i\theta}T). \tag{7.70}$$

Since the factor $\sqrt{-i}e^{i\theta/2}$ appears in every mode of the integral measures (including the measure for the trivial false vacuum saddle point), it is a total phase and can be discarded. Together with the result (7.65), we see that the Minkowski result is related to the Euclidean result by the analytic continuation $\mathcal{T} \to ie^{-i\theta}T$.

We expect that the false vacuum saddle point is connected with the complex saddle point since $\mathrm{Im}\mathcal{I}[\tilde{x}_F^\theta] = \mathrm{Im}\mathcal{I}[\tilde{x}_B^\theta] = 0$.[23] Thus we multiply the integral measure in the expansion around the complex bounce by $1/2$ and define the modified measure as

$$\widetilde{\mathcal{D}\Delta z_B} = \frac{1}{2}\prod_n \frac{1}{\sqrt{2\pi}}\,\mathrm{d}\tilde{g}_n^B, \tag{7.71}$$

where $\mathrm{d}\tilde{g}_1^B = \mathrm{d}\tilde{c}_1^B$. We denote the modified Z_B^M as $\tilde{Z}_B^M$, giving us

$$\langle \mathrm{FV}|e^{-iHT}|\mathrm{FV}\rangle = \mathcal{N}^2 Z_F^{M,\epsilon} + \mathcal{N}^2\tilde{Z}_B^{M,\epsilon}. \tag{7.72}$$

Now let us fix the normalization factor $\mathcal{N}$ in Eq. (7.72). We impose the normalization condition:

$$\mathcal{N}^2\ Z_F^{M,\epsilon} = 1. \tag{7.73}$$

This means that under small fluctuations, the false vacuum will always evolve into itself. Then we have

$$\langle \mathrm{FV}|e^{-iHT}|\mathrm{FV}\rangle = \langle \mathrm{FV}|\mathbf{1} + iM(T)|\mathrm{FV}\rangle = 1 + \frac{\tilde{Z}_B^{M,\epsilon}}{Z_F^{M,\epsilon}}. \tag{7.74}$$

We can recognize that

$$\langle \mathrm{FV}|M(T)|\mathrm{FV}\rangle = -i\,\frac{\tilde{Z}_B^{M,\epsilon}}{Z_F^{M,\epsilon}}. \tag{7.75}$$

[23] Had we not fixed $V(x_+) = 0$, we would have $iS_M^\theta[\tilde{x}_F] \neq 0$. But then $iS_M^\theta[\tilde{x}_B]$ will be shifted by the same quantity, leading no physical consequences after normalization.

Therefore,

$$\mathrm{Im}\langle \mathrm{FV}|M(T)|\mathrm{FV}\rangle = -\mathrm{Re}\left(\frac{\tilde{Z}_B^{M,\epsilon}}{Z_F^{M,\epsilon}}\right). \tag{7.76}$$

As we have shown in the last section, at NLO, the result can be obtained simply from the Euclidean one by the replacement $\mathcal{T} \to iT$ (the regulator ϵ is not important here). We finally obtain

$$\frac{\tilde{Z}_B^{M,\epsilon}}{Z_F^{M,\epsilon}} = -\frac{T}{2}\sqrt{\frac{B}{2\pi}}\left|\left(\frac{\det'[-\partial_\tau^2 + U''(x_B)]}{\det[-\partial_\tau^2 + U''(x_+)]}\right)\right|^{-1/2} e^{-B}. \tag{7.77}$$

Note that this is a real result as exactly the optical theorem requires, see Eq. (7.76). The imaginary unit i has been canceled by the i in iT obtained from the inverse Wick rotation $\mathcal{T} \to iT$. Substituting the above result into Eq. (7.76), one arrives at

$$\mathrm{Im}\langle \mathrm{FV}|M(T)|\mathrm{FV}\rangle = \frac{T}{2}\sqrt{\frac{B}{2\pi}}\left|\frac{\det'[-\partial_\tau^2 + U''(x_B)]}{\det[-\partial_\tau^2 + U''(x_+)]}\right|^{-1/2} e^{-B}. \tag{7.78}$$

Note the nontrivial cancellation of the minus sign in Eq. (7.76) by the one in Eq. (7.77), implying the validity of the optical theorem. Looking back into Eq. (6.32), we have

$$\begin{aligned} p(\text{false vacuum decay})_{\text{one single complex bounce}} &= T\,\Gamma \\ &\equiv T\sqrt{\frac{B}{2\pi}}\left|\frac{\det'[-\partial_\tau^2 + U''(x_B)]}{\det[-\partial_\tau^2 + U''(x_+)]}\right|^{-1/2} e^{-B}, \end{aligned} \tag{7.79}$$

identical to the result obtained in the Euclidean path integral. Note that, had we not introduced the complex bounce, we would have no way to prove this result. And this may explain why the instanton techniques can be used to describe real-time Minkowski process such as tunneling.

We can obtain the exponential decay law in a similar way as in the multiple-instanton argument for the Euclidean path integral given by Callan and Coleman [37]. The intuitive picture is the following. The particle, initially trapped in the false vacuum, can penetrate into the barrier region between the turning point p and x_+ due to its quantum nature. Every single complex bounce describes a collision of the particle on the outer wall in the barrier region. And the probability in Eq. (7.79) is the escape probability for the particle to penetrate outside of the barrier for one single collision. Namely, the surviving probability is $1-p$ which is the first order expansion of e^{-p}. During the history, collisions happen again and again which leads to an exponential surviving probability $e^{-\Gamma T}$. The mathematical derivation of this statement can be carried out by completely repeating the argument in Ref. [37] which will be omitted here.

The derivation and argument can be straightforwardly generalized to quantum field theory and one obtains Eq. (2.32)

7.5 The physical meaning of the negative eigenvalue λ_0^B

From both the Euclidean formalism and the Minkowski formalism, we see that the imaginary part of the false vacuum energy or the M matrix is intrinsically related the existence

of the negative eigenvalue λ_0^B of the fluctuation operator $-\partial_\tau^2 + U''(x_B)$. In the Euclidean formalism, the negative mode corresponds to deformations of the bounce.[24] The field configurations generated by these deformations are $\hat{x}(\tau;\zeta)$ discussed in Secs. 6.1 and 2.1. In the neighborhood of the bounce, these configurations can be expressed linearly as $\hat{x}(\tau;\zeta) = x_B(\tau) + \zeta\, f_0^B(\tau)$ for $\zeta \in \mathbb{R}$. The existence of these configurations makes us analytically continue ζ to imaginary values.

In the Minkowski formalism, we shall expect that the negative mode also corresponds to deformations of the complex bounce. In the neighborhood of the complex bounce, the generated configurations can be expressed as $\hat{\tilde{x}}(t;\zeta) = \tilde{x}_B^\theta(t) + \zeta\, \tilde{f}_0^B(t)$ obtained from the Euclidean ones via the map $\tau \to ie^{-i\theta}t$. Amusingly, though $\hat{\tilde{x}}(t;\zeta)$ is a complex function, $\hat{\tilde{x}}(t=0;\zeta)$ is real and $\hat{\tilde{x}}(t=0;\zeta) = \hat{x}(\tau=0;\zeta)$. Since it is essentially these deformed configurations that are responsible for the imaginary part in the M matrix, according to the optical theorem (6.32) one can deduce that

$$\int \mathrm{d}\tilde{g}_0^B \text{ in Minkowski path integral} \sim \int \mathrm{d}\zeta\; P(\mathrm{FV} \to x_{\mathrm{exit}}(\zeta) \equiv \hat{\tilde{x}}(t=0;\zeta)). \tag{7.80}$$

Here $P(\mathrm{FV} \to x_{\mathrm{exit}}(\zeta))$ is the probability for a particle to transit from the false vacuum to $x_{\mathrm{exit}}(\zeta)$. Indeed, $x_{\mathrm{exit}}(\zeta)$ are the intermediate states $\{\mathbf{q}_n\}$ in Eq. (6.32). We do not need to worry about the seeming energy violation for a particle exiting at a point away from the classical turning point $\mathbf{p}$ since the false vacuum is an approximate energy eigenstate while a particle escaping at a particular point is a position eigenstate at $t = 0$. This "energy violation" is allowed by the uncertainty principle. We emphasize that, after tunneling, the particle is in a superposition of the position eigenstates and the energy expectation value of this superposition of states is equal to the one before tunneling.

In this interpretation, we have a physical picture why there is a particular factor $1/2$ in the path integral measure for $\mathrm{d}\tilde{g}_0^B$. According to the correspondence (7.80), associating a factor $1/2$ to $\mathrm{d}\tilde{g}_0$ amounts to constraining the final states after tunneling to be $\hat{\tilde{x}}(t = 0;\zeta > b)$. These states are simply the position eigenstates outside of the turning point. The reason for this constraint was explained in Refs. [46, 47]. Roughly speaking, the physical decay rate is defined in a timescale for which the escape wave function $\Psi(x;t=0)$ has no support in the inner region with respect to the turning point $\mathbf{p}$. That is, the false vacuum decays exponentially for intermediate times between the short time scale of the sloshing stage inside the metastable well and the long time scale in which the wave function begins to flow back into the metastable minimum. In Gamow's language, this physical definition corresponds to a pure outgoing boundary condition. In Appendix. D, we give a derivation of the decay rate from the WKB method, closely following Ref. [42].

Since the integral $\mathrm{d}\tilde{g}_0^B$ is weighted by an Gaussian $\exp(-|\lambda_0^B||\tilde{g}_0^B|^2/2)$, the probability distribution function (PDF) after tunneling is expected to be

$$|\Psi(x,t=0)|^2 \sim e^{-\frac{1}{2}|\lambda_0^B|\,\zeta^2} \sim e^{-\frac{1}{2}\frac{|\lambda_0^B|}{(f_0^B(0))^2}(x_{\mathrm{exit}}-x_p)^2}, \tag{7.81}$$

where we have used

$$x_{\mathrm{exit}} = \hat{\tilde{x}}(0;\zeta) = \hat{x}(0;\zeta) = x_B(0) + \zeta\, f_0^B(0) \tag{7.82}$$

[24] In the thin-wall limit, these deformations are dilations.

and $x_B(0) = x_p$ with x_p being the coordinate of the classical turning point $\mathbf{p}$. Eq. (7.81) is a Gaussian distribution around the classical turning point. Considering the fact that there is no support inside the turning point for the wave function in the exponential decay regime, our construction of the optical theorem implies a half-Gaussian distribution after tunneling. The half width at half minimum is

$$L_{\rm HWHM} = \sqrt{\frac{(2\ln 2)\,(f_0^B(0))^2}{|\lambda_0^B|}}. \tag{7.83}$$

The negative eigenvalue λ_0^B gets a physical meaning! Of course, one can anticipate that this clean formula is an ideal case where the true vacuum has a much wider region than the false vacuum. In any realistic situation, this formula receives modifications.

In the context of quantum field theory, $x(\tau)$ is simply replaced by $\Phi(\tau, \mathbf{x})$ in the Lagrangian. And every exit point is replaced by a bubble configuration $\varphi(r \equiv |\mathbf{x}|; \tau = 0)$. After the false vacuum decay, we generally have a superposition state of all the quantum bubbles with radius the same as or bigger than the critical one. Let us denote the bounce solution in field theory as $\varphi_B(\rho)$ (recall $\rho = \sqrt{\tau^2 + r^2}$). Similar to $\hat{x}(\tau; \zeta)$, we have the linearized relation

$$\hat{\varphi}(\rho; \zeta) = \varphi_B(\rho; \zeta) + \zeta\, \phi_0^B(\rho) \tag{7.84}$$

where $\phi_0^B(\rho)$ is the negative mode. The field configurations at $\tau = 0$ are

$$\hat{\varphi}(r; \zeta) = \varphi_B(r) + \zeta\, \phi_0^B(r). \tag{7.85}$$

The radii of the bubbles can be effectively defined as the peak of the derivative of the field configurations with respect to r:[25]

$$\left.\frac{\partial^2 \hat{\varphi}(r; \zeta)}{\partial r^2}\right|_{r=R} = 0; \tag{7.86}$$

$$\left.\frac{\partial^2 \varphi_B(r)}{\partial r^2}\right|_{r=R_c} = 0. \tag{7.87}$$

Here we have changed the notations; we use R_c to denote the radius of the critical bubble and leave R to denote the radius of a general nucleated bubble. From Eq. (7.85), we have

$$\zeta = -\frac{\left.\frac{\partial^2 \varphi_B(r)}{\partial r^2}\right|_R}{\left.\frac{\partial^2 \phi_0^B(r)}{\partial r^2}\right|_R} \equiv \zeta(R). \tag{7.88}$$

If $R = R_c$, then $\zeta = 0$ as expected.

We should have a PDF in terms of the radius of the quantum bubbles

$$\Psi(R) \sim e^{-\frac{1}{2}\,|\lambda_0^B|\,\zeta(R)^2}. \tag{7.89}$$

[25] We restrict our discussion to the thin-wall cases, otherwise the concepts of the bubble wall and its position become unclear.

Here λ_0^B denotes the negative eigenvalue of the operator $-\Delta^{(4)}+U''(\varphi_B)$. In the thin-wall approximation, one can even obtain a closed form for $\zeta(R)$ and $\Psi(R)$. $\varphi_B(r)$ takes the form (cf. Eq (2.37))

$$\varphi_B(r) = v\tanh[\gamma(r-R_c)], \tag{7.90}$$

where $R_c = 12\gamma/(gv)$. The negative-mode eigenfunction is

$$\phi_0^B(r) = -S_E[\varphi_B]^{-1/2}\,\partial_r\varphi_B. \tag{7.91}$$

The negative eigenvalue is $\lambda_0^B = -3/R_c^2$. A direct calculation gives

$$\zeta(R) = \frac{S_E[\varphi_B]^{1/2}\tanh[\gamma(R-R_c)]}{\gamma\left(1-3\tanh^2[\gamma(R-R_c)]\right)}. \tag{7.92}$$

$\zeta(R_c) = 0$ as it should be. Note that, since the linearized relation (7.84) is valid only in the neighborhood of the bounce, Eq. (7.92) is also valid only in the neighborhood of R_c. Thus the pole in Eq. (7.92) can be understood as a signal that we go into the non-linear region.

The state Eq. (7.89) looks like a spherically symmetric wave. It is anticipated that decoherence will collapse the superposition state to classical bubbles. The possible phenomenological consequences of the half-Gaussian PDF for the nucleated bubbles will be pursued elsewhere.

Chapter 8

Conclusion and Perspectives

In the SM, current experimental data and theoretical calculations suggest that the electroweak vacuum is unstable but with a lifetime much longer than the Universe, leading to the metastable scenario. This motivates an extremely intriguing picture that the SM could be extrapolated up to the Planck scale without any new heavy degrees of freedom in principle. Since there is a variety of phenomena that cannot be explained by the SM such as dark matter and the matter-antimatter asymmetry, the metastable scenario may imply that all these phenomena might be explained by feebly coupled "hidden particles" with masses below the electroweak scale. This possibility implies that the best strategy to find these particles does not lie in the construction of more powerful colliders to probe the energy frontier but in experiments at the intensity frontier that are sensitive to very small coupling constants. Because of this, the computations on the electroweak lifetime in the SM are very important. Previous studies have been focused on the precision calculations of the couplings but paid less attention to the tunneling process itself. In particular, though the couplings have been calculated at two-loop order, the radiative effects on the vacuum transition have not been investigated with a matched precision. Radiative effects may be important because, in the false vacuum decay, there is an inhomogeneous background while the precision couplings do not account for the particular effects from the inhomogeneity of the background. With these motivations, in this thesis we have, based on the works [59, 60], developed a systematic method to handle the radiative effects on false vacuum decay in the Higgs-Yukawa theory. We have given both an elaborated theoretical study on deriving the formalism using the effective action and a detailed numerical study. In particular, we have derived the Green's functions for the Euclidean Dirac operator with an $O(4)$-symmetric mass term. Both the general formalism and the Green's functions we have derived can be applied to more realistic calculations in the SM which will be pursued in a future project.

In addition to the problem of electroweak metastability in flat spacetime, this question has also been studied in curved spacetimes. One typical example is that the bubble nucleation may be catalyzed by a black hole. Indeed, recent studies suggest that microscopic black holes could dramatically reduce the lifetime of the electroweak vacuum in some parameter space of the Higgs potential with possible higher dimensional operators induced by new physics or gravity effects. Since such microscopic black holes could be generated via evaporation by primordial black holes, the constraint that the electroweak vacuum has a lifetime longer than the Universe puts important constraints on inflation during or after which primordial black holes can be produced. However, one particularly important issue in the studies of bubble nucleation around black holes is the ambiguity of the interpretation of the bounce solution. On the one hand, one may begin with a pure Schwarzschild spacetime and study the vacuum decay using the Callan-Coleman formalism, thus expecting it to describe a quantum transition. On the other hand, the

Euclidean Schwarzschild spacetime, obtained by Wick rotation of the Schwarzschild time from the Minkowski Schwarzschild metric, has a natural periodicity in time and therefore one expects a thermal interpretation. In this thesis, we have clarified the physical meaning of an $O(3) \times O(2)$ bounce solution in the Euclidean Schwarzschild spacetime [56]. We have proposed a correspondence between two different interpretations for such bounce. It can be either interpreted as a thermal transition of vacuum in the static region outside of a Schwarzschild black hole or a quantum tunneling in a maximally extended Kruskal-Szekeres spacetime. The thermal and quantum interpretations are given by the static observers or the freely falling observers, respectively. In particular, we found that the Matsubara modes in the thermal interpretation can be mapped to the circular harmonic modes from the $O(2)$ symmetry (from the $O(3) \times O(2)$) in the tunneling interpretation. The transition probabilities in these two interpretations are shown to agree with each other. We also showed that this correspondence is general and can be applied to the Rindler horizon and the de Sitter horizon.

The correspondence between these two interpretations is due to thermofield dynamics which relates a thermal state to a pure quantum state by doubling the Fock space. Thus the thermal field theory in the static region outside of a Schwarzschild black hole and the (Euclidean version of the) quantum field theory in the maximally extended Kruskal-Szekeres spacetime turn out to live in the same Euclidean spacetime. This correspondence, however, brings a new paradox related to black holes. That is, for freely falling observers, if they calculate the tunneling probability in a Schwarzschild spacetime background, they would not get the agreement with the thermal transition probability obtained by the external static observers. This paradox is originated from the curious fact that while the black hole horizon shares a similar local structure with other horizons, it is very different in the global structure. This paradox might imply that the Hawking radiation for a Schwarzschild black hole cannot be purely thermal such that a thermal field theory cannot be employed to describe the physical processes observed by the external static observers, including the vacuum transition. This will be investigated in the future.

The correspondence again could provide a guiding principle in studying thermal phase transitions. The decay rate of vacuum decay at finite temperature has so far no rigorous derivation from first principles. We, therefore, have suggested a formula for the thermal decay rate that can be consistent with the Unruh effect and the black hole complementarity principle. Further, we have also formalized the decay formula in a way that it can be used to systematically account for the higher order quantum and thermal corrections that will be investigated elsewhere. We leave a detailed comparison between our formula and Linde's or Affleck's formula to a future project.

Although false vacuum decay has been applied in a plenty of phenomenological studies, it has not been presented in a real-time description before. In the last part of this thesis, we have provided a real-time formalism for quantum tunneling. We have found that the false vacuum decay rate can be derived from the unitarity of the evolution operator. Specifically, the decay rate can be given by the imaginary part of the M-matrix in the S-matrix with $S = \mathbf{1}+iM$, where S is the transition amplitude from the false vacuum to itself. In this way, we have constructed an optical theorem for the unstable vacuum. The real-time formalism forces us to directly deal with the Minkowski transition amplitude instead of a Euclidean one as Callan and Coleman originally did. However, for the potentials of interest, there

are no nontrivial classical solutions with the correct boundary conditions for false vacuum decay. Thus, one finds no way to apply the method of steepest descent in order to perform the Minkowski path integral. In our work, we have applied Picard-Lefschetz theory to the path integral, within which we complexify the paths and deform the integration contour such that it passes through complex saddle points. This is allowed as long as the deformed contour gives the same integration result. We have identified a particular complex saddle point that corresponds to the bounce solution in the Euclidean field theory, which we refer to as the complex bounce. Then the integration on the Lefschetz thimble that is generated by the steepest flows from the complex bounce is shown to give a one-loop result identical with one obtained by Callan and Coleman.

Our derivation of the decay rate in real time has important consequences. According to the optical theorem, the decay rate obtained is responsible for the transitions from the false vacuum to all the intermediate states, including the most typical one for the critical bubble. In this way, our theory predicts a probability distribution for the nucleated bubbles. We will investigate the possible phenomenological consequences of this observation in the future.

Acknowledgement

I would like to express my gratitude here to the various people who supported me in completing this work during the past years.

First of all, I would like to thank my supervisor Björn Garbrecht for his guidance on my Ph.D. study. I have greatly benefited from sharing his expertise in the fields of quantum field theory and particle physics. I, in particular, want to express my gratitude to Björn for his great patience on my language barrier that I encountered at the early stage of my Ph.D. study. Certainly, his profound knowledge and rigorous scholarship have helped me to become an independent researcher. I am also grateful to Peter Millington and Carlos Tamarit, in collaborations with whom most of the results in this thesis were achieved. Peter teaches me a lot on false vacuum decay while Carlos always patiently answers my questions from different topics.

I also benefited from the great courses given by Andreas Weiler and Patrick Vaudrevange as well as the useful discussions with them on supersymmetry and beyond the standard model. I am in particularly inspired by the discussions in the seminars that Andreas has put great efforts to organize. I would also give a special thank to Marco Drewes for his very nice advice and help with pursuing my future research career.

I would also thank many other colleagues in the T70, T30 and T75 theory groups at TUM for many valuable discussions in the seminars or the coffee time. They are Juan S. Cruz, Kåre Fridell, Dario Gueter, Julia Harz, Juraj Klarić, Philipp Klose, Jamie McDonald, Gramos Qerimi, Llibert Aresté Soló, Konstantin Springmann, Jian Wang, Yan-Bing Wei, Giovanni Zattera, Hong Zhang, Yi Zhu.

Finally, I would like to thank my friends and family who made my life and study in Munich a pleasant one. Most importantly there are my parents, to whom I owe so much during all the previous years. I would also thank my friends, Hua Chen, Qi-Bo Chen, Zheng Liu, Zi-Liang Wang, You-Quan Zhou, to name a few.

My last thank is devoted to my wife Fang-Ping Fan for her incredible patience and willingness to respect my decision to do a Ph.D. here in Munich. Thanks for waiting for me for all those years.

Appendix

Appendix A

Functional Determinant

In this appendix, we will introduce two different ways, the Gel'fand-Yaglom method, and the Green's function method, of evaluating the functional determinants of ordinary differential operators and compare them. We will take the seminal model of particle tunneling (cf. Sec. 2.1) as an application. These methods can also be applied to false vacuum decay because the $O(4)$-symmetry of the background allows the decomposition of a four-dimensional partial differential operator into a hyperradial operator and the Laplace-Beltrami operator. The angular spectrum can be exactly solved. Thus, the evaluation of the determinant of a four-dimensional hyperspherically symmetric partial differential operator can be essentially reduced to evaluating the determinant of a hyperradial ordinary differential operator.

A.1 Gel'fand-Yaglom Method

The Gel'fand-Yaglom method is based on the following powerful theorem. In this section, we closely follow Ref. [42].

A.1.1 Gel'fand-Yaglom theorem

Consider the equation

$$(-\partial_\tau^2 + W(\tau))\,\psi(\tau) = \lambda\,\psi(\tau), \tag{A.1}$$

where $W(\tau)$ is some bounded function of $\tau \in [-\mathcal{T}/2, \mathcal{T}/2]$. Let us define $\psi_\lambda(\tau)$ as the solution of this equation obeying the following boundary conditions:

$$\psi_\lambda(-\mathcal{T}/2) = 0, \quad \partial_\tau \psi_\lambda(\tau)|_{\tau=-\mathcal{T}/2} = 1. \tag{A.2}$$

The determinant of the operator $-\partial_\tau^2 + W(\tau)$ is defined as

$$\det(-\partial_\tau^2 + W(\tau)) = \prod_n \lambda_n, \tag{A.3}$$

where the λ_n satisfy

$$(-\partial_\tau^2 + W(\tau))\,\psi_{\lambda_n}(\tau) = \lambda_n\,\psi_{\lambda_n}(\tau), \tag{A.4}$$

with boundary conditions $\psi_{\lambda_n}(-\mathcal{T}/2) = \psi_{\lambda_n}(\mathcal{T}/2) = 0$.

The Gel'fand-Yaglom theorem states that

$$\frac{\det[-\partial_\tau^2 + W^{(1)}(\tau) - \lambda]}{\det[-\partial_\tau^2 + W^{(2)}(\tau) - \lambda]} = \frac{\psi_\lambda^{(1)}(\mathcal{T}/2)}{\psi_\lambda^{(2)}(\mathcal{T}/2)}. \tag{A.5}$$

Applying the above formula to the case $\lambda = 0$ and taking the limit $\mathcal{T} \to \infty$, we obtain the ratio that we have in our decay rate formula.

A.1.2 Evaluating the ratio of the functional determinants

The functional determinant ratio in the tunneling rate now can be readily evaluated. We first consider the case $W^{(1)}(\tau) = U''(x_+) \equiv m^2$. The solution to Eq. (A.1) with the boundary conditions (A.2) is

$$\psi_0^{(1)}(\tau) = \frac{1}{m}\sinh[m(\tau + \mathcal{T}/2)]. \tag{A.6}$$

Thus $\psi_0^{(1)}(\mathcal{T}/2) = e^{m\mathcal{T}}/2m$ for large $\mathcal{T}$.

Next, let us consider the case $W^{(2)}(\tau) = U''(x_B(\tau))$. We have to evaluate the primed determinant. Following Coleman, we can do this by evaluating the full determinant on a finite interval $[-\mathcal{T}/2, \mathcal{T}/2]$, dividing it by its smallest *finite* eigenvalue near zero, λ_0 (to be distinguished from the negative eigenvalue λ_0^B), and finally letting $\mathcal{T}$ go to infinity. $\psi_0^{(2)}(\tau)$ can be constructed from an arbitrary basis of solutions. Actually, it is sufficient to know its asymptotic behavior at $\pm\mathcal{T}/2$ in order to apply formula (A.5). Consider the equation

$$\left(-\partial_\tau^2 + U''(x_B(\tau))\right)\psi(\tau) = 0. \tag{A.7}$$

One solution in the basis can be

$$x_1(\tau) = B^{-1/2}\,\frac{\mathrm{d}x_B(\tau)}{\mathrm{d}\tau} \to \pm\,\frac{A}{\sqrt{m}}\,e^{-m|\tau|},\ \text{as } \tau \to \pm\infty, \tag{A.8}$$

where A is determined by the asymptotic behaviour of $x_1(\tau)$ (cf. Eq. (A.11)). Note that $\psi_0^{(2)}(\tau)$ cannot be $x_1(\tau)$ because $x_1(\tau)$ does not satisfy the particular boundary conditions given below Eq. (A.4). For the classical bounce, we have

$$\frac{1}{2}\left(\frac{\mathrm{d}x_B(\tau)}{\mathrm{d}\tau}\right)^2 - U(x_B(\tau)) = 0. \tag{A.9}$$

Therefore $\mathrm{d}x_B(\tau)/d\tau = \sqrt{2U(x_B(\tau))}$ which leads to

$$\tau = \int_{x_p}^{x} \mathrm{d}x\,\frac{1}{\sqrt{2U(x)}}. \tag{A.10}$$

Using the asymptotic behaviour Eq. (A.8), one has

$$m\tau \equiv m\int_{x_p}^{x} \mathrm{d}x\,\frac{1}{\sqrt{2U(x)}} = -\ln\left[B^{-1/2}\,m^{3/2}\,A^{-1}\,(x_+ - x)\right] + \mathcal{O}(x_+ - x). \tag{A.11}$$

Denote another independent solution to Eq. (A.7) as $x_2(\tau)$. One can choose the normalization for $x_2(\tau)$ such that

$$x_1\,\partial_\tau x_2 - x_2\,\partial_\tau x_1 = 2\,A^2. \tag{A.12}$$

Therefore, we can deduce its asymptotic behaviour

$$x_2(\tau) \to \frac{A}{\sqrt{m}}\,e^{m|\tau|},\ \text{as } \tau \to \pm\infty. \tag{A.13}$$

According to the boundary conditions (A.2), one can construct $\psi_0^{(2)}(\tau)$ as

$$\psi_0^{(2)}(\tau) = -\frac{1}{2\sqrt{m}A}\left(e^{m\mathcal{T}/2}\,x_1(\tau) + e^{-m\mathcal{T}/2}\,x_2(\tau)\right) \tag{A.14}$$

leading to $\psi_0^{(2)}(\mathcal{T}/2) = -1/m$.

Now let us subtract the smallest positive eigenvalue λ_0. Since λ_0 is small, we can expand $\psi_{\lambda_0}(\tau) = \psi_0^{(2)}(\tau) + \delta\psi_{\lambda_0}(\tau)$ in the eigenequation. Hence, one has

$$(-\partial_\tau^2 + U''(x_B(\tau)))\,\delta\psi_{\lambda_0}(\tau) = \lambda_0\,\psi_0^{(2)}(\tau). \tag{A.15}$$

The solution can be constructed directly as

$$\psi_{\lambda_0}(\tau) = \psi_0^{(2)}(\tau) - \frac{\lambda_0}{2\,A^2}\int_{-\mathcal{T}/2}^{\tau} d\tau'\,[x_2(\tau)x_1(\tau') - x_1(\tau)x_2(\tau')]\,\psi_0^{(2)}(\tau') \tag{A.16}$$

and

$$\psi_{\lambda_0}(\mathcal{T}/2) = -\frac{1}{m} + \frac{\lambda_0}{4mA^2}\int_{-\mathcal{T}/2}^{\mathcal{T}/2} d\tau'\,[e^{m\mathcal{T}}x_1^2(\tau') - e^{-m\mathcal{T}}x_2^2(\tau')]. \tag{A.17}$$

Since $x_1(\tau)$ is normalized, we arrive at

$$\psi_{\lambda_0}(\mathcal{T}/2) \approx -\frac{1}{m} + \frac{\lambda_0}{4mA^2}\,e^{m\mathcal{T}}. \tag{A.18}$$

By requiring the boundary condition $\psi_{\lambda_0}(\mathcal{T}/2) = 0$, we obtain $\lambda_0 = 4\,A^2/e^{m\mathcal{T}}$. In total, we have

$$\frac{\det'[-\partial_\tau^2 + U''(x_B)]}{\det[-\partial_\tau^2 + U''(x_+)]} = \frac{\psi_0^{(2)}(\mathcal{T}/2)}{\lambda_0\,\psi_0^{(1)}(\mathcal{T}/2)} = -\frac{1}{2\,A^2}. \tag{A.19}$$

Note that this is a *negative* number, indicating the existence of a negative eigenvalue in the eigen spectrum of operator $-\partial_\tau^2 + U''(x_B(\tau))$. Had we used a kink solution $\bar{x}(\tau)$ (see Appendix A.3) instead of the bounce $x_B(\tau)$, the asymptotic behaviour in Eq. (A.8) will be different and leads a positive result in Eq. (A.19) [42]. Substituting the above result into Eq. (2.24), we have

$$\Gamma = \sqrt{\frac{B}{\pi\hbar}}\,e^{-B/\hbar}\,A, \tag{A.20}$$

where we have kept $\hbar$ explicitly since we will compare with the WKB method in Appendix D.

A.2 Green's function method

Now we will introduce the Green's function method for calculating the fluctuation determinant due to Baacke and Junker [121, 122, 123, 124] (see also Ref. [61]).

Suppose we have the following eigenequations

$$G_1^{-1}\psi_n^{(1)}(\tau) \equiv [-\partial_\tau^2 + W^{(1)}(\tau)]\psi_n^{(1)}(\tau) = \lambda_n^{(1)}\psi_n^{(1)}(\tau), \tag{A.21}$$

$$G_2^{-1}\psi_n^{(1)}(\tau) \equiv [-\partial_\tau^2 + W^{(2)}(\tau)]\psi_n^{(2)}(\tau) = \lambda_n^{(2)}\psi_n^{(2)}(\tau), \tag{A.22}$$

Then

$$Q \equiv \ln \frac{\det[-\partial_\tau^2 + W^{(1)}(\tau)]}{\det[-\partial_\tau^2 + W^{(2)}(\tau)]} = \sum_n \ln \frac{\lambda_n^{(1)}}{\lambda_n^{(2)}}. \tag{A.23}$$

In order to obtain an expression for the fluctuation determinant in terms of the Green's functions, we consider the operator

$$G_i^{-1}(s) = G_i^{-1} + s, \tag{A.24}$$

where $i = 1, 2$ and $s \in \mathbb{R}$ is an auxiliary parameter. The Green's functions can be written as

$$G_i(\tau, \tau', s) = \sum_n \frac{\psi_n^{(i)*}(\tau)\, \psi_n^{(i)}(\tau')}{\lambda_n^{(i)} + s}. \tag{A.25}$$

Integrating $G_i(\tau, \tau, s)$ over τ, we obtain

$$\int \mathrm{d}\tau\, G_i(\tau, \tau, s) = \sum_n \frac{1}{\lambda_n^{(i)} + s} \tag{A.26}$$

by virtue of the orthonormality of the eigenfunctions.

Further, we integrate over s up to some UV cut-off Λ, giving

$$\int_0^{\Lambda^2} \mathrm{d}s \int \mathrm{d}\tau\, G_i(\tau, \tau, s) = -\sum_n \ln \frac{\lambda_n^{(i)}}{\lambda_n^{(i)} + \Lambda}. \tag{A.27}$$

Comparing this with Eq. (A.23), we get

$$\ln \frac{\det[-\partial_\tau^2 + W^{(1)}(\tau)]}{\det[-\partial_\tau^2 + W^{(2)}(\tau)]} = \lim_{\Lambda\to\infty} -\int_0^{\Lambda} \mathrm{d}s \int \mathrm{d}\tau \Big(G_1(\tau, \tau, s) - G_2(\tau, \tau, s)\Big). \tag{A.28}$$

A.3 Gel'fand-Yaglom method vs. Green's function method

Let us compare the Gel'fand-Yaglom method with the Green's function method for the kink instanton:

$$\bar{x}(\tau) = v \tanh\left(\frac{\mu}{\sqrt{2}}\tau\right) \tag{A.29}$$

which gives $B \equiv S_E[\bar{x}] = 4\sqrt{2}\mu^3/\lambda$. Note that the kink solution is not the bounce solution in the degenerate limit, that is, the double-well model, because the kink solution approaches different vacua at $\tau \to \pm\infty$. But we still use B to denote the kink action.

Now $x_1(\tau)$ has the following asymptotic behavior

$$x_1(\tau) = B^{-1/2} \frac{\mathrm{d}\bar{x}(\tau)}{\mathrm{d}\tau} \to \frac{A}{\sqrt{m}}\, e^{-m|\tau|}, \text{ as } \tau \to \pm\infty, \tag{A.30}$$

where $A = 2\sqrt{3}\mu$, $m = \sqrt{2}\mu$. The normalization condition (A.12) gives us

$$x_2(\tau) \to \pm\frac{A}{\sqrt{m}} e^{m|\tau|}. \tag{A.31}$$

These asymptotic behaviors introduce an additional minus sign in $\psi_0^{(2)}(\tau)$ and hence in the formula (A.19). Finally, we have

$$\frac{\det'(-\partial_\tau^2 + U''(\bar{x}))}{\det(-\partial_\tau^2 + U''(x_+))} = \frac{1}{24\mu^2}. \tag{A.32}$$

On the other hand, the functional determinant ratio can be calculated via the Green's function method,

$$\ln \frac{\det(-\partial_\tau^2 + U''(\bar{x}))}{\det(-\partial_\tau^2 + U''(x_+))} = -\int_{-\infty}^{\infty} \mathrm{d}\tau \int_0^{\infty} \mathrm{d}s \, \Big(G(\bar{x};\tau,\tau,s) - G(x_+;\tau,\tau,s) \Big). \tag{A.33}$$

We first solve the Green's functions for the kink background. Defining $u \equiv \tanh(\mu\tau/\sqrt{2})$, we have

$$\left(\frac{\mathrm{d}}{\mathrm{d}u}(1-u^2)\frac{\mathrm{d}}{\mathrm{d}u} - \frac{\varpi^2}{1-u^2} + 6 \right) G(\bar{x};u,u',s) = -\left(\frac{\sqrt{2}}{\mu}\right)\delta(u-u'), \tag{A.34}$$

where $\varpi^2 = 4 + 2s/\mu^2$. The Green's function to the above equation has been analytically solved in Ref. [114]. The Green's function can be decomposed into two parts of contributions from the discrete and continuum spectrum, respectively. The contribution from the discrete spectrum is

$$G_d(\bar{x};u,u',s) = \frac{\sqrt{2}}{\mu}\left(-\frac{3}{2}\frac{uu'}{1-\varpi^2}\sqrt{1-u^2}\sqrt{1-u'^2} - \frac{3}{4}\frac{1}{4-\varpi^2}(1-u^2)(1-u'^2) \right), \tag{A.35}$$

where the second term is for the time-translational zero mode that needs to be subtracted. The contribution from the continuum spectrum is

$$\begin{aligned} G_c(\bar{x};u,u',s) = \frac{\sqrt{2}}{\mu}\Bigg\{ & \frac{3}{2}\frac{uu'}{1-\varpi^2}\sqrt{1-u^2}\sqrt{1-u'^2} + \frac{3}{4}\frac{1}{4-\varpi^2}(1-u^2)(1-u'^2) \\ & + \left(\frac{1}{2\varpi}\theta(u-u')\left(\frac{1-u}{1+u}\right)^{\frac{\varpi}{2}}\left(\frac{1+u'}{1-u'}\right)^{\frac{\varpi}{2}} \frac{3u^2+3u\varpi+\varpi^2-1}{(1+\varpi)(2+\varpi)}\frac{3u'^2-3u'\varpi+\varpi^2-1}{(1-\varpi)(2-\varpi)} \right. \\ & \left. + (u \leftrightarrow u') \right) \Bigg\}. \end{aligned} \tag{A.36}$$

Taking the coincident limit, we obtain

$$\begin{aligned} G(\bar{x};u,u,s) \equiv & \, G_d(\bar{x};u,u,s) + G_c(\bar{x};u,u,s) \\ = & \frac{\sqrt{2}}{\mu}\left(\frac{1}{2\varpi} + \frac{3}{2}(1-u^2)\sum_{n=1}^{2}(-1)^n \frac{n-1-u^2}{\varpi(\varpi^2-n^2)} \right). \end{aligned} \tag{A.37}$$

Since $\varpi \to 2$ when $s \to 0$, one might think that the $n=2$ term will bring a trouble because of the infrared divergence when doing the integral over s. However, this infrared divergence is exactly due to the time-translational zero mode and should be subtracted. We introduce an infrared regulator δ as well as an ultraviolet regulator Λ. Doing the integral, we get

$$-\int_{-\infty}^{\infty}\mathrm{d}\tau\int_0^{\infty}\mathrm{d}s\; G(\bar{x};\tau,\tau,s) = -(\sqrt{\Lambda}-\sqrt{2}\mu)\int_{-\infty}^{\infty}\mathrm{d}\tau - \ln(24\mu^2) + \ln\delta, \tag{A.38}$$

where the first term is proportional to $\mathcal{T}$ and will be canceled when we consider the functional determinant ratio; the last term comes from the zero mode and should be subtracted in order to obtain the primed determinant.

A similar calculation gives the functional determinant evaluated at the false vacuum,

$$-\int_{-\infty}^{\infty} \mathrm{d}\tau \int_{0}^{\infty} \mathrm{d}s \; G(x_+;\tau,\tau,s) = -(\sqrt{\Lambda} - \sqrt{2}\mu) \int_{-\infty}^{\infty} \mathrm{d}\tau. \tag{A.39}$$

Therefore, we finally arrive at the same result as in Eq. (A.32).

Appendix B

Fermionic Green's Function

In this appendix, we describe in detail the derivation of the hyperspherically symmetric, fermionic Green's function in the presence of an inhomogeneous mass $m(\rho) \equiv \kappa\varphi_B(\rho)$.

B.1 Angular-momentum recoupling

We will first give a review about the recoupling of spin and orbital angular momenta in four dimensions (see, e.g., Refs. [133, 134, 135]) which closely follows Ref. [134]. See Ref. [136] for a comparable discussion in the context of the fermion determinant.

The generators of the rotations on $\mathbb{R}^4$ are

$$M_{\mu\nu} = -i\left(x_\mu \frac{\partial}{\partial_\nu} - x_\nu \frac{\partial}{\partial_\mu}\right), \tag{B.1}$$

of them only six are independent because of the antisymmetry under interchange of the indices μ and ν, i.e. $M_{\mu\nu} = -M_{\nu\mu}$. They are

$$N_1 \equiv M_{23}\,, \quad N_2 \equiv M_{31}\,, \quad N_3 \equiv M_{12}, \tag{B.2a}$$
$$N_1' \equiv M_{41}\,, \quad N_2' \equiv M_{42}\,, \quad N_3' \equiv M_{43}. \tag{B.2b}$$

These form a basis $\{N_i, N_i'\}$ of the Lie algebra $\mathfrak{o}(4)$:

$$\big[N_i, N_j\big] = i\epsilon_{ijk}N_k, \tag{B.3a}$$
$$\big[N_i, N_j'\big] = i\epsilon_{ijk}N_k', \tag{B.3b}$$
$$\big[N_i', N_j'\big] = i\epsilon_{ijk}N_k, \tag{B.3c}$$

where ϵ_{ijk} is the Levi-Civita tensor.

It is convenient to introduce another basis $\{A_i, A_i'\}$:

$$A_i \equiv \frac{1}{2}\big(N_i + N_i'\big), \qquad A_i' \equiv \frac{1}{2}\big(N_i - N_i'\big), \tag{B.4}$$

satisfying

$$\big[A_i, A_j\big] = i\epsilon_{ijk}A_k, \tag{B.5a}$$
$$\big[A_i, A_j'\big] = 0, \tag{B.5b}$$
$$\big[A_i', A_j'\big] = i\epsilon_{ijk}A_k'. \tag{B.5c}$$

The two sets of operators $\mathbf{A} \equiv \{A_i\}$ and $\mathbf{A}' \equiv \{A_i'\}$ form two commuting $\mathfrak{o}(3)$ algebras, reflecting the fact that the $\mathfrak{o}(4)$ algebra is equal to the direct sum of two $\mathfrak{o}(3)$ algebras, i.e. $\mathfrak{o}(4) = \mathfrak{o}(3) \oplus \mathfrak{o}'(3)$. Correspondingly the $O(4)$ group is locally isomorphic to the direct

product of two $O(3)$ groups, i.e. $O(4) \simeq O(3) \otimes O'(3)$. The states in the basis $\{N_i, N'_i\}$ and $\{A_i, A'_i\}$ will be indexed by the labels (p, q) and $\{j, j'\}$, respectively. These labels are related via

$$p = j \ + \ j' \ , \qquad q = j \ - \ j'. \tag{B.6}$$

Eigenstates of $\mathbf{A}^2$ and $\mathbf{A}'^2$ have eigenvalues $j(j+1)$ and $j'(j'+1)$, respectively. Eigenstates of the total orbital angular momentum operator

$$\frac{1}{2}\, M \cdot M \equiv \frac{1}{2}\, M_{\mu\nu} M_{\mu\nu} = \mathbf{N}^2 + \mathbf{N}'^2 = 2\big(\mathbf{A}^2 + \mathbf{A}'^2\big) \tag{B.7}$$

have eigenvalues $p(p+2) + q^2 \ = \ 2[j(j+1) + j'(j'+1)]$ and transform as $\{j/2, j'/2\}$ representations with partition numbers $(\frac{j+j'}{2}, \frac{j-j'}{2})$.

Under spatial reflection: $x_i \to -x_i$, $x_4 \to x_4$, we have $N_i \to N_i$, $N'_i \to -N'_i$ and $A_i \leftrightarrow A'_i$. The spatial reflection symmetry of $O(4)$ therefore forces $j = j'$ for the total angular momentum eigenstates. Thus, the total orbital angular momentum eigenstates transform as $\{j/2, j/2\}$ representations of $O(4)$ with partition numbers $(j, 0)$, and $\frac{1}{2}\, M \cdot M$ has eigenvalues $4j(j+1)$.

In the case of the spin group $\mathrm{Spin}(4) \simeq SU_L(2) \otimes SU_R(2)$, we have the generators

$$\Sigma_{\mu\nu} = -\,\frac{i}{4}\,\big[\gamma_\mu, \gamma_\nu\big], \tag{B.8}$$

with the six independent operators

$$S_1 \equiv \Sigma_{23} \ , \qquad S_2 \equiv \Sigma_{31} \ , \quad S_3 \equiv \Sigma_{12}, \tag{B.9a}$$

$$S'_1 \equiv \Sigma_{41} \ , \qquad S'_2 \equiv \Sigma_{42} \ , \quad S'_3 \equiv \Sigma_{43}, \tag{B.9b}$$

forming a basis of the Lie algebra $\mathfrak{so}(4)$:

$$\big[S_i, S_j\big] = i\epsilon_{ijk} S_k, \tag{B.10a}$$

$$\big[S_i, S'_j\big] = i\epsilon_{ijk} S'_k, \tag{B.10b}$$

$$\big[S'_i, S'_j\big] = i\epsilon_{ijk} S_k. \tag{B.10c}$$

As before, we can introduce another basis $\{S^L_i, S^R_j\}$:

$$S^L_i \equiv \frac{1}{2}\big(S_i + S'_i\big), \qquad S^R_i \equiv \frac{1}{2}\big(S_i - S'_i\big), \tag{B.11}$$

satisfying

$$\big[S^L_i, S^L_j\big] = i\epsilon_{ijk} S^L_k, \tag{B.12a}$$

$$\big[S^L_i, S^R_j\big] = 0, \tag{B.12b}$$

$$\big[S^R_i, S^R_j\big] = i\epsilon_{ijk} S^R_k. \tag{B.12c}$$

Analogous to $\mathbf{A}_i$ and $\mathbf{A}'_i$, the sets of operators $\mathbf{S}^L \equiv \{S^L_i\}$ and $\mathbf{S}^R \equiv \{S^R_i\}$ form two commuting $\mathfrak{su}(2)$ algebras, reflecting the fact that the $\mathfrak{so}(4)$ algebra is equal to the direct sum of two $\mathfrak{su}(2)$ algebras, i.e. $\mathfrak{so}(4) = \mathfrak{su}_L(2) \oplus \mathfrak{su}_R(2)$. Correspondingly, the $SO(4)$ group is locally isomorphic to the direct product of two $SU(2)$ groups, i.e. $SO(4) \simeq SU_L(2) \otimes SU_R(2)$. The operators $\mathbf{S}^L$ act on the subspace generated by the projector

$P_L = \frac{1}{2}(\mathbb{I}_4 - \gamma_5)$, and the operators $\mathbf{S}^R$ act on the subspace generated by the projector $P_R = \frac{1}{2}(\mathbb{I}_4 + \gamma_5)$. We call spinors that transform in these two subspaces left and right handed, respectively. Left-handed spinors transform as $\{1/2, 0\}$ representations and are labeled by the partition numbers $(1/2, +1/2)$; right-handed spinors transform as $\{0, 1/2\}$ representations and are labeled by the partition numbers $(1/2, -1/2)$.

In terms of the above generators, we can write the Dirac operator in the form

$$\gamma \cdot \partial_{(x)} \; + \; m(\rho) = \gamma \cdot \hat{x} \left[\hat{x} \cdot \partial_{(x)} \; - \; \frac{M \cdot \Sigma}{\rho} \; + \; \gamma \cdot \hat{x} \, m(\rho) \right] \equiv \gamma \cdot \hat{x} \tilde{D}^{-1}, \tag{B.13}$$

where $\hat{x}_\mu \equiv x_\mu / |x| \equiv x_\mu / \rho$. If we can find the Green's function $\tilde{D}$ of the operator $\tilde{D}^{-1}$, the Green's function of the complete Dirac operator will be given by $D = \gamma \cdot \hat{x} \tilde{D}$. We then aim to find the eigenstates of $M \cdot \Sigma$, i.e. the simultaneous eigenstates of $\frac{1}{2}M^2$, $\frac{1}{2}\Sigma^2$ and the total angular momentum $K^2 \equiv \frac{1}{2}(M + \Sigma)^2$.

First we consider the eigenstates of $\frac{1}{2}M^2$. A basis of them is spanned by

$$\begin{aligned} |(j,0), \ell, m_\ell\rangle = \sum_{m_j, m'_j} & \big(j/2, m_j, j/2, m'_j \big| \ell, m_\ell\big) \\ & \times \; |j/2, m_j\rangle \otimes |j/2, m'_j\rangle \, , \end{aligned} \tag{B.14}$$

where $\big(j/2, m_j, j/2, m'_j \big| \ell, m_\ell\big)$ are the Clebsch-Gordan coefficients for the branching $O(3) \supset O(2)$. The quantum number ℓ labels the irreducible representations of $O(3)$ and m_ℓ those of $O(2)$.

Second, the basis of eigenstates of $\frac{1}{2}\Sigma^2$ can be chosen as

$$\begin{aligned} |(s, \pm s), s, m_s\rangle = \sum_{m_s^L, m_s^R} & \big(s^L, m_s^L, s^R, m_s^R \big| s, m_s\big) \\ & \times \; |s^L, m_s^L\rangle \otimes |s^R, m_s^R\rangle \, , \end{aligned} \tag{B.15}$$

with $s = 1/2$. Since either $s^L = m_s^L = 0$ or $s^R = m_s^R = 0$, the Clebsch-Gordan coefficients simplify, and we have

$$|(s, +s), s, m_s\rangle = |s, m_s\rangle \otimes |0, 0\rangle \, , \tag{B.16a}$$

$$|(s, -s), s, m_s\rangle = |0, 0\rangle \otimes |s, m_s\rangle \, . \tag{B.16b}$$

In order to find the eigenstates of $M \cdot \Sigma$, we need to consider the coupling between the representation of $O(4)$ and that of Spin(4). We first couple the states transforming under $O(3)$ with those under $SU_L(2)$, leading to the quantum numbers J and m_J, and then proceed similarly for $O'(3)$ and $SU_R(2)$, leading to the quantum numbers J' and m'_J. Finally, we couple the two resulting states, replacing the quantum numbers m_J, m'_J by L, M. There is a unitary transformation relating these two couplings [133]:

$$\begin{aligned} & |(j,0), (s, \pm s); \{J, J'\}, L, M\rangle \\ & \quad = \sum_{\ell, m_\ell, m_s} (-i)^\ell \big[(2J+1)(2J'+1)(2\ell+1)(2s+1)\big]^{1/2} \\ & \qquad \times \begin{Bmatrix} j/2 & (s \pm s)/2 & J \\ j/2 & (s \mp s)/2 & J' \\ \ell & s & L \end{Bmatrix} \big(\ell, m_\ell, s, m_s | L, M\big) \\ & \qquad \times \; |(j,0); \ell, m_\ell\rangle \otimes |(s, \pm s); s, m_s\rangle \, , \end{aligned} \tag{B.17}$$

where the summations run over $\ell = j, j-1, \ldots, 0$, $m_\ell = \ell, \ell-1, \ldots, -\ell$ and $m_s = \pm s$. The expression within curly braces is the Wigner $9j$-symbol. We have also introduced a phase $(-i)^\ell$ that depends on the explicit representation of the individual product states. The various quantum numbers take values

$$J = j/2 + (s \pm s)/2, |j/2 - (s \pm s)/2|, \tag{B.18a}$$
$$J' = j/2 + (s \mp s)/2, |j/2 - (s \mp s)/2|, \tag{B.18b}$$
$$L = J + J', J + J' - 1, \ldots, |J - J'|, \tag{B.18c}$$
$$M = L, L-1, \ldots, -L, \tag{B.18d}$$

and, correspondingly, the partition numbers take values

$$P \equiv J + J' = \; j \; + \; s, |j \; - \; s|, \tag{B.19a}$$
$$Q \equiv J - J' = \; \pm s, \mp s. \tag{B.19b}$$

The states have the following eigenvalues of the total angular momentum:

$$\begin{aligned} K^2 \to P(P+2) + Q^2 &= 2[J(J+1) + J'(J'+1)] \\ &= \begin{cases} j^2 \; + \; 3j \; + \; 3/2 \, , & P = j \; + \; s \; , \; j \; > \; 0 \, , \\ j^2 \; + \; j \; - \; 1/2 \, , & P = j \; - \; s \; , \; j \; > \; 0, \\ 3/2 \, , & P = s \; , \; j = 0. \end{cases} \end{aligned} \tag{B.20}$$

It follows then that

$$\begin{aligned} M \cdot \Sigma &= K^2 \; - \; \frac{1}{2} M^2 \; - \; \frac{1}{2} \Sigma^2 \\ &\to \; \mathcal{J} \; \equiv \; P(P+2) \; + \; Q^2 \; - \; j(j+2) \; - \; 2s(s+1) \\ &= \begin{cases} j \, , & P = j \; + \; s \; , \; j \; > \; 0, \\ -(j+2) \, , & P = j \; - \; s \; , \; j \; > \; 0, \\ 0 \, , & P = s \; , \; j \; = \; 0. \end{cases} \end{aligned} \tag{B.21}$$

In the coordinate representation, the orbital angular momentum states are given by the four-dimensional hyperspherical harmonics

$$Y_{j\ell m_\ell}(\mathbf{e}_x) = \langle \mathbf{e}_x | (j,0), \ell, m_\ell \rangle \, , \tag{B.22}$$

where the four-dimensional unit vector is

$$\mathbf{e}_x = (\cos\chi, \sin\chi\cos\theta, \sin\chi\sin\theta\sin\varphi, \sin\chi\sin\theta\cos\varphi). \tag{B.23}$$

In terms of these coordinates, the hyperspherical harmonics in four dimensions are given by [137]

$$\begin{aligned} Y_{j\ell m_\ell}(\mathbf{e}_x) = 2^\ell \, \Gamma(\ell+1) \left(\frac{2(j+1)(j-\ell)!}{\pi(j+\ell+1)!} \right)^{\frac{1}{2}} \\ \times \; \sin^\ell(\chi) C_{j-\ell}^{\ell+1}(\cos\chi) Y_{\ell m_\ell}(\theta, \varphi), \end{aligned} \tag{B.24}$$

where $Y_{\ell m_\ell}$ are the usual three-dimensional spherical harmonics. The spin states can be written

$$\xi_{\pm,m_s} = \frac{1}{2}(\mathbb{I} \mp \gamma_5) \begin{pmatrix} \xi_{m_s} \\ \xi_{m_s} \end{pmatrix} = \langle \xi | (s, \pm s), s, m_s \rangle \,, \tag{B.25}$$

where we have defined $\xi_{+s} = (1\ 0)^\mathsf{T}$, $\xi_{-s} = (0\ 1)^\mathsf{T}$. We can then introduce the *spin hyperspherical harmonic*

$$\begin{aligned} Y^{j,\pm}_{JJ'LM}(\mathbf{e}_x) &= \langle \xi; \mathbf{e}_x | (j,0), (s, \pm s); \{J, J'\}, L, M \rangle \\ &= \sum_{\ell, m_\ell, m_s} (-i)^\ell \big[(2J+1)(2J'+1)(2\ell+1)(2s+1)\big]^{1/2} \\ &\quad \times \begin{Bmatrix} j/2 & (s \pm s)/2 & J \\ j/2 & (s \mp s)/2 & J' \\ \ell & s & L \end{Bmatrix} \big(\ell, m_\ell, s, m_s | L, M\big) \\ &\quad \times \xi_{\pm,m_s} Y_{j\ell m_\ell}(\mathbf{e}_x). \end{aligned} \tag{B.26}$$

B.2 Green's function: hyperspherical problem

After reviewing the recoupling of spin and orbital angular momenta, we now can derive the fermionic Green's function for a radially varying mass $m(\rho)$. The Dirac equation in Euclidean space takes the form

$$\big[\gamma \cdot \partial_{(x)} \ + \ m(\rho)\big] D(x, x') = \delta^4(x - x'). \tag{B.27}$$

One can make the following ansatz for the solution:

$$D(x, x') = \sum_\lambda \big[a_\lambda(\rho, \rho') \ + \ b_\lambda(\rho, \rho')\, \gamma \cdot x\big] \tilde{D}_\lambda(\mathbf{e}_x, \mathbf{e}'_x), \tag{B.28}$$

where $\lambda = \{j, \pm, J, J', L, M\}$ is a multi-index and

$$\tilde{D}_\lambda(\mathbf{e}_x, \mathbf{e}'_x) = [Y^{j,\pm}_{JJ'LM}(\mathbf{e}'_x)]^* Y^{j,\pm}_{JJ'LM}(\mathbf{e}_x). \tag{B.29}$$

Given the completeness of the eigenstates in Eq. (B.17), this leads to the equation

$$\begin{aligned} &\gamma \cdot x \left[\frac{x \cdot \partial_{(x)} - \mathcal{J}}{\rho^2}\, a_\lambda(\rho, \rho') \ + \ m(\rho) b_\lambda(\rho, \rho')\right] \tilde{D}_\lambda(\mathbf{e}_x, \mathbf{e}'_x) \\ &+ \left[m(\rho) a_\lambda(\rho, \rho') \ + \ \left(\frac{\partial}{\partial \rho} + \frac{\mathcal{J}+3}{\rho}\right) \rho\, b_\lambda(\rho, \rho')\right] \tilde{D}_\lambda(\mathbf{e}_x, \mathbf{e}'_x) \\ &= \frac{\delta(\rho - \rho')}{\rho^3}\, \tilde{D}_\lambda(\mathbf{e}_x, \mathbf{e}'_x), \end{aligned} \tag{B.30}$$

where we have used Eq. (B.13) and the relation

$$\gamma \cdot \hat{x}\, M \cdot \Sigma\, \gamma \cdot \hat{x} = -\, M \cdot \Sigma \ - \ 3. \tag{B.31}$$

The radial equation only depends on the orbital angular momentum quantum number j and the partition number P. The two linearly independent components of Eq. (B.30)

allow us to eliminate b_λ such that we obtain a second-order equation. Substituting for the allowed values for $\mathcal{J}$ from Eq. (B.21) leads to

$$\Bigg[-\frac{\mathrm{d}^2}{\mathrm{d}\rho^2} - \frac{3}{\rho}\frac{\mathrm{d}}{\mathrm{d}\rho} + \frac{j(j+2)}{\rho^2} + m^2(\rho) + \frac{\mathrm{d}\ln m(\rho)}{\mathrm{d}\rho}\left(\frac{\mathrm{d}}{\mathrm{d}\rho} - \frac{\mathcal{J}}{\rho}\right)\Bigg] a_\lambda(\rho,\rho') = \frac{m(\rho)\delta(\rho-\rho')}{\rho'^3}. \tag{B.32}$$

Note that, for a constant mass, this coincides with the spherical Klein-Gordon equation, as one would expect.

We are ultimately interested in the coincident limit of the fermionic Green's function. It is therefore useful to evaluate the dyadic product of the eigenstates in Eq. (B.17) and to trace over all but P and j. This can be simplified dramatically, since we may take the angle $\chi = 0$ without loss of generality. Doing so, $\ell = 0$ in all non-vanishing contributions, and we find the result

$$\sum_{Q,L,M,\pm} |\,\langle \mathbf{e}_x|(j,0),(s,\pm s);(P,Q),L,M\rangle\,|^2 = \frac{1}{4\pi^2}\,(j+1)\,\mathcal{K}\,\mathbb{I}_4, \tag{B.33}$$

where

$$\mathcal{K} = \begin{cases} j\,+\,2\,, & P = j\,+\,s\,,\ j\,>\,0, \\ j\,, & P = j\,-\,s\,,\ j\,>\,0, \\ 2\,, & P = s\,,\ j\,=\,0. \end{cases} \tag{B.34}$$

Note that summing over the allowed values for P, we recover the corresponding result from Ref. [59], appearing in the coincident Green's function of the scalar field. Putting everything together, we arrive at the following expression for the coincident fermionic Green's function:

$$D(x,x) = \frac{1}{4\pi^2}\sum_{P,j}(j+1)\,\mathcal{K}\left[\mathbb{I}_4 + \frac{\mathcal{J} - x\cdot\partial_{(x)}}{m\rho}\,\gamma\cdot\hat{x}\right] a_j(\rho), \tag{B.35}$$

where $a_j(\rho) \equiv a_\lambda(\rho,\rho)$.

B.3 Green's function: planar problem

In the thin-wall limit, we may apply the planar-wall approximation, neglecting the damping term and replacing j/R by the continuous variable $|\mathbf{k}|$ (the three-momentum in the hyperplane of the bubble wall). In addition, we consistently replace $\delta(\rho-\rho')/\rho'^3$ by $\delta(\rho-\rho')/R^3$ on the right-hand side of the radial equation (B.30). Equation (B.32) then becomes

$$\left[-\partial_z^2 + \mathbf{k}^2 + m^2(z) + \frac{\mathrm{d}\ln m(z)}{\mathrm{d}z}\,(\partial_z - h\,|\mathbf{k}|)\right] a_h(\mathbf{k};z,z') = \frac{m(z)\,\delta(z-z')}{R^3}, \tag{B.36}$$

where we have replaced ρ by the variable z and $h = \pm$, coming from the partition number P in Eq. (B.21). Defining $\tilde{a}_h(\mathbf{k}; z, z') \equiv R^3\, a_h(\mathbf{k}; z, z')$, we arrive at the final form

$$\begin{aligned}&\left[-\partial_z^2 + \mathbf{k}^2 + m^2(z) + \frac{\mathrm{d}\ln m(z)}{\mathrm{d}z}\,(\partial_z - h\,|\mathbf{k}|)\right]\tilde{a}_h(\mathbf{k}; z, z') \\ &= m(z)\,\delta(z - z'). \end{aligned} \tag{B.37}$$

Substituting Eq. (B.35) into Eq. (4.29) with $a_\lambda(\rho, \rho')$ replaced by $a_h(\mathbf{k}; z, z')$ and employing the representations of the gamma matrices in Eq. (5.8), the fermion tadpole can be written as

$$\begin{aligned}\Pi_D(\varphi_B; x)\,\varphi_B(x) =&\ -\kappa\,\mathrm{tr_S}\,D(\varphi_B; x, x) \\ =&\ -\frac{\kappa}{\pi^2}\sum_{h=\pm}\int \mathrm{d}|\mathbf{k}|\,\mathbf{k}^2\,\tilde{a}_h(\mathbf{k}; z, z')\,. \end{aligned} \tag{B.38}$$

The numerical results from the main part of this work have been checked by simultaneously solving Eq. (B.37) and using the expression for the fermion tadpole in Eq. (B.38) to compute the radiative effects.

Appendix C

General Argument for the Analytic Continuation between Euclidean and Minkowski Functional Determinants

In this appendix, we aim to give a general argument on the analytic continuation $\mathcal{T} \to ie^{-i\theta}T$ between the Euclidean functional determinant to that with a general θ value.

C.1 Analytic continuation of eigenfunctions and eigenvalues

To be general, we consider a fluctuation determinant around a background field $\bar{\phi}$ in a scalar field theory. $\bar{\phi}$ is a (real or complex) saddle point in the expansion of the path integral which interpolates between two vacuum configurations. The asymptotic vacua are not necessarily the same. For a time contour analytically continued by a rotation of an angle $-\theta$ in the clockwise direction in the complex plane, the eigenvalue problem of the fluctuation operator is given by

$$\mathcal{M}_\theta \Delta\phi_\theta^\lambda(t,\mathbf{x}) \equiv \left[e^{2i\theta}\frac{\mathrm{d}^2}{\mathrm{d}t^2} - \nabla^2 + U''(\bar{\phi}(t,\mathbf{x}))\right]\Delta\phi_\theta^\lambda(t,\mathbf{x}) = \lambda\Delta\phi_\theta^\lambda(t,\mathbf{x}), \tag{C.1}$$

where the background $\bar{\phi}$ satisfies

$$\left[e^{2i\theta}\frac{\mathrm{d}^2}{\mathrm{d}t^2} - \nabla^2 + U'(\bar{\phi}(t,\mathbf{x}))\right]\bar{\phi} = 0. \tag{C.2}$$

For $\theta = \epsilon$ one recovers the Minkowski result, while for $\theta = \pi/2$ one obtains the Euclidean one.

As we have seen in the Chap. 7, the analytic continuation between the eigenfunctions and the parameters wherein can be analyzed by the normalization properties of the eigenfunctions. The normalization properties can be determined by the asymptotic behaviors of the eigenfunctions as we will now show.

The field configuration $\bar{\phi}$ has the following asymptotic behavior

$$\bar{\phi}(t,\mathbf{x}) \to \phi_\pm, \text{ as } t \to \pm\infty, \tag{C.3}$$

where $\phi_\pm$ are the vacuum configurations. The potential near the vacua can be approximated by harmonic potentials

$$U_\pm(\phi) = \frac{m_\pm^2}{2}(\phi - \phi_\pm)^2, \tag{C.4}$$

where $m_\pm^2 \equiv U''(\phi_\pm)$ are the effective masses in the vacua. Inserting this into Eq. (C.2), one can see that the solution $\bar{\phi}$ approaches the vacua $\phi_\pm$ exponentially fast, as long as $\theta \geq 0^+$:

$$\bar{\phi}(t) \to \phi_\pm + Ce^{\mp(i\cos\theta+\sin\theta)\sqrt{m_\pm^2+\mathbf{k}_\pm^2}t} \quad \text{for} \quad t \to \pm\infty. \tag{C.5}$$

Thus for large $|t|$ the background $\bar{\phi}$ will then sit at the vacua up to exponentially suppressed corrections. Hence $U''(\bar{\phi}) \to m_\pm^2$ and we get asymptotic equations of the form

$$\left[e^{2i\theta}\frac{\mathrm{d}^2}{\mathrm{d}t^2} - \nabla^2 + m_\pm^2\right]\Delta\phi_\theta^\lambda(t,\mathbf{x}) = \lambda\Delta\phi_\theta^\lambda(t,\mathbf{x}). \tag{C.6}$$

From the above equation, one immediately obtains the asymptotic behaviors of the eigenfunctions

$$\Delta\phi_\theta^\lambda(t,\mathbf{x}) \sim \exp\left[e^{-i\theta}\sqrt{\lambda-\mathbf{k}_\pm^2-m_\pm^2}\ t\right]e^{i\mathbf{k}_\pm\cdot\mathbf{x}},\ t\to\pm\infty, \tag{C.7}$$

or

$$\Delta\phi_\theta^\lambda(t,\mathbf{x}) \sim \exp\left[-e^{-i\theta}\sqrt{\lambda-\mathbf{k}_\pm^2-m_\pm^2}\ t\right]e^{i\mathbf{k}_\pm\cdot\mathbf{x}},\ t\to\pm\infty. \tag{C.8}$$

We can consider *real or imaginary* $\mathbf{k}$ so that we may capture both oscillating sine, cosine as well as real exponentials (we restrict to purely real or purely imaginary because a Hermitian ∇^2 requires real eigenvalues $\mathbf{k}^2$). Despite the complex notation for the exponentials, it will be understood that in the Euclidean spacetime the norm involves no complex conjugation, as it is always possible to construct a basis of real eigenfunctions, or of complex eigenfunctions paired in reciprocal pairs with real scalar products. The absence of complex conjugation in the scalar products will be important for showing analytic continuation of $\det\mathcal{M}_\theta$ from $\det\mathcal{M}_{\pi/2} \equiv \det\mathcal{M}_E$.

Of the values of λ, $\mathbf{k}$ in the asymptotic solutions above, some will correspond to normalizable full solutions, either in the proper or improper sense. Solutions that are normalizable in the improper way will have an oscillating asymptotic behavior, either in the temporal or spatial direction. In the spatial directions, this happens for real $\mathbf{k}_\pm$, while in the temporal direction this happens for values of λ such that $e^{-i\theta}\sqrt{\lambda+\mathbf{k}_\pm^2+m_\pm^2}$ is purely imaginary.

Properly normalizable solutions correspond to functions that decay at infinity in the time and spatial directions. This happens for purely imaginary $\mathbf{k}$ and for that when $e^{-i\theta}\sqrt{\lambda+\mathbf{k}_\pm^2+m_\pm^2}$ contains a real part that gives the decaying behavior. Acoording to the node theorem, the spectrum of properly normalizable solutions is discrete.

No matter whether they are part of the continuum or discrete spectrum, we can classify the eigenfunctions as "temporally oscillating" or "temporally decaying" according to their asymptotic behavior in the time direction. The associated eigenvalues λ are of the form:

$$\text{Temporally oscillating: } e^{-i\theta}\sqrt{\lambda_{osc}-\mathbf{k}_\pm^2-m_\pm^2} = i\kappa_{\theta,\pm},\ \kappa_{\theta,\pm}\in\mathbb{R},\ \text{continuous } \lambda_{osc} \tag{C.9a}$$

$$\text{Temporally decaying: } \sqrt{\lambda_{dec}-\mathbf{k}_\pm^2-m_\pm^2} = \beta_{\theta,\pm} \in \mathbb{R}^+. \tag{C.9b}$$

We will explain the phase chosen in Eq. (C.9b) later.

Given solutions to the eigenequations (not necessarily normalizable) for a given value of θ, one can obtain solutions for another value of θ by analytic continuation in the time variable. This is because that both the background and fluctuation equations for arbitrary θ can be obtained by analytic continuation from Euclidean time. Thus we may construct all our solutions by rotating from Euclidean time: $\tau \to ie^{-i\theta}t$. A key concern is that solutions that are (im)properly normalizable for one value of θ are not necessarily so for another value. However, one can construct (im)properly normalizable solutions for arbitrary θ by supplementing the analytic continuation of the time variable with complex rotations of the parameters in the solutions. We analyze this problem for the temporally decaying and temporally oscillating solutions respectively.

A temporally decaying Euclidean solution goes as

$$\Delta\phi_E^\lambda(\tau,\mathbf{x}) \propto \exp\left(\mp\beta_{E,\pm}\tau\right),\ \tau\to\pm\infty, \beta_{E,\pm}\in\mathbb{R}^+. \tag{C.10}$$

The analytic continuation to arbitrary θ, obtained by substituting $\tau \to ie^{-i\theta}t$ gives

$$\Delta\phi_\theta^\lambda(\tau,\mathbf{x}) \propto \exp\left(\mp ie^{-i\theta}\beta_{E,\pm}t\right) = \exp(\mp\sin\theta\beta_{E,\pm}t)\exp(\mp i\cos\theta\beta_{E,\pm}t),\ t\to\pm\infty, \beta_{E,\pm}>0. \tag{C.11}$$

As long as $\theta \geq 0^+$, the rotated solution will still be temporally decaying. Therefore its normalizability properties will be identical to the Euclidean case and the straightforward rotation of Euclidean temporally decaying solutions gives acceptable eigenfunctions for a rotated time contour. This means that the eigenvalues are not changed: $\beta_{E,\pm} \to \beta_{\theta,\pm}$. This explains the phase in Eq. (C.9b) is indeed chosen such as to maintain the parameter $\beta_{\theta,\pm}$ real for all values $\theta \in (0, 2\pi]$.

A temporally oscillating Euclidean solution has the asymptotic behavior

$$\Delta\phi_E^\lambda(\tau,\mathbf{x}) \propto \exp\left(i\kappa_{E,\pm}\tau\right),\ \tau\to\pm\infty, \tag{C.12}$$

where $\kappa_{E,\pm} \in \mathbb{R}$ depend on the free parameters that define the Euclidean solutions. The analytic continuation in time gives

$$\Delta\phi_\theta^\lambda(\tau,\mathbf{x}) \propto \exp\left(-e^{-i\theta}\kappa_{E,\pm}t\right),\ t\to\pm\infty. \tag{C.13}$$

It will blow up in one of the time directions and hence is not an acceptable eigenfunction. However, one can complexify the free parameters of the original Euclidean solution, doing $\kappa_{E,\pm} \to -ie^{i\theta}\kappa_{\theta,\pm}$(note both $\kappa_{E,\pm}$ and $\kappa_{\theta,\pm}$ are real) and arrive at a new solution that is normalizable in the improper sense. This means that the eigenvalues for general θ corresponding to temporally oscillating solutions are obtained from the Euclidean eigenvalues by appropriate complex rotations. In the Euclidean case, one would have e.g.

$$\lambda_E = \kappa_{E,\pm}^2 + \mathbf{k}_\pm^2 + m_\pm^2, \quad \kappa_{E,\pm}, \mathbf{k}_\pm \in \mathbb{R} \tag{C.14}$$

while after the κ rotation, the corresponding eigenvalue for arbitrary θ will be

$$\lambda_\theta = -e^{2i\theta}\kappa_{\theta,\pm}^2 + \mathbf{k}_\pm^2 + m_\pm^2, \quad \kappa_{\theta,\pm}, \mathbf{k}_\pm \in \mathbb{R}. \tag{C.15}$$

Note that the eigenvalues for a rotated time contour can be complex because the fluctuation operator is only Hermitian for $\theta = 0, \pi/2$.

C.2 Orthonormal property and the completeness of the analytically continued eigenfunctions

Before we move onto the calculation of the functional determinant of the fluctuation operator, we must check the orthonormal property and the completeness of the continued eigenfunctions. In the following, parameterize the Euclidean eigenfunctions in terms of the constants defining their asymptotic behavior at either end, e.g., at $\tau = +\infty$. And we will supress the subscript "+" for clarity.

We first check the orthonormal property. As we emphasized earlier, the scalar product is defined without complex conjugation. And the continued eigenfunctions remain orthogonal with respect to such a product because they are obtained by analytic rotations of Euclidean ones, which are themselves orthogonal.[26] What we really need to do is fixing the normalization factor. For discrete eigenfunctions, we thus write $\Delta\phi_\theta(t,\mathbf{x}) = \sqrt{N}\Delta\phi_E(ie^{-i\theta}t,\mathbf{x})$ where N is a normalization factor. The scalar product for them is:

$$\int \mathrm{d}t\mathrm{d}^3\mathbf{x}\ \Delta\phi_\theta^\lambda(t,\mathbf{x})\Delta\phi_\theta^{\lambda'}(t,\mathbf{x}) = N\int \mathrm{d}t\mathrm{d}^3\mathbf{x}\ \Delta\phi_E^\lambda(ie^{-i\theta}t,\mathbf{x})\Delta\phi_E^{\lambda'}(ie^{-i\theta}t,\mathbf{x}). \tag{C.16}$$

Since the Euclidean eigenfunctions are analytic in time, using the Cauchy theorem the integration contour can be rotated without changing the value of the integral (note that the discrete eigenfunctions vanish for large values of complex time along the arcs that join the rotated axes). One can rotate the integral (C.16) via $t \to -ie^{i\theta}\tau$, giving

$$\int \mathrm{d}t\mathrm{d}^3\mathbf{x}\ \Delta\phi_\theta^\lambda(t,\mathbf{x})\Delta\phi_\theta^{\lambda'}(t,\mathbf{x}) = -ie^{i\theta}N\int \mathrm{d}\tau\mathrm{d}^3\mathbf{x}\ \Delta\phi_E^\lambda(\tau,\mathbf{x})\Delta\phi_E^{\lambda'}(\tau,\mathbf{x}) = -ie^{i\theta}N\delta_{\lambda\lambda'}, \tag{C.17}$$

where we used the Euclidean orthogonality condition. Thus we have $N = ie^{-i\theta}$.

For a possible continuum spectrum with temporally decaying solutions, we can use a similar argument and obtain the same normalization constant. In this case, we expect that the norm only diverges when integrating over spatial directions. Then the Euclidean scalar products will go as

$$\int \mathrm{d}\tau\mathrm{d}^3\mathbf{x}\ \Delta\phi_{E,-}^{(\beta_E,\mathbf{k})}(\tau,\mathbf{x})\Delta\phi_{E,+}^{(\beta_E,\mathbf{k}')}(\tau,\mathbf{x}) = \delta^3(\mathbf{k}-\mathbf{k}'), \tag{C.18}$$

where $+,-$ denote elements of a pair of reciprocal eigenfunctions. For the eigenfunctions with arbitrary θ (recall $\beta_E \to \beta_\theta$ in the analytic continuation), $\Delta\phi_\theta^{(\beta_\theta,\mathbf{k})}(t,\mathbf{x}) = \sqrt{N}\Delta\phi_E^{(\beta_\theta,\mathbf{k})}(ie^{-i\theta}t,\mathbf{x})$ we will have

$$\begin{aligned}\int \mathrm{d}t\mathrm{d}^3\mathbf{x}\ \Delta\phi_{E,-}^{(\beta_\theta,\mathbf{k})}(t,\mathbf{x})\Delta\phi_{E,+}^{(\beta'_\theta,\mathbf{k}')}(t,\mathbf{x}) &= -ie^{i\theta}N\int \mathrm{d}\tau\mathrm{d}^3\mathbf{x}\ \Delta\phi_{E,-}^{(\beta_\theta,\mathbf{k})}(\tau,\mathbf{x})\Delta\phi_{E,+}^{(\beta'_\theta,\mathbf{k}')}(\tau,\mathbf{x}) \\ &= -ie^{i\theta}N\delta_{\beta_\theta,\beta'_\theta}\delta^3(\mathbf{k}-\mathbf{k}').\end{aligned} \tag{C.19}$$

Again, $N = ie^{-i\theta}$ gives the appropriate normalization. In the case of temporally oscillating solutions one has to consider the effect of the analytic continuation of the κ parameter.

[26] We assume that the parameters $\{\kappa_E,\mathbf{k}\}$ or $\{\beta_E,\mathbf{k}\}$ can indeed parameterize a complete orthonormal basis in the space of all the eigenfunctions. This should be taken, however, with caution. If this is not true, then our analysis will still applies to the planar-wall case where $\mathbf{k}$ becomes a conserved quantity [138].

In this case, the Euclidean scalar products take

$$\int \mathrm{d}\tau \mathrm{d}^3x\, \Delta\phi_{E,-}^{(\kappa_E,\mathbf{k})}(\tau,\mathbf{x})\Delta\phi_{E,+}^{(\kappa'_E,\mathbf{k}')}(\tau,\mathbf{x}) = \delta(\kappa_E-\kappa'_E)\delta^3(\mathbf{k}-\mathbf{k}'). \tag{C.20}$$

For a rotated time contour, the corresponding eigenfunctions are obtained by analytic continuation of τ and κ_E:

$$\Delta\phi_\theta^{(\kappa_\theta,\mathbf{k})}(t,\mathbf{x}) = \sqrt{N'}\Delta\phi_E^{(-ie^{i\theta}\kappa_\theta,\mathbf{k})}(ie^{-i\theta}t,\mathbf{x}). \tag{C.21}$$

Thus one has

$$\int \mathrm{d}t\mathrm{d}^3\mathbf{x}\, \Delta\phi_{\theta,-}^{(\kappa_\theta,\mathbf{k})}(t,\mathbf{x})\Delta\phi_{\theta,+}^{(\kappa'_\theta,\mathbf{k}')}(t,\mathbf{x}) = -ie^{i\theta}N' \int \mathrm{d}\tau\mathrm{d}^3\mathbf{x}\, \Delta\phi_{E,-}^{(-ie^{i\theta}\kappa_\theta,\mathbf{k})}(\tau,\mathbf{x})\Delta\phi_{E,+}^{(-ie^{i\theta}\kappa'_\theta,\mathbf{k}')}(\tau,\mathbf{x})$$
$$= -ie^{i\theta}N'\delta(-ie^{i\theta}(\kappa_\theta-\kappa'_\theta))\delta^3(\mathbf{k}-\mathbf{k}') = N'\delta(\kappa_\theta-\kappa'_\theta)\delta^3(\mathbf{k}-\mathbf{k}'). \tag{C.22a}$$

This fixes the normalization $N'=1$. Note that when rotating the integration contour after applying the Cauchy theorem, the contributions from the integration along the arcs at infinite complex time are also expected to vanish in this case, because of the oscillating nature of the solution—as opposed to the exponential decay of the previous eigenfunctions.

Now we check the completeness of the continued eigenfunctions. Consider the sum over projection operators

$$\mathcal{I}_\theta = \sum_{dec,disc} \Delta\phi_\theta^\lambda(x)\Delta\phi_\theta^\lambda(x') + \sum\!\!\!\!\!\!\int_{dec,cont} \mathrm{d}^3\mathbf{k}\, \Delta\phi_{\theta,-}^{(\beta_\theta,\mathbf{k})}(x)\Delta\phi_{\theta,+}^{(\beta_\theta,\mathbf{k})}(x')$$
$$+ \int_{osc} \mathrm{d}\kappa_\theta \mathrm{d}^3k\, \Delta\phi_{\theta,-}^{(\kappa_\theta,\mathbf{k})}(x)\Delta\phi_{\theta,+}^{(\kappa_\theta,\mathbf{k})}(x'). \tag{C.23}$$

where "dec,disc/cont" refer to temporally decaying eigenfunctions belonging to the discrete/continous spectrum, and "osc" refers to the temporally oscillating solutions in the continuum spectrum. Using the relation to the Euclidean eigenfunctions with the appropriate normalization obtained above, we have:

$$\begin{aligned}
\Delta\phi_\theta^\lambda(t,\mathbf{x}) &= \sqrt{ie^{-i\theta}}\Delta\phi_E^\lambda(ie^{-i\theta}\tau,\mathbf{x}) \quad \text{decaying, discrete,}\\
\Delta\phi_\theta^{(\beta_\theta,\mathbf{k})}(t,\mathbf{x}) &= \sqrt{ie^{-i\theta}}\Delta\phi_E^{(\beta_\theta,\mathbf{k})}(ie^{-i\theta}\tau,\mathbf{x}) \quad \text{decaying, continuum,}\\
\Delta\phi_\theta^{(\kappa_\theta,\mathbf{k})}(x) &= \Delta\phi_E^{(-ie^{i\theta}\kappa_\theta,\mathbf{k})}(ie^{-i\theta}\tau,\mathbf{x}) \quad \text{oscillating, continuum.}
\end{aligned} \tag{C.24}$$

The above implies, after analytic continuation of the integral in κ_θ in (C.23) to an integral over $ie^{-i\theta}\kappa_E$ (where $\kappa_E\in\mathbb{R}$)

$$\mathcal{I}_\theta = ie^{-i\theta}\left(\sum_{dec,disc} \Delta\phi_E^\lambda(ie^{-i\theta}t,\mathbf{x})\Delta\phi_E^\lambda(ie^{-i\theta}t',\mathbf{x}') + \sum\!\!\!\!\!\!\int_{dec,cont} \mathrm{d}^3\mathbf{k}\, \Delta\phi_{E,-}^{(\beta_\theta,\mathbf{k})}(ie^{-i\theta}t,\mathbf{x})\right.$$
$$\left.\times\Delta\phi_{E,+}^{(\beta_\theta,\mathbf{k})}(ie^{-i\theta}t',\mathbf{x}') + \int_{osc} \mathrm{d}\kappa_E\mathrm{d}^3\mathbf{k}\, \Delta\phi_{E,-}^{(\kappa_E,\mathbf{k})}(ie^{-i\theta}t,\mathbf{x})\Delta\phi_{E,+}^{(\kappa_E,\mathbf{k})}(ie^{-i\theta}t,\mathbf{x})\right).$$

The term in parenthesis is nothing but the sum over projectors over the Euclidean eigenfunctions, analytically continued in time. Assuming a complete Euclidean basis, this is nothing but $\delta(ie^{-i\theta}(t-t'))\delta^3(\mathbf{x}-\mathbf{x}')$. Thus,

$$\mathcal{I}_\theta = ie^{-i\theta}\delta(ie^{-i\theta}(t-t'))\delta^3(\mathbf{x}-\mathbf{x}') = \delta(t-t')\delta^3(\mathbf{x}-\mathbf{x}'). \tag{C.25}$$

In summary, the sum over the rotated projectors onto the rotated eigenfunctions is equal to the identity, which shows that the rotated basis is complete.

C.3 Analytic continuation of the functional determinants

Given the orthonormal eigenfunctions for arbitrary θ and given the completeness, the differential operator $\mathcal{M}_\theta$ can be expanded into a basis of orthogonal projectors:

$$\mathcal{M}_\theta(x,x') = \sum_{dec,disc} \lambda \Delta\phi^\lambda_\theta(x)\Delta\phi^\lambda_\theta(x') + \sum\!\!\!\!\!\!\int_{dec,cont} \mathrm{d}^3\mathbf{k}\ \lambda(\mathbf{k})\,\Delta\phi^{(\beta_\theta,\mathbf{k})}_{\theta,-}(x)\Delta\phi^{(\beta_\theta,\mathbf{k})}_{\theta,+}(x') + \int_{osc} \mathrm{d}\kappa_\theta \mathrm{d}^3\mathbf{k}\ \lambda_\theta(\kappa_\theta,\mathbf{k})\,\Delta\phi^{(\kappa_\theta,\mathbf{k})}_{\theta,-}(x)\Delta\phi^{(\kappa_\theta,\mathbf{k})}_{\theta,+}(x'). \tag{C.26}$$

The determinant is a sum of the spectrum

$$\log\det\mathcal{M}_\theta = \mathrm{tr}\,\log\mathcal{M}_\theta = \sum_{dec,disc}\log\lambda + V^{(3)}\sum\!\!\!\!\!\!\int_{dec,cont}\frac{\mathrm{d}^3\mathbf{k}}{(2\pi)^3}\,\log\lambda(\mathbf{k}) + V^{(4)}_\theta\int_{osc}\frac{\mathrm{d}\kappa_\theta\mathrm{d}^3\mathbf{k}}{(2\pi)^4}\,\log\lambda_\theta(\kappa_\theta,\mathbf{k}). \tag{C.27}$$

Above, $V^{(3)} = (2\pi)^3\delta^3_{\mathbf{k}}(0)$ is the three-dimensional volume of the $\mathbf{k}$-space, and $V^{(4)}_\theta = (2\pi)^4\delta_{\kappa_\theta}(0)\delta^3_{\mathbf{k}}(0)$ the full four-dimensional volume of the dual space of the $\{\kappa_\theta,\mathbf{k}\}$ space.

Now we argue that the determinant in Eq. (C.27) only depends on θ through the volume factors, in a way consistent with the replacement of Euclidean time $\mathcal{T}$ with $\mathcal{T}\to ie^{i\theta}T$. Compared to the Euclidean case, as argued before the eigenvalues of the temporally decaying solutions are invariant under rotations of the time contour, so that their contributions to the determinant are as in Euclidean space.

Regarding the contribution from the last integral in Eq. (C.27), one can express the eigenvalues in terms of the Euclidean ones through the above motivated κ rotation:

$$\lambda_\theta(\kappa_\theta,\mathbf{k}) = \lambda_E(-ie^{i\theta}\kappa_\theta,\mathbf{k}). \tag{C.28}$$

In this way,

$$V^{(4)}_\theta\int_{osc}\mathrm{d}\kappa_\theta\mathrm{d}^3\mathbf{k}\ \log\lambda_\theta(\kappa_\theta,\mathbf{k}) = V^{(4)}_\theta\int_{osc}\mathrm{d}\kappa_\theta\mathrm{d}^3\mathbf{k}\ \log\lambda_E(-ie^{i\theta}\kappa_\theta,\mathbf{k}). \tag{C.29}$$

Using the Cauchy theorem to rotate the integral $\kappa_\theta\to ie^{-i\theta}\kappa_E$, one has

$$\log\det\mathcal{M}^{\mathrm{cont}}_\theta = ie^{-i\theta}V^{(4)}_\theta\int_{osc}\mathrm{d}\kappa_E\mathrm{d}^3\mathbf{k}\ \log\lambda_E(\kappa_E,\mathbf{k}), \tag{C.30}$$

meaning that the contribution to the determinant from the continuous spectrum for general θ is simply obtained from Euclidean result by the analytic continuation $V^{(4)}_E\to ie^{-i\theta}V^{(4)}_\theta$ or $\mathcal{T}\to ie^{-i\theta}T$. The integration along the temporal arcs at infinity vanishes when one chooses a proper regularization scheme [138].

Although the argument given so far is general and should be in principle applicable to a general saddle point $\bar\phi$, including the bounce, we give some explicit simple examples below.

C.4 Examples

Constant vacuum configuration

In this case the background is constant, we have a constant effect mass $m \equiv U''(\bar{\phi})$. The eigenfunctions are simply plane waves and the spectrum is continuous. In Euclidean spacetime, the eigenfunctions are

$$\Delta\phi_E^{(\kappa_E,\mathbf{k})}(\tau,\mathbf{x}) = \frac{1}{(2\pi)^2} e^{i\hat{k}\cdot\hat{x}}, \tag{C.31}$$

where $\hat{x} = (\tau, \mathbf{x})$ is the Euclidean position four-vector, and $\hat{k} = (\kappa_E, \mathbf{k})$. The reciprocal eigenfunctions are simply obtained by substituting $\hat{k}$ with $-\hat{k}$, so that one gets

$$\int \mathrm{d}^4\hat{x}\, \Delta\phi^{\hat{k}}_{E,-}(\hat{x})\Delta\phi^{\hat{k}'}_{E,+}(\hat{x}) = \delta^4(\hat{k}-\hat{k}'). \tag{C.32}$$

The eigenvalues are given by $\delta_{mn}\hat{k}^m\hat{k}^n + m^2 \equiv \hat{k}^2 + m^2$ and the determinant is

$$\log\det\mathcal{M}_E = V_E^{(4)} \int \frac{\mathrm{d}^4\hat{k}}{(2\pi)^4}\ \log(\hat{k}^2+m^2) = \int \mathrm{d}^4\hat{x}\, U_{\mathrm{CW}}. \tag{C.33}$$

The result is the spacetime integral of the CW potential evaluated at the vacuum, as it should be.

In Minkowski space the eigenfunctions are also improperly normalizable plane waves. With Lorentz notation $x^\mu = (t, \mathbf{x})$, $k^\mu = (k^0, \mathbf{k})$, these are:

$$\Delta\phi^k(x) = \frac{1}{(2\pi)^2} e^{ik\cdot x}. \tag{C.34}$$

Note how the solutions can be obtained from the Euclidean ones in (C.31) by doing $\tau \to ie^{-i\theta}t$, $\kappa_E \to -ie^{i\theta}k^0$, with $\theta = 0$.[27] Again, the above Minkowski solutions are normalized as in Eq. (C.32), and are eigenfunctions of $\mathcal{M}_{\theta=0}$ with eigenvalues $-k^2 + m^2$. The determinant is then

$$\log\det\mathcal{M}_0 = V_0^{(4)} \int \frac{d^4k}{(2\pi)^4} \log(-k^2+m^2), \tag{C.35}$$

which can be related to the Euclidean result by analytic continuation of $\mathcal{T} \to ie^{-i\theta}T$ for $\theta = 0$.

Quantum mechanical kink

The quantum mechanical kink solves the equation

$$\left[-\frac{\mathrm{d}^2}{\mathrm{d}\tau^2} + U'(\bar{\phi})\right]\bar{\phi} = 0. \tag{C.36}$$

[27] In the Minkowski path integral, we have ϵ as a regulator in both the $i\epsilon$-prescription (for picking the vacuum) and the complex bounce. But arriving here, we can safely take $\theta = 0$.

with a potential

$$U(\phi) = -\frac{1}{2}\mu^2\phi^2 + \frac{\lambda}{4!}\phi^4. \tag{C.37}$$

The solution is $\bar{\phi} = v\tanh\gamma(\tau - \tau_0)$, with $\gamma = \mu/\sqrt{2}$. Writing $u = \tanh\gamma(\tau - \tau_0)$, the eigenvalue equation

$$\left[-\frac{\mathrm{d}^2}{\mathrm{d}\tau^2} + U''(\bar{\phi})\right]\Delta\phi_E(\tau) = \lambda\Delta\phi_E(\tau) \tag{C.38}$$

becomes

$$\left[\frac{\mathrm{d}}{\mathrm{d}u}(1-u^2)\frac{\mathrm{d}}{\mathrm{d}u} - \frac{\varpi^2}{1-u^2} + 6\right]\Delta\phi_E(u) = 0, \quad \varpi^2 = 4 - \lambda/\gamma^2. \tag{C.39}$$

The solutions are the associated Legendre functions of second degree and order ϖ:

$$\Delta\phi_E(u) = \sqrt{N_E(\varpi)}P_2^{\varpi}(u), \tag{C.40}$$

with $N_E(\varpi)$ is a normalization constant.

First, one may note that the effective mass of the scalar field in the (degenerate) vacuum, reached by the kink at $\tau = \infty$, is given by

$$m^2 = 4\gamma^2. \tag{C.41}$$

From the work [114] we know there are only 2 discrete eigenvalues corresponding to $\varpi = 1$ (with a positive eigenvalue $\lambda = 3\gamma^2$) and $\varpi = 2$ (giving a zero mode, associated with time translations). There is no negative mode because the kink is not a true bounce which should be like a kink-anti-kink configuration. There are continuum modes associated with complex ϖ.

To understand this in terms of asymptotic expansions, for $\varpi \neq 1$ we may relate the Legendre functions to Jacobi polynomials, writing

$$P_2^{\varpi}(u) = \frac{1}{\cos(\varpi\pi/2)}\left(\frac{u+1}{u-1}\right)^{\frac{\varpi}{2}}(3-\varpi)_{\varpi}P_2^{-\varpi,\varpi}(u), \quad |u| < 1,\, \varpi \neq 1. \tag{C.42}$$

The asymptotic expansions for $\tau \to \pm\infty$—corresponding to $u = \pm 1$—give

$$\begin{aligned} P_2^{\varpi}(\tau) &\sim \frac{1}{2\cos(\varpi\pi/2)}(-1)^{\frac{\varpi}{2}}e^{\gamma\varpi\tau}(3-\varpi)_{\varpi}(1-\varpi)(2-\varpi),\ \tau \to \infty, \\ P_2^{\varpi}(\tau) &\sim \frac{1}{2\cos(\varpi\pi/2)}(-1)^{\frac{\varpi}{2}}e^{\gamma\varpi\tau}(3-\varpi)_{\varpi}(1+\varpi)(2+\varpi),\ \tau \to -\infty. \end{aligned} \tag{C.43}$$

For $\varpi = 1$ one has $P_2^1(u) = -3u\sqrt{1-u^2}$, which gives

$$\begin{aligned} P_2^1(\tau) &\sim -6e^{-\gamma\tau},\ \tau \to \infty, \\ P_2^1(\tau) &\sim 6e^{\gamma\tau},\ \tau \to -\infty. \end{aligned} \tag{C.44}$$

Note how for $\varpi = 1, 2$ we recover a suppressed behaviour at both ends, in accordance with the fact that there is a discrete mode. There are no other values of $\varpi \neq 1, 2$ for

which we have a decaying behaviour for both $\tau = \pm\infty$, which confirms that there are only two discrete modes. Furthermore, the continuum spectrum can only come from oscillating solutions, which demand complex ϖ:

$$\varpi = \frac{i\kappa_E}{\gamma} = \frac{2i\kappa_E}{m_+}, \kappa_E \in \mathbb{R}. \tag{C.45}$$

In this case the continuum eigenvalues are

$$\lambda_{cont} = \gamma^2(4 - \varpi^2) = m^2 + \kappa_E^2, \tag{C.46}$$

where we used (C.41). This is in accordance with our general result for the Euclidean eigenvalues in the continuum, (C.14). The eigenfunctions in the continuum are then of the form

$$\Delta\phi_E^{\kappa_E}(u) = \sqrt{N_E(\kappa_E)}\, P_2^{\varpi}(u)\Big|_{\varpi=\frac{2i}{m}\kappa_E}. \tag{C.47}$$

The reciprocal eigenfunctions are obtained by simply changing the sign of κ_E, as follows from the identity

$$\int_{-1}^{1} \frac{du}{1-u^2} P_2^{i\xi}(u) P_2^{-i\xi'}(u) = \frac{2\sinh\pi\xi}{\xi}\delta(\xi - \xi'), \tag{C.48}$$

which implies that our eigenfunctions (C.47) satisfy

$$\int_{-\infty}^{\infty} \mathrm{d}\tau\ \Delta\phi_{E,-}^{\kappa_E}\phi(\tau)\Delta\phi_{E,+}^{\kappa'_E}\phi(\tau) = \frac{m^2}{2\kappa} N_E(\kappa_E)\sinh\frac{2\kappa_E\pi}{m}\,\delta(\kappa_E - \kappa'_E). \tag{C.49}$$

This fixes the Euclidean normalization constant as

$$N_E(\kappa_E) = \frac{2\kappa_E}{m^2\sinh\frac{2\kappa_E\pi}{m}}. \tag{C.50}$$

For a rotated time countour, one can rewrite the equation for the fluctuations in terms of a variable $\tilde{u} = v\tanh\gamma i e^{-i\theta}(t - t_0)$. The resulting equation is identical to (C.39), after substituting u with $\tilde{u}$. Thus its solutions will be the associated Legendre functions evaluated at $\tilde{u}$. This is equivalent to the analytic continuation of the Euclidean solutions with the substitution $\tau \to ie^{-i\theta}t$.

The asymptotic expansions can be obtained from (C.43), (C.44) by the same analytic continuation, giving

$$\begin{aligned}
P_2^{\varpi}(ie^{-i\theta}t) &\sim \frac{1}{2\cos(\varpi\pi/2)}(-1)^{\frac{\varpi}{2}} e^{\gamma\varpi t\sin\theta} e^{i\gamma\varpi t\cos\theta}(3-\varpi)_{\varpi}(1-\varpi)(2-\varpi),\ t\to\infty,\\
P_2^{\varpi}(ie^{-i\theta}t) &\sim \frac{1}{2\cos(\varpi\pi/2)}(-1)^{\frac{\varpi}{2}} e^{\gamma\varpi t\sin\theta} e^{i\gamma\varpi t\cos\theta}(3-\varpi)_{\varpi}(1+\varpi)(2+\varpi),\ t\to-\infty,\\
P_2^{1}(ie^{-i\theta}t) &\sim -6e^{-\gamma t\sin\theta} e^{-i\gamma\cos\theta t},\ t\to\infty,\\
P_2^{1}(ie^{-i\theta}t) &\sim 6e^{\gamma t\sin\theta} e^{i\gamma\cos\theta t},\ t\to-\infty.
\end{aligned}$$

Again, for $\varpi = 1, 2$ the solutions decay at infinite time for $\theta > 0$, and define valid discrete modes. For asymptotic oscillatory solutions we need

$$e^{-i\theta}\gamma\varpi = \kappa_\theta,\ \kappa_\theta \in \mathbb{R}, \Rightarrow \varpi = \frac{e^{i\theta}\kappa_\theta}{\gamma} = \frac{2e^{i\theta}\kappa_\theta}{m}. \tag{C.51}$$

These values of ϖ can be obtained from the corresponding Euclidean ones, (C.45), by an analytic continuation $\kappa_E \to -ie^{i\theta}\kappa_\theta$, as expected from our general arguments. The continuum eigenvalues can be obtained by doing the same substitution in (C.14), which gives a result agreeing with (C.15).

The normalization of the continuum eigenfunctions for arbitrary θ follows from relating the solutions to the Euclidean ones, as in the first section. We now have

$$\Delta\phi_\theta^{\kappa_\theta}(t) = \sqrt{N}\Delta\phi_E^{-ie^{i\theta}\kappa_\theta}(ie^{-i\theta}t) \tag{C.52}$$

and the same arguments used in (C.22a) imply that the rotated functions are orthogonal, and $N = 1$. The relation between the determinants follows from the arguments of the first section.

As a check on whether one should rotate the κ parameter of the solutions in the discrete spectrum, we plot the continuation of the discrete modes $P_2^1(\tanh\tau), P_2^1(\tanh\tau)$ that arises when substituting both $\tau \to ie^{-i\theta}t$, and modifying the indices $1 \to -ie^{i\theta}t$,$2 \to -2ie^{i\theta}t$. As can be seen in Fig. C.1, this gives rise to an exponential blowup of the solutions, which can be understood from (C.51): for $\varpi \neq 1, 2$ one gets the same exponential for $t \to \pm\infty$, so that the solution blows up at one end.

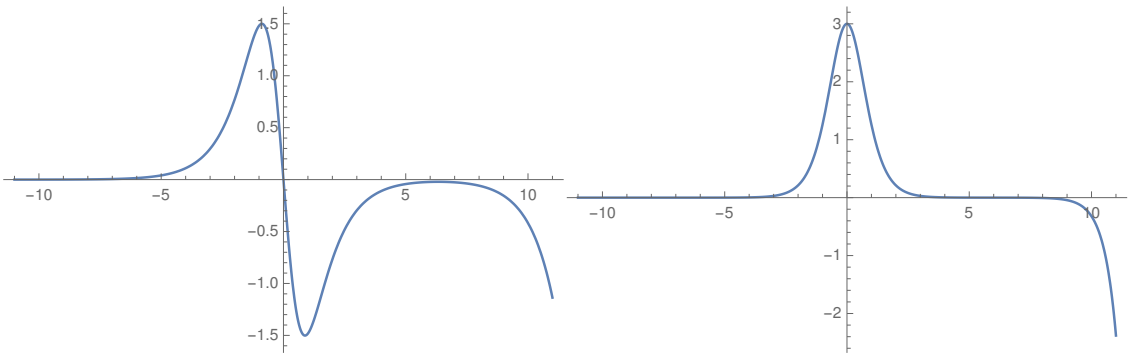

Figure C.1: Left. Double continutation of $P_2^1(\tanh\tau)$ with $\theta = 0.99\pi/2$. Right. Double continutation of $P_2^2(\tanh\tau)$ with $\theta = 0.99999\pi/2$

A further test concerns verifying (C.17) for the continuation of the discrete eigenfunctions P_2^1, P_2^2. Doing numerical integration this can be seen to hold (tested for $\theta = b\pi/2$, with $b \in \{0.01, 1\}$, with an accuracy in one part in 10^{12}).

QFT kink in planar-wall limit

The thin-wall tunneling problem in four-dimensional spacetime is analogous to the quantum mechanical kink, but with additional spatial degrees of freedom. We consider a scalar theory with the same potential as in (C.37). In hyperspherical coordinates, and assuming an $O(4)$ symmetry for the scalar background, the latter must satisfy

$$\left[-\frac{\mathrm{d}^2}{\mathrm{d}\rho^2} - \frac{3}{\rho}\frac{\mathrm{d}}{\mathrm{d}\rho} + U'(\bar{\phi})\right]\bar{\phi}(\rho) = 0. \tag{C.53}$$

In the thin-wall approximation, the $(1/\rho)\mathrm{d}/\mathrm{d}\rho$ term in the bounce equation can be neglected, the equation becomes the same as in quantum mechanics and one has again the kink as a solution (but now as a function of the Euclidean radial coordinate ρ):

$$\bar{\phi}(\rho) = v \tanh \gamma(\rho - R), \tag{C.54}$$

where R is meant to be large, so that the configuration interpolates between the two vacua at $\phi = \pm v$. For very large R, within a given region the wall will look planar. Its profile is a function of a single coordinate that we may identify with the Euclidean time. In this way we are back to a quantum mechanical kink background.

Interpreting the bounce background as depending on the Euclidean time, the eigenequations become

$$\left[-\frac{\mathrm{d}^2}{\mathrm{d}\tau^2} - \nabla^2 + U''(\bar{\phi}(\tau))\right] \Delta\phi = \lambda \Delta\phi. \tag{C.55}$$

Expanding in eigenfunctions of the 3d Laplacian, we write

$$\Delta\phi(\tau, \mathbf{x}) = \varphi(\tau) e^{i\mathbf{k}\cdot\mathbf{x}}, \tag{C.56}$$

so that one has

$$\left[-\frac{\mathrm{d}^2}{\mathrm{d}\tau^2} + U''(\bar{\phi}(\tau))\right] \varphi = (\lambda - \mathbf{k}^2)\varphi. \tag{C.57}$$

This is identical to the equation (C.38) of the fluctuations of the quantum mechanical kink, after replacing $\lambda \to \lambda - \mathbf{k}^2$. Thus proceeding as before we change variables to $u = \tanh \gamma(\tau - R)$ and find solutions in terms of Legendre polynomials $P_2^{\varpi}(u)$, but now with eigenvalues given by

$$\lambda = \gamma^2(4 - \varpi^2) + \mathbf{k}^2. \tag{C.58}$$

There is a continuum spectrum depending on $\mathbf{k}$, while for ϖ there are again 2 discrete choices $\varpi = 1, 2$ giving temporally decaying solutions, and a continuum giving temporally oscillating solutions. The latter have ϖ as in (C.45), and continuum eigenvalues of the form

$$\lambda = m^2 + \kappa_E^2 + \mathbf{k}^2, \tag{C.59}$$

exactly as in (C.14). The properly normalized real Euclidean eigenfunctions in the continuum are:

$$\Delta\phi_E^{(\kappa_E, \mathbf{k})} \phi(\hat{x}) = \sqrt{\frac{N_E(\kappa_E)}{(2\pi)^3}}\, P_2^{\varpi}(u)\Big|_{\varpi = \frac{2i}{m}\kappa_E} e^{i\mathbf{k}\cdot\mathbf{x}}, \tag{C.60}$$

with $N_E(\kappa_E)$ given by (C.50), and with the reciprocal eigenfunctions obtained by changing $\kappa_E, \mathbf{k}$ with $-\kappa_E, -\mathbf{k}$. The scalar products go as

$$\int \mathrm{d}^4x\; \Delta\phi_{E,-}^{(\kappa_E, \mathbf{k})}(\hat{x}) \Delta\phi_{E,+}^{(\kappa'_E, \mathbf{k}')}(\hat{x}) = \delta(\kappa_E - \kappa'_E)\delta^3(\mathbf{k} - \mathbf{k}'). \tag{C.61}$$

The contribution to the determinant of the continuum modes is then

$$\log\det\mathcal{M}_E = V_E^{(4)}\int\frac{\mathrm{d}^4\hat{k}}{(2\pi)^4}\log(\hat{k}^2+m^2), \tag{C.62}$$

where we defined a 4 vector $\hat{k}=(\kappa_E,\mathbf{k})$.

The continuation to rotated time of the eigenfunctions and determinant goes exactly as in the kink case, as the only difference now is the $\mathbf{k}$ dependence in the eigenfunctions and eigenvalues, which is not changed by the analytic continuation process.

A very subtle point is that Eq. (C.62) is not equal to the spacetime integral of the Coleman-Weinberg potential. This is because $V_E^{(4)}$ is defined as $(2\pi)^4\delta_{\kappa_E}(0)\delta^3_{\mathbf{k}}(\mathbf{0})$ which is not necessarily equal to $\int\mathrm{d}^4x$ due to the nontrivial background $\bar{\phi}$. See Ref. [138].

Appendix D

Decay Rate from the WKB Method

In this appendix, we rederive the decay rate (A.20) from solving the static Schrödinger equation using the WKB expansion. This derivation closely follows the calculation of the ground energy in a symmetric double-well potential given in Ref. [42].

Before we start, we find it helpful to comment on the unit system used in our field theory version of the action for quantum mechanics:

$$S_E = \int \mathrm{d}t \left[\frac{1}{2} \left(\frac{\mathrm{d}x}{\mathrm{d}\tau} \right)^2 - V(x) \right]. \tag{D.1}$$

Here, we have set the mass for the particle to be one such that the kinetic term looks like that in field theory. This makes the "field", $x(\tau)$, have unusual dimension. We first fix the time τ with energy dimension -1, i.e., $[\tau] = -1$. Therefore the "field" $x(\tau)$ has the energy dimension $-1/2$. That is,

$$[\tau] = -1,\ [x] = -\frac{1}{2},\ [V(x)] = 1,\ [V''(x)] = [m^2] = 2. \tag{D.2}$$

Further from Eq. (A.8), we have $[A] = 1$. (This is consistent with that $A = 2\sqrt{3}\mu$ in the kink example. See below Eq. (A.30).)

For $x_p < x < x_+$ (see Fig. 2.1), we have the following WKB wave function

$$\psi_{\mathrm{WKB}}(x) = \frac{c_1}{\sqrt{\kappa(x)}}\, e^{\frac{1}{\hbar}\int_{x_p}^{x} dx'\,\kappa(x')} + \frac{c_2}{\sqrt{\kappa(x)}}\, e^{-\frac{1}{\hbar}\int_{x_p}^{x} dx'\,\kappa(x')}, \tag{D.3}$$

where $\kappa(x) = \sqrt{2(U(x) - E)}$. We are going to match this wavefunction with those near the turning points x_p and x_+. Let us first consider the region around x_+. In this region, the potential is $U = m^2(x_+ - x)^2/2$ and we expect an approximately ground state in this parabolic potential. For a wave function, due to the normalization

$$\int \mathrm{d}x\ \psi^2_{\mathrm{WKB}}(x) = 1, \tag{D.4}$$

we have

$$[\psi_{\mathrm{WKB}}(x)] = \frac{1}{4},\ [\kappa(x)] = \frac{1}{4},\ [c_1] = [c_2] = \frac{1}{2}. \tag{D.5}$$

The dimensional system will help us to check the consistency of the equations and expressions. For such a bound state, we have to consider the quantum ground energy, writing $E = \hbar m\,(1/2 + \varepsilon)$ where ε denotes a small correction. Expand $\kappa(x)$ as

$$\kappa(x) = \sqrt{2U(x)} - \frac{E}{\sqrt{2U(x)}}, \tag{D.6}$$

and substitute the above equation to Eq. (D.3). Using

$$\int_{x_p}^{x} \mathrm{d}x' \sqrt{2U(x')} = \int_{x_p}^{x_+} \mathrm{d}x' \sqrt{2U(x')} + \int_{x_+}^{x} \mathrm{d}x' \sqrt{2U(x')}$$
$$= \frac{B}{2} - \frac{1}{2} m (x_+ - x)^2. \tag{D.7}$$

We obtain

$$\psi_{\mathrm{WKB}}(x) = \frac{c_1}{\sqrt{m(x_+ - x)}}\, e^{\frac{1}{\hbar}\left(\frac{B}{2} - \frac{1}{2}m(x_+ - x)^2 + Em^{-1}\ln(B^{-1/2}m^{3/2}A^{-1}(x_+ - x))\right)}$$
$$+ \frac{c_2}{\sqrt{m(x_+ - x)}}\, e^{-\frac{1}{\hbar}\left(\frac{B}{2} - \frac{1}{2}m(x_+ - x)^2 + Em^{-1}\ln(B^{-1/2}m^{3/2}A^{-1}(x_+ - x))\right)}, \tag{D.8}$$

where we have used Eq. (A.11). Substituting $E = \hbar m\,(1/2 + \varepsilon)$ into the above expression, we finally have

$$\psi_{\mathrm{WKB}}(x) = \Big(c_1\, e^{B/2\hbar} B^{-1/4} A^{-1/2} m^{1/4} e^{-\frac{m}{2\hbar}(x_+ - x)^2}$$
$$+ \frac{c_2}{m^{5/4}(x_+ - x)}\, e^{-B/2\hbar} B^{1/4} A^{1/2} e^{\frac{m}{2\hbar}(x_+ - x)^2} \Big) \times [1 + \mathcal{O}(\varepsilon)]. \tag{D.9}$$

To fix the coefficients, we need to match $\psi_{\mathrm{WKB}}(x)$ to the solutions of the Schrödinger equation. First, we consider the match to the solution of the following equation

$$-\frac{\hbar^2}{2}\,\partial_x^2 \psi(x) + \frac{1}{2} m^2\,(x - x_+)^2\,\psi(x) = E\,\psi(x) \tag{D.10}$$

for$|x - x_+| \gg \hbar$. Since ε is a small number, we will solve this problem perturbatively around $\varepsilon = 0$. For $\varepsilon = 0$, we have two solutions

$$\psi_1(x) = m^{1/4}\, e^{-m(x_+ - x)^2/2\hbar}, \tag{D.11}$$

and

$$\psi_2(x) = \frac{1}{m^{1/4}(x_+ - x)}\, e^{m(x_+ - x)^2/2\hbar}, \tag{D.12}$$

where the latter is valid for $|x - x_+| \gg \hbar$. The factors of $m^{1/4}$ and $m^{-1/4}$ are included for dimensional reason. For nonvanishing ε, writing $\psi(x) = \psi_1(x) + \delta\psi(x)$, we have

$$-\frac{\hbar^2}{2}\,\partial_x^2 \delta\psi(x) + \frac{1}{2}\, m^2 (x - x_+)^2\,\delta\psi(x) = (\hbar m)\varepsilon\,\psi_1(x). \tag{D.13}$$

The solution can be readily seen to be

$$\psi(x) = \psi_1(x) - \varepsilon \int_x^\infty dx'\,\psi_1(x')\,[\psi_1(x')\psi_2(x) - \psi_2(x')\psi_1(x)], \tag{D.14}$$

where $\psi(x)$ vanishes for $x \to \infty$. This automatically takes care of the match for $x - x_+ \gg \hbar$. For $x - x_+ \ll \hbar$, we can approximately use the following relation

$$\int_x^\infty dx'\,\psi_1^2(x') \approx \int_{-\infty}^\infty dx'\,\psi_1^2(x') = \sqrt{\pi\hbar} \tag{D.15}$$

to obtain

$$\psi(x) = N\left[m^{1/4}e^{-m(x_+-x)^2/2\hbar}\left[1+\mathcal{O}(\varepsilon)\right] - \frac{\varepsilon\sqrt{\pi\hbar}}{m^{1/4}(x_+-x)}\,e^{m(x_+-x)^2/2\hbar}\right], \tag{D.16}$$

where we have included a normalization factor. Comparing Eq. (D.16) with Eq. (D.9), we have

$$m\varepsilon = -\frac{c_2}{c_1}\sqrt{\frac{B}{\pi\hbar}}\,e^{-B/\hbar}\,A. \tag{D.17}$$

The ratio c_2/c_1 can be determined by doing the match around x_p. In this region, $U(x) = U'(x_p)(x-x_p)$. The state is not a bound state and we can simply take $E=0$. Hence, we have the the following Schrödinger equation,

$$-\frac{\hbar^2}{2}\,\partial_x^2\psi(x) + U'(x_p)(x-x_p)\,\psi(x) = 0. \tag{D.18}$$

Defining $y = x - x_p$ and $y = (\hbar^2/(2U'(x_p)))^{1/3}z$, we have

$$\partial_z^2\psi(z) - z\psi(z) = 0. \tag{D.19}$$

The solutions to this equation are Airy functions. The asymptotic forms of the Airy functions are well known:

$$Ai(z) \to \frac{1}{2\sqrt{\pi}}\,z^{-1/4}\,\exp\left(-\frac{2}{3}\,z^{3/2}\right) \text{ for } z\to+\infty, \tag{D.20}$$

$$Ai(z) \to \frac{1}{\sqrt{\pi}}\,|z|^{-1/4}\,\cos\left(\frac{2}{3}\,|z|^{3/2} - \frac{\pi}{4}\right) \text{ for } z\to-\infty. \tag{D.21}$$

and

$$Bi(z) \to \frac{1}{\sqrt{\pi}}\,z^{-1/4}\,\exp\left(\frac{2}{3}\,z^{3/2}\right) \text{ for } z\to+\infty, \tag{D.22}$$

$$Bi(z) \to \frac{1}{\sqrt{\pi}}\,|z|^{-1/4}\,\cos\left(\frac{2}{3}\,|z|^{3/2} + \frac{\pi}{4}\right) \text{ for } z\to-\infty. \tag{D.23}$$

This gives the following connection formulas: if for $x > x_p$, we have

$$\frac{c_1}{\sqrt{\kappa(x)}}\,\exp\left[\int_{x_p}^{x} dx'\,\kappa(x')\right] + \frac{c_2}{\sqrt{\kappa(x)}}\,\exp\left[-\int_{x_p}^{x} dx'\,\kappa(x')\right], \tag{D.24}$$

then the solution for $x < x_p$ takes the form

$$\frac{2\,c_2}{\sqrt{k(x)}}\,\cos\left[\int_{x}^{x_p} dx'\,k(x') - \frac{\pi}{4}\right] - \frac{c_1}{\sqrt{k(x)}}\,\sin\left[\int_{x}^{x_p} dx'\,k(x') - \frac{\pi}{4}\right], \tag{D.25}$$

where $k(x) = \sqrt{-2U(x)}$ and we have used $\kappa(x) \sim \sqrt{z}$ for $z > 0$ and $k(x) \sim \sqrt{|z|}$ for $z < 0$.

To have a pure outgoing boundary condition for $x < x_p$, we let $c_1 = i\,2c_2$. This gives us

$$m\varepsilon = \frac{i}{2}\sqrt{\frac{B}{\pi\hbar}}\,e^{-B/\hbar}\,A, \tag{D.26}$$

which is imaginary. Finally, we obtain the decay rate

$$\Gamma = \frac{2}{\hbar}\,\mathrm{Im}E = \sqrt{\frac{B}{\pi\hbar}}\,e^{-B/\hbar}\,A, \tag{D.27}$$

in agreement with the result derived from the path integral.

Bibliography

[1] M. E. Peskin and D. V. Schroeder, *An Introduction to quantum field theory*, CRC Press.

[2] S. M. Carroll, *Spacetime and geometry: An introduction to general relativity*, San Francisco, USA, Addison-Wesley (2004).

[3] G. Aad *et al.* [ATLAS Collaboration], "Observation of a new particle in the search for the Standard Model Higgs boson with the ATLAS detector at the LHC," Phys. Lett. B **716**, 1 (2012) [arXiv:1207.7214 [hep-ex]].

[4] S. Chatrchyan *et al.* [CMS Collaboration], "Observation of a new boson at a mass of 125 GeV with the CMS experiment at the LHC," Phys. Lett. B **716**, 30 (2012) [arXiv:1207.7235 [hep-ex]].

[5] [CDF and D0 Collaborations and Tevatron Electroweak Working Group], "Combination of CDF and D0 results on the mass of the top quark using up to 5.8 fb-1 of data," arXiv:1107.5255 [hep-ex].

[6] G. Isidori, G. Ridolfi and A. Strumia, "On the metastability of the standard model vacuum," Nucl. Phys. B **609**, 387 (2001) [hep-ph/0104016].

[7] G. Degrassi, S. Di Vita, J. Elias-Miró, J. R. Espinosa, G. F. Giudice, G. Isidori and A. Strumia, "Higgs mass and vacuum stability in the Standard Model at NNLO," JHEP **1208**, 098 (2012) [arXiv:1205.6497 [hep-ph]].

[8] D. Buttazzo, G. Degrassi, P. P. Giardino, G. F. Giudice, F. Sala, A. Salvio and A. Strumia, "Investigating the near-criticality of the Higgs boson," JHEP **1312**, 089 (2013) [arXiv:1307.3536 [hep-ph]].

[9] L. Di Luzio, G. Isidori and G. Ridolfi, "Stability of the electroweak ground state in the Standard Model and its extensions," Phys. Lett. B **753**, 150 (2016) [arXiv:1509.05028 [hep-ph]].

[10] S. Chigusa, T. Moroi and Y. Shoji, "State-of-the-Art Calculation of the Decay Rate of Electroweak Vacuum in the Standard Model," Phys. Rev. Lett. **119**, 211801 (2017) [arXiv:1707.09301 [hep-ph]].

[11] A. Andreassen, W. Frost and M. D. Schwartz, "Scale Invariant Instantons and the Complete Lifetime of the Standard Model," Phys. Rev. D **97**, no. 5, 056006 (2018) [arXiv:1707.08124 [hep-ph]].

[12] S. R. Coleman and E. J. Weinberg, "Radiative Corrections as the Origin of Spontaneous Symmetry Breaking," Phys. Rev. D **7**, 1888 (1973).

[13] R. Gregory, I. G. Moss and B. Withers, "Black holes as bubble nucleation sites," JHEP **1403**, 081 (2014) [arXiv:1401.0017 [hep-th]].

[14] P. Burda, R. Gregory and I. Moss, "Gravity and the stability of the Higgs vacuum," Phys. Rev. Lett. **115**, 071303 (2015) [arXiv:1501.04937 [hep-th]].

[15] P. Burda, R. Gregory and I. Moss, "Vacuum metastability with black holes," JHEP **1508**, 114 (2015) [arXiv:1503.07331 [hep-th]].

[16] P. Burda, R. Gregory and I. Moss, "The fate of the Higgs vacuum," JHEP **1606**, 025 (2016) [arXiv:1601.02152 [hep-th]].

[17] E. W. Kolb and M. S. Turner, "The Early Universe," Front. Phys. **69**, 1 (1990).

[18] S. Dodelson, *Modern Cosmology*, Amsterdam, Netherlands, Academic Press (2003).

[19] K. Kajantie, M. Laine, K. Rummukainen and M. E. Shaposhnikov, "Is there a hot electroweak phase transition at m(H) larger or equal to m(W)?," Phys. Rev. Lett. **77**, 2887 (1996) [hep-ph/9605288].

[20] M. Gurtler, E. M. Ilgenfritz and A. Schiller, "Where the electroweak phase transition ends," Phys. Rev. D **56**, 3888 (1997) [hep-lat/9704013].

[21] J. F. Gunion, R. Vega and J. Wudka, "Higgs triplets in the standard model," Phys. Rev. D **42**, 1673 (1990).

[22] J. M. Cline and P. A. Lemieux, "Electroweak phase transition in two Higgs doublet models," Phys. Rev. D **55**, 3873 (1997) [hep-ph/9609240].

[23] M. Carena, M. Quiros and C. E. M. Wagner, "Electroweak baryogenesis and Higgs and stop searches at LEP and the Tevatron," Nucl. Phys. B **524**, 3 (1998) [hep-ph/9710401].

[24] L. Fromme, S. J. Huber and M. Seniuch, "Baryogenesis in the two-Higgs doublet model," JHEP **0611**, 038 (2006) [hep-ph/0605242].

[25] S. Profumo, M. J. Ramsey-Musolf and G. Shaughnessy, "Singlet Higgs phenomenology and the electroweak phase transition," JHEP **0708**, 010 (2007) [arXiv:0705.2425 [hep-ph]].

[26] V. Barger, P. Langacker, M. McCaskey, M. J. Ramsey-Musolf and G. Shaughnessy, "LHC Phenomenology of an Extended Standard Model with a Real Scalar Singlet," Phys. Rev. D **77**, 035005 (2008) [arXiv:0706.4311 [hep-ph]].

[27] P. Fileviez Perez, H. H. Patel, M. J. Ramsey-Musolf and K. Wang, "Triplet Scalars and Dark Matter at the LHC," Phys. Rev. D **79**, 055024 (2009) [arXiv:0811.3957 [hep-ph]].

[28] G. C. Dorsch, S. J. Huber and J. M. No, "A strong electroweak phase transition in the 2HDM after LHC8," JHEP **1310**, 029 (2013) [arXiv:1305.6610 [hep-ph]].

[29] E. Witten, "Cosmic Separation of Phases," Phys. Rev. D **30**, 272 (1984).

[30] A. Kosowsky, M. S. Turner and R. Watkins, "Gravitational radiation from colliding vacuum bubbles," Phys. Rev. D **45**, 4514 (1992).

[31] C. Caprini, R. Durrer, T. Konstandin and G. Servant, "General Properties of the Gravitational Wave Spectrum from Phase Transitions," Phys. Rev. D **79**, 083519 (2009) [arXiv:0901.1661 [astro-ph.CO]].

[32] C. Caprini *et al.*, "Science with the space-based interferometer eLISA. II: Gravitational waves from cosmological phase transitions," JCAP **1604**, 001 (2016) [arXiv:1512.06239 [astro-ph.CO]].

[33] V. A. Kuzmin, V. A. Rubakov and M. E. Shaposhnikov, "On the Anomalous Electroweak Baryon Number Nonconservation in the Early Universe," Phys. Lett. **155B**, 36 (1985).

[34] M. E. Shaposhnikov, "Baryon Asymmetry of the Universe in Standard Electroweak Theory," Nucl. Phys. B **287**, 757 (1987).

[35] D. E. Morrissey and M. J. Ramsey-Musolf, "Electroweak baryogenesis," New J. Phys. **14**, 125003 (2012) [arXiv:1206.2942 [hep-ph]].

[36] B. Garbrecht, "Why is there more matter than antimatter? Calculational methods for leptogenesis and electroweak baryogenesis," arXiv:1812.02651 [hep-ph].

[37] C. G. Callan, Jr. and S. R. Coleman, "The Fate of the False Vacuum. 2. First Quantum Corrections," Phys. Rev. D **16** (1977) 1762.

[38] J. S. Langer, "Theory of the condensation point," Annals Phys. **41** (1967) 108 [Annals Phys. **281** (2000) 941].

[39] J. S. Langer, "Statistical theory of the decay of metastable states," Annals Phys. **54** (1969) 258.

[40] I. Y. Kobzarev, L. B. Okun and M. B. Voloshin, "Bubbles in Metastable Vacuum," Sov. J. Nucl. Phys. **20** (1975) 644 [Yad. Fiz. **20** (1974) 1229].

[41] S. R. Coleman, "The Fate of the False Vacuum. 1. Semiclassical Theory," Phys. Rev. D **15** (1977) 2929 [Erratum-ibid. D **16** (1977) 1248].

[42] S. R. Coleman, *Aspects of symmetry: selected Erice lectures*, Cambridge University Press, 1988.

[43] I. Affleck, "Quantum Statistical Metastability," Phys. Rev. Lett. **46**, 388 (1981).

[44] A. D. Linde, "Fate of the False Vacuum at Finite Temperature: Theory and Applications," Phys. Lett. **100B**, 37 (1981).

[45] A. D. Linde, "Decay of the False Vacuum at Finite Temperature," Nucl. Phys. B **216**, 421 (1983) Erratum: [Nucl. Phys. B **223**, 544 (1983)].

[46] A. Andreassen, D. Farhi, W. Frost and M. D. Schwartz, "Direct Approach to Quantum Tunneling," Phys. Rev. Lett. **117**, 231601 (2016) [arXiv:1602.01102 [hep-th]].

[47] A. Andreassen, D. Farhi, W. Frost and M. D. Schwartz, "Precision decay rate calculations in quantum field theory," Phys. Rev. D **95**, 085011 (2017) [arXiv:1604.06090 [hep-th]].

[48] E. Witten, "Analytic Continuation Of Chern-Simons Theory," AMS/IP Stud. Adv. Math. **50**, 347 (2011) [arXiv:1001.2933 [hep-th]].

[49] E. Witten, "A New Look At The Path Integral Of Quantum Mechanics," arXiv:1009.6032 [hep-th].

[50] J. L. Gervais and B. Sakita, "Extended Particles in Quantum Field Theories," Phys. Rev. D **11**, 2943 (1975).

[51] A. D. Plascencia and C. Tamarit, "Convexity, gauge-dependence and tunneling rates," JHEP **1610**, 099 (2016) [arXiv:1510.07613 [hep-ph]].

[52] A. R. Brown, "The Thin-Wall Approximation in Vacuum Decay: a Lemma," Phys. Rev. D **97** (2018) no.10, 105002 [arXiv:1711.07712 [hep-th]].

[53] R. F. Dashen, B. Hasslacher and A. Neveu, "Nonperturbative Methods and Extended Hadron Models in Field Phys. Rev. D **10** (1974) 4114; *ibid.* 4130; *ibid.* 4138.

[54] M. Laine and A. Vuorinen, "Basics of Thermal Field Theory," Lect. Notes Phys. **925**, pp.1 (2016) [arXiv:1701.01554 [hep-ph]].

[55] E. J. Weinberg, "Classical solutions in quantum field theory : Solitons and Instantons in High Energy Physics," Cambridge University Press, 2012.

[56] W. Y. Ai, "Correspondence between Thermal and Quantum Vacuum Transitions around Horizons," JHEP **1903**, 164 (2019) [arXiv:1812.06962 [hep-th]].

[57] W. G. Unruh, "Notes on black hole evaporation," Phys. Rev. D **14**, 870 (1976).

[58] L. Susskind, L. Thorlacius and J. Uglum, "The Stretched horizon and black hole complementarity," Phys. Rev. D **48**, 3743 (1993) [hep-th/9306069].

[59] B. Garbrecht and P. Millington, "Green's function method for handling radiative effects on false vacuum decay," Phys. Rev. D **91**, 105021 (2015) [arXiv:1501.07466 [hep-th]].

[60] W. Y. Ai, B. Garbrecht and P. Millington, "Radiative effects on false vacuum decay in Higgs-Yukawa theory," Phys. Rev. D **98**, 076014 (2018) [arXiv:1807.03338 [hep-th]].

[61] B. Garbrecht and P. Millington, "Self-consistent solitons for vacuum decay in radiatively generated potentials," Phys. Rev. D **92**, 125022 (2015) [arXiv:1509.08480 [hep-ph]].

[62] N. Tetradis, "Black holes and Higgs stability," JCAP **1609**, 036 (2016) [arXiv:1606.04018 [hep-ph]].

[63] D. Gorbunov, D. Levkov and A. Panin, "Fatal youth of the Universe: black hole threat for the electroweak vacuum during preheating," JCAP **1710**, 016 (2017) [arXiv:1704.05399 [astro-ph.CO]].

[64] D. Canko, I. Gialamas, G. Jelic-Cizmek, A. Riotto and N. Tetradis, "On the Catalysis of the Electroweak Vacuum Decay by Black Holes at High Temperature," Eur. Phys. J. C **78**, 328 (2018) [arXiv:1706.01364 [hep-th]].

[65] K. Mukaida and M. Yamada, "False Vacuum Decay Catalyzed by Black Holes," Phys. Rev. D **96**, 103514 (2017) [arXiv:1706.04523 [hep-th]].

[66] R. Gregory, K. M. Marshall, F. Michel and I. G. Moss, "Negative modes of Coleman-De Luccia and black hole bubbles," Phys. Rev. D **98**, 085017 (2018) [arXiv:1808.02305 [hep-th]].

[67] L. Parker, "Particle creation in expanding universes," Phys. Rev. Lett. **21**, 562 (1968).

[68] L. Parker, "Quantized fields and particle creation in expanding universes. 1.," Phys. Rev. **183**, 1057 (1969).

[69] L. Parker, "Quantized fields and particle creation in expanding universes. 2.," Phys. Rev. D **3**, 346 (1971) Erratum: [Phys. Rev. D **3**, 2546 (1971)].

[70] S. A. Fulling, "Nonuniqueness of canonical field quantization in Riemannian space-time," Phys. Rev. D **7**, 2850 (1973).

[71] Ya. B. Zel'dovich, "Generation of waves by a rotating body," ZhETF Pis. Red.14, 270 (1970).

[72] S. W. Hawking, "Particle Creation by Black Holes," Commun. Math. Phys. **43**, 199 (1975) Erratum: [Commun. Math. Phys. **46**, 206 (1976)].

[73] J. M. Bardeen, B. Carter and S. W. Hawking, "The Four laws of black hole mechanics," Commun. Math. Phys. **31**, 161 (1973).

[74] W. Israel, "Thermo field dynamics of black holes," Phys. Lett. A **57**, 107 (1976).

[75] L. Susskind and L. Thorlacius, "Gedanken experiments involving black holes," Phys. Rev. D **49**, 966 (1994) [hep-th/9308100].

[76] A. R. Brown and E. J. Weinberg, "Thermal derivation of the Coleman-De Luccia tunneling prescription," Phys. Rev. D **76**, 064003 (2007) [arXiv:0706.1573 [hep-th]].

[77] S. R. Coleman and F. De Luccia, "Gravitational Effects on and of Vacuum Decay," Phys. Rev. D **21**, 3305 (1980).

[78] Y. Takahasi and H. Umezawa, "Thermo field dynamics," Collect. Phenom. **2**, 55 (1975).

[79] A. Einstein and N. Rosen, "The Particle Problem in the General Theory of Relativity," Phys. Rev. **48**, 73 (1935).

[80] S. W. Hawking, "Gravitational Instantons," Phys. Lett. A **60**, 81 (1977).

[81] M. Spradlin, A. Strominger and A. Volovich, "Les Houches lectures on de Sitter space," hep-th/0110007.

[82] J. D. Bekenstein, "Black holes and the second law," Lett. Nuovo Cim. **4**, 737 (1972).

[83] S. W. Hawking, "Breakdown of Predictability in Gravitational Collapse," Phys. Rev. D **14**, 2460 (1976).

[84] S. D. Mathur, "The Information paradox: A Pedagogical introduction," Class. Quant. Grav. **26**, 224001 (2009) [arXiv:0909.1038 [hep-th]].

[85] A. Almheiri, D. Marolf, J. Polchinski and J. Sully, "Black Holes: Complementarity or Firewalls?," JHEP **1302**, 062 (2013) [arXiv:1207.3123 [hep-th]].

[86] D. N. Page, "Information in black hole radiation," Phys. Rev. Lett. **71**, 3743 (1993) [hep-th/9306083].

[87] J. Maldacena and L. Susskind, "Cool horizons for entangled black holes," Fortsch. Phys. **61**, 781 (2013) [arXiv:1306.0533 [hep-th]].

[88] A. Einstein, B. Podolsky and N. Rosen, "Can quantum mechanical description of physical reality be considered complete?," Phys. Rev. **47**, 777 (1935).

[89] N. Cabibbo, L. Maiani, G. Parisi and R. Petronzio, "Bounds on the Fermions and Higgs Boson Masses in Grand Unified Theories," Nucl. Phys. B **158**, 295 (1979).

[90] P. Q. Hung, "Vacuum Instability and New Constraints on Fermion Masses," Phys. Rev. Lett. **42**, 873 (1979).

[91] M. Lindner, "Implications of Triviality for the Standard Model," Z. Phys. C **31**, 295 (1986).

[92] M. Sher, "Electroweak Higgs Potentials and Vacuum Stability," Phys. Rept. **179**, 273 (1989).

[93] M. Sher, "Precise vacuum stability bound in the standard model," Phys. Lett. B **317**, 159 (1993) [Addendum: Phys. Lett. B **331**, 448 (1994)] [hep-ph/9307342].

[94] J. A. Casas, J. R. Espinosa and M. Quirós, "Improved Higgs mass stability bound in the standard model and implications for supersymmetry," Phys. Lett. B **342**, 171 (1995) [hep-ph/9409458].

[95] J. A. Casas, J. R. Espinosa and M. Quirós, "Standard model stability bounds for new physics within LHC reach," Phys. Lett. B **382**, 374 (1996) [hep-ph/9603227].

[96] C. P. Burgess, V. Di Clemente and J. R. Espinosa, "Effective operators and vacuum instability as heralds of new physics," JHEP **0201**, 041 (2002) [hep-ph/0201160].

[97] G. Isidori, V. S. Rychkov, A. Strumia and N. Tetradis, "Gravitational corrections to standard model vacuum decay," Phys. Rev. D **77**, 025034 (2008) [arXiv:0712.0242 [hep-ph]].

[98] N. Arkani-Hamed, S. Dubovsky, L. Senatore and G. Villadoro, "(No) Eternal Inflation and Precision Higgs Physics," JHEP **0803**, 075 (2008) [arXiv:0801.2399 [hep-ph]].

[99] F. Bezrukov and M. Shaposhnikov, "Standard Model Higgs boson mass from inflation: Two loop analysis," JHEP **0907**, 089 (2009) [arXiv:0904.1537 [hep-ph]].

[100] L. J. Hall and Y. Nomura, "A Finely-Predicted Higgs Boson Mass from A Finely-Tuned Weak Scale," JHEP **1003**, 076 (2010) [arXiv:0910.2235 [hep-ph]].

[101] J. Ellis, J. R. Espinosa, G. F. Giudice, A. Hoecker and A. Riotto, "The Probable Fate of the Standard Model," Phys. Lett. B **679**, 369 (2009) [arXiv:0906.0954 [hep-ph]].

[102] J. Elias-Miró, J. R. Espinosa, G. F. Giudice, G. Isidori, A. Riotto and A. Strumia, "Higgs mass implications on the stability of the electroweak vacuum," Phys. Lett. B **709**, 222 (2012) [arXiv:1112.3022 [hep-ph]].

[103] F. Bezrukov, M. Y. Kalmykov, B. A. Kniehl and M. Shaposhnikov, "Higgs Boson Mass and New Physics," JHEP **1210**, 140 (2012) [arXiv:1205.2893 [hep-ph]].

[104] I. Masina, "Higgs boson and top quark masses as tests of electroweak vacuum stability," Phys. Rev. D **87**, no. 5, 053001 (2013) [arXiv:1209.0393 [hep-ph]].

[105] V. Branchina and E. Messina, "Stability, Higgs Boson Mass and New Physics," Phys. Rev. Lett. **111**, 241801 (2013) [arXiv:1307.5193 [hep-ph]].

[106] V. Branchina, E. Messina and A. Platania, "Top mass determination, Higgs inflation, and vacuum stability," JHEP **1409**, 182 (2014) [arXiv:1407.4112 [hep-ph]].

[107] V. Branchina, E. Messina and M. Sher, "Lifetime of the electroweak vacuum and sensitivity to Planck scale physics," Phys. Rev. D **91**, 013003 (2015) [arXiv:1408.5302 [hep-ph]].

[108] V. Branchina, F. Contino and A. Pilaftsis, "Protecting the Stability of the EW Vacuum from Planck-Scale Gravitational Effects," Phys. Rev. D **98**, 075001 (2018) [arXiv:1806.11059 [hep-ph]].

[109] Z. Lalak, M. Lewicki and P. Olszewski, "Higher-order scalar interactions and SM vacuum stability," JHEP **1405**, 119 (2014) [arXiv:1402.3826 [hep-ph]].

[110] A. Eichhorn, H. Gies, J. Jaeckel, T. Plehn, M. M. Scherer and R. Sondenheimer, "The Higgs Mass and the Scale of New Physics," JHEP **1504**, 022 (2015) [arXiv:1501.02812 [hep-ph]].

[111] I. M. Gel'fand and A. M. Yaglom, "Integration in functional spaces and it applications in quantum physics," J. Math. Phys. **1** (1960) 48.

[112] J. Baacke and G. Lavrelashvili, "One loop corrections to the metastable vacuum decay," Phys. Rev. D **69**, 025009 (2004) [hep-th/0307202].

[113] G. V. Dunne and H. Min, "Beyond the thin-wall approximation: Precise numerical computation of prefactors in false vacuum decay," Phys. Rev. D **72**, 125004 (2005) [hep-th/0511156].

[114] B. Garbrecht and P. Millington, "Fluctuations about the Fubini-Lipatov instanton for false vacuum decay in classically scale invariant models," Phys. Rev. D **98**, 016001 (2018) [arXiv:1804.04944 [hep-th]].

[115] B. Garbrecht and P. Millington, "Constraining the effective action by a method of external sources," Nucl. Phys. B **906** (2016) 105 [arXiv:1509.07847 [hep-th]].

[116] R. Jackiw, "Functional evaluation of the effective potential," Phys. Rev. D **9**, 1686 (1974).

[117] J. M. Cornwall, R. Jackiw and E. Tomboulis, "Effective Action for Composite Operators," Phys. Rev. D **10**, 2428 (1974).

[118] M. A. Bezuglov and A. I. Onishchenko, "Two-loop corrections to false vacuum decay in scalar field theory," arXiv:1805.06482 [hep-ph].

[119] B. Garbrecht and P. Millington, "Constraining the effective action by a method of external sources," Nucl. Phys. B **906**, 105 (2016) [arXiv:1509.07847 [hep-th]].

[120] R. V. Konoplich, "Calculation of Quantum Corrections to Nontrivial Classical Solutions by Means of the Zeta Function," Theor. Math. Phys. **73**, 1286 (1987) [Teor. Mat. Fiz. **73**, 379 (1987)].

[121] J. Baacke and S. Junker, "Quantum corrections to the electroweak sphaleron transition," Mod. Phys. Lett. A **8**, 2869 (1993) [hep-ph/9306307].

[122] J. Baacke and S. Junker, "Quantum fluctuations around the electroweak sphaleron," Phys. Rev. D **49**, 2055 (1994) [hep-ph/9308310].

[123] J. Baacke and S. Junker, "Quantum fluctuations of the electroweak sphaleron: Erratum and addendum," Phys. Rev. D **50**, 4227 (1994) [hep-th/9402078].

[124] J. Baacke, "One-loop corrections to the instanton transition in the Abelian Higgs model: Gel'fand-Yaglom and Green's function methods," Phys. Rev. D **78**, 065039 (2008) [arXiv:0803.4333 [hep-th]].

[125] F. Pham, "Vanishing homologies and the n variable saddlepoint method," Proc. Symp. Pure Math. **40** (1983) 319.

[126] M. V. Berry and C. J. Howls, "Hyperasymptotics for integrals with saddles," Proc. Roy. Soc. Lond **A 434** (1991) 657.

[127] A. Cherman and M. Unsal, "Real-Time Feynman Path Integral Realization of Instantons," arXiv:1408.0012 [hep-th].

[128] Y. Tanizaki and T. Koike, "Real-time Feynman path integral with Picard-Lefschetz theory and its applications to quantum tunneling," Annals Phys. **351**, 250 (2014) [arXiv:1406.2386 [math-ph]].

[129] G. Basar, G. V. Dunne and M. Unsal, "Resurgence theory, ghost-instantons, and analytic continuation of path integrals," JHEP **1310**, 041 (2013) [arXiv:1308.1108 [hep-th]].

[130] J. Écalle, "Les fonctions resurgentes," volumes I-III, Publications mathématiques d'Orsay, France (1981).

[131] E. Delabaere, "Introduction to the Écalle theory," in *Computer Algebra and differential equations*, E. Delabaere ed., London Math. Society Lecture Note Series 193, Cambridge University Press, Cambridge U.K.(1994).

[132] O. Costin, "Asymptotics and Borel summability," Chapman & Hall/CRC, U.S.A. (2009).

[133] L. C. Biedenharn, "Wigner Coefficients for the R4 Group and Some Applications," J. Math. Phys. **2**, no. 3, 433 (1961).

[134] P. Van Isacker, In *Symmetries in Science V*, Ed. B. Gruber et al., Plenum Press, New York, 1991.

[135] J. Schwinger, *On angular momentum*, Dover Publications, New York, 2015.

[136] J. Avan and H. J. De Vega, "INVERSE SCATTERING TRANSFORM AND INSTANTONS OF FOUR-DIMENSIONAL YUKAWA AND ϕ^4 THEORIES," Nucl. Phys. B **269** (1986) 621.

[137] Z.-Y. Wen and J. Avery, "Some properties of hyperspherical harmonics", J. Math. Phys. **26** (1985) 396.

[138] W. Y. Ai, B. Garbrecht and C. Tamarit, "Functional methods for false vacuum decay in real time," arXiv:1905.04236 [hep-th].